SENSING AND IMAGING OF HYALURONIDASE ACTIVITY USING A LONG-LIVED FLUOROPHORE

DISSERTATION

Presented to the Graduate Council of the
Graduate School of Biomedical Sciences

University of North Texas
Health Science Center at Fort Worth

In Partial Fulfillment of the Requirements

For the Degree of
Doctor of Philosophy

By
Rahul Chib
Fort Worth, Texas
April 2016

Acknowledgements

First and foremost, I would like to express my sincere gratitude to my mentors, Dr. Zygmunt Gryczynski and Dr. Ignacy Gryczynski, whose guidance, understanding, patience and dedication have helped me to accomplish my goals as a graduate student and complete my doctoral studies. They introduced me to this amazing colorful world of fluorescence spectroscopy. I could not have imagined having a better advisors and mentors for my Ph.D. study. I truly appreciate the trust they placed in me throughout my doctoral research, and I will always be grateful to them for the experience I have gained working in their laboratory.

Besides my advisors, I would also like to thank my dissertation committee members: Dr. Rafal Fudala, guided me in each and every step of this project. Dr. Fudala also helped me with the cellular imaging experiments. I would also like to thank Dr. Julian Borejdo, for his insightful comments and encouragement, but also for the questions he posed which incited me to widen my research from various perspectives. Dr. Andras Lacko also served on my committee and gave interesting inputs on this research work. Dr. Lacko's lab was very helpful in cell based studies, especially Dr. Nirupama Sabnis, who provided her guidance in all cellular studies. I would also like to thank my university member, Dr. Michael Allen, for being really supportive during all my committee meetings.

I am also thankful to various other members of Center for Fluorescence Technologies and Nanomedicine (CFTN): Dr. Sangram Raut, for patiently teaching me to operate various instruments, answering all my questions, and helping me with experimental design. I would also like to thank Dr. Irina Akopova, for helping me with AFM experiments and cell culture and Dr.

Ryan Rich, for helping with several other experiments. My livelihood in the lab was sustained in great part by a number of ‘nerdy’ graduate students in the lab, Sunil Shah, Divya Duggal, Hung Doan, Sebastian Requena, Joe Kimball and Janhavi Nagwekar were phenomenal company. They came up with ideas, helped me perform experiments and constructively critiqued the results. I would also like to thank our collaborators, Dr. Mark Mummert, Dr. Beata Grobelna, Dr. Bo. W. Laursen, Dr. Thomas J. Sorensen and Dr. Ilkay Bora for providing samples used in this project.

I would like to express my deep appreciation to my friends who provided so much support and encouragement throughout this process. They include, Mukul Sonker, Rashmi Goyat, Ankur Jain, Yogesh Mishra, Manoj Prajapat, Nikhil Gaidhani, Ina Mishra, Divya Duggal, Sunil Shah, Steffi Daniel, and all members of CBIM family.

The Department of Cell Biology, Immunology and Microbiology and UNT Health Science Center campus has been my home for last four and half year. Moreover, I want to thank them for the financial assistance during my time here. I would like to thank everyone that I have interacted with. I have been humbled by their friendship and hospitality. This community has become my home away from home.

Most importantly, none of this would have been possible without the love and support of my family: my parents (Praveen Chib and Neerja Chib), my grandma (Chanderkanta Chib), my two sisters (Bharti and Shivani), my brother-in-law (Tarun), and my nephew and niece (Ishaan and Ishita). They have been immensely supportive, patient and understanding and I will never take their love for granted.

Table of Contents

List of illustrations

Chapter 1

Chapter 2

Chapter 3

Figure 5: Fluorescence intensity decays of 2 uM HA-FRET (donor) in synthetic urine incubated with 35U/mL of HA-ase enzyme for 90 minutes. Excitation used was 470 nm laser. Donor emission was observed at 520 nm using a 495 long pass filter before detector. Decays were fitted using multi-exponential function and chi square values were used to access the goodness of fit.

Chapter 4

Scheme1. Flow chart of preparation of ADOTA doped silica thin films. Insert: molecular structure of N-(ω-butanoic acid)-azatriangulenium tetrafluoroborate (ADOTA).

Scheme 2: Schematic of the front face arrangement used for steady state and time resolved fluorescence measurements. In this scheme, S represents the sample used for measurement, M is the mirror, F is long pass filter before detector, L is lens.

Figure 1: AFM showing the surface topography of the silica thin layer prepared by the sol gel process.

Figure 2: Top panel: absorption spectrum of N-(ω-butanoic acid)-azatriangulenium tetrafluoroborate (ADOTA). in silica thin film. Bottom panel: absorption spectrum of ADOTA in PVA film.

Figure 3: Normalized excitation and emission spectrum of *N*-(ω-butanoic acid)-azatriangulenium tetrafluoroborate (ADOTA) in silica thin film (red) and in PVA film (blue).

Figure 4:Top panel: fluorescence emission spectrum (red line) and anisotropy (blue circle) of *N*-(ω-butanoic acid)-azatriangulenium tetrafluoroborate (ADOTA) in silica thin film. Bottom panel: fluorescence emission spectrum (blue line) and anisotropy (blue circle) of ADOTA in PVA film.

Figure 5: Top Panel: fluorescence intensity decay of *N*-(ω-butanoic acid)-azatriangulenium tetrafluoroborate (ADOTA) in silica thin film (Ex: 470nm, Obs: 560nm). Bottom panel: fluorescence intensity decay of ADOTA in PVA film (Ex: 470nm, Obs: 560nm).

Figure 6: Top panel: fluorescence intensity decay of *N*-(ω-butanoic acid)-azatriangulenium tetrafluoroborate (ADOTA) in silica thin film (Ex: 470nm, Obs: 620nm). Bottom panel: fluorescence intensity decay of ADOTA in PVA film (Ex: 470nm, Obs: 620nm).

Figure 7- Lifetime distribution (Lorentzian Model) of *N*-(ω-butanoic acid)-azatriangulenium tetrafluoroborate (ADOTA) in silica thin film and PVA film. (Top Panel) This figure represents the fluorescence lifetime distribution when observed at 560 nm. (Bottom Panel) This figure represents fluorescence lifetime distribution observed at 620 nm. ADOTA is more heterogeneous at 560 nm (Silica Thin $Film_{FWHM}$ =15.05 ns, PVA $Film_{FWHM=}$3.22 ns) compared to observation at 620 nm (Silica Thin $Film_{FWHM}$ = 12.71ns, PVA $Film_{FWHM=}$2.45 ns)

Figure 8: Top panel: Fluorescence anisotropy decay of *N*-(ω-butanoic acid)-azatriangulenium tetrafluoroborate (ADOTA) in silica thin film (Ex: 470nm, Obs: 560nm). Bottom panel: fluorescence anisotropy decay of ADOTA in PVA film (Ex: 470nm, Obs: 560nm).

Figure 9: Top panel: Fluorescence anisotropy decay of *N*-(ω-butanoic acid)-azatriangulenium tetrafluoroborate (ADOTA) in silica thin film (Ex: 470nm, Obs: 620nm). Bottom panel: fluorescence anisotropy decay of ADOTA in PVA film (Ex: 470nm, Obs: 620nm).

Chapter 5

Scheme 1: Schematic representation for the assay system and its response to the enzyme hyaluronidase. (A) shows the covalent binding of ADOTA fluorophore to the COOH group of hyaluronic acid. (B) Shows the undigested HA-ADOTA probe and cleaved probe following enzymatic action

Scheme 2: Synthetic procedure for the preparation of p-aminophenyl-ADOTA BF_4

Figure 1: The absorption spectrum of HA-ADOTA probe in PBS (pH 7.4). The concentration of ADOTA in HA-ADOTA probe is 13.96 μM. HA-ADOTA probe in the assay system is 70 nM.

Figure 2 : (A)- Shows the normalized emission spectra of free ADOTA fluorophore in PBS (pH 7.4) and the emission spectra of HA-ADOTA probe (70nM ADOTA) in PBS (pH 7.4) when excited using a 470 nm light source. (B)- The excitation and emission spectra of heavily labeled HA-ADOTA (70 nM ADOTA) probe before and after enzymatic cleavage. The large spectral overlap between excitation and emission spectra is responsible for an efficient excitation energy migration (HOMO-FRET) between ADOTA molecules. The energy migration between ADOTA molecules is responsible for the self-quenching process. (C)- Pictorial representation of the change in the color of HA-ADOTA solution before and after hyaluronidase cleavage.

Figure 3: The change is fluorescence emission of HA-ADOTA probe (70 nM ADOTA, PBS pH7.4) after incubation with different amount of hyaluronidase enzyme. The fluorescence emission spectra was collected for 150 minutes. A 470 nm laser was used for the excitation and the experiments were performed in triplicate and a same increase in fluorescence intensity was observed.

Figure 4: Change is the ratio of emission intensity (560nm/605nm) of the assay system (70 nm ADOTA) in PBS buffer (PBS 7.4) at room temperature vs reaction time in the presence of different amount hyaluronidase. A 470 nm laser was used for excitation and all the experiments were performed in triplicate

Figure 5: The calibration curve for the intensity ratio of HA-ADOTA (70 nM ADOTA) probe in PBS (pH 7.4) at 100 minute as a function of hyaluronidase level (A) 0-20 U/ml, (B) 0-100 U/ml.

Figure 6: The fluorescence intensity decay of HA-ADOTA probe (70 nm ADOTA, 0.6mg/ml HA) in PBS (pH 7.4) in the absence and presence of hyaluronidase. In the presence of enzyme, an increase in the fluorescence lifetime was observed. Without the enzyme at 0 min 3 components are needed to fit the data with amplitudes of 0.16, 0.53 and 0.31 with the lifetime of 18 ns, 0.41 ns and 3.23 ns. With 100U/ml of hyaluronidase at 160 minutes, the decay was fitted using 2 components with amplitudes of 0.74 and 0.26 with lifetime of 18.85 ns and 1.83 ns. All fluorescence lifetime measurements were performed in triplicate.

Figure 7: The time dependent change in the fluorescence lifetime of HA-ADOTA probe (70 nM ADOTA) in PBS (pH 7.4) in the absence and presence of hyaluronidase.

Figure 8: (A) Change is the ratio of emission intensity (560nm/605nm) from cell culture media as a function of change in time. A 470 nm excitation was used and the reaction was continued for 150 min at room temperature. All the experiments were performed in triplicate. (B) change in the color of fluorescence emission of HA-ADOTA probe in culture media before and after enzymatic cleavage.

Chapter 6

Figure 1: Fluorescence lifetime decay of HA-ADOTA probe in media collected from DU-145 cells after 72 hours. An increase in amplitude weighted fluorescence lifetime was observed after

the cleavage of HA-ADOTA by hyaluronidase for 15 minutes produced by the DU-145 cells. The data is the representation of three independent experiments.

Figure 2: Fluorescence lifetime images of PZ-HPV-7 (Healthy prostate cells) and DU-145 cancer cell lines with and without HA-ADOTA. The long fluorescence lifetime of ~16 ns was observed for digested HA-ADOTA probe by hyaluronidase in DU-145 cells.

Figure 3: Time gated analysis of background from DU-145 cells (A) and DU-145 cells with HA-ADOTA (B) after 15 minute of incubation with 2ns, 5ns, 10ns, 15ns and 20 ns gating after the excitation pulse. The data is the representation of three independent experiments.

Chapter 1

Introduction

Color is one of the most interesting characteristics of any material in nature. It is one of the most important mechanisms of nature to provide information to attract or intimidate and is the basic sign of visual communication. Colors are basically just interpretation of varying wavelength or energy of light in the brain and its perception varies not only within species but also between individuals. Humans rely on their optical sense to differentiate between colors of varying information and to interpret symbols encoded in nature like danger, ripeness of food etc.

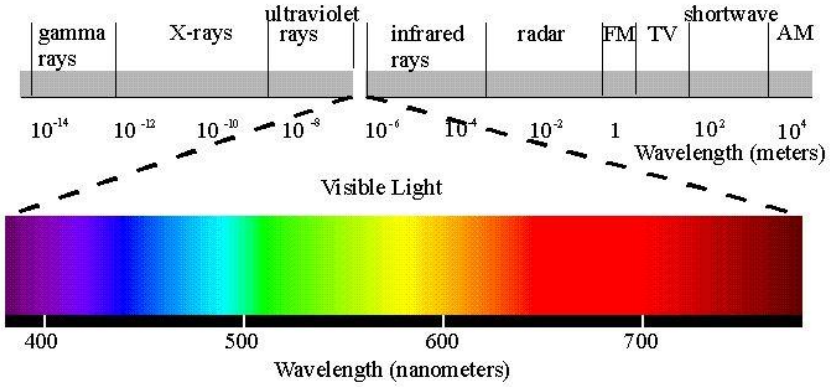

Figure 1: The electromagnetic spectrum with the human visible part zoomed out.

The section of electromagnetic spectrum that is perceived by the human eye stretches from near ultra-violet at about 390 nm to the red at 700 nm [1]. Even though colorants (dyes) were produced a long time ago from natural resources especially by major colony owning empires in France and England, their organic synthesis on industrial scale started in Germany in the middle of 19th century with the foundation of many companies like Bayer and Hoesch. The global industrial market for dyes and pigments is expected to grow over $26 Billion by the year 2017. The total

global market for biological imaging dyes is estimated to be roughly around $14.5 billion in year 2017. This includes contrast and nuclear reagents, proteins and quantum dots [2-6].

1. Introduction to photophysical phenomena

Light emission from a material is called luminescence. Luminescence is emission of UV, visible or infra-red light by electronically excited species. Depending on the energy source, luminescence is then described as electro, chemo, radio, bio or photoluminescence. Photoluminescence is the emission process occurring from a material when energy is provided by electromagnetic radiation of UV, visible and infra-red region of the spectrum. The term luminescence was first introduced by the physicist and science historian, Eilhardt Wiedemann in year 1888 [7]. Fluorescence, phosphorescence and delayed fluorescence are known forms of photoluminescence. The term fluorescence was first coined by Sir George Stoke, a physicist and professor of mathematics at Cambridge in his famous paper entitled "*On the refrangibility of light*" in 1852 [8]. However, the observation of fluorescence phenomena had been reported in the literature way before this time. In 1565, a Spanish physician and botanist, Nicolas Monardes reported a wonderful blue emission from an infusion of wood brought from Mexico, which was used to treat kidney and urinary disease. The medicinal property and blue color of the wood was known to the Aztecs. As it was an expensive medicine, its counterfeit were also available in the market. Therefore, it was of great interest to detect these counterfeits which emitted yellow color in solution. This was the first application of the phenomena that would be later called as "*fluorescence*". This wood was later characterized as *Lignum Nephriticum*. In 1833, Sir David Brewster described the beautiful red fluorescence of chlorophyll when a beam of light passes from green alcoholic extract of leaves, in the article "*On the color of natural bodies"* [9,10]. In

1845, Sir John Hershel reported the blue light emission from quinine sulfate solution and called this phenomenon as “Epipolic dispersion”.

Although, it is not clear who demonstrated the term phosphorescence, the term phosphor, a material that glows in the dark, has been in use since the middle ages. There are various examples of minerals that glow in the dark, and one such widely known mineral is *Bolognian phosphor* found by Cobbler from Bologna named Vincenzo Cascariolo in 1602. Later in 1900, many well-known scientists like Pringsheim, Levshin, J. Perrin, F. Perrin, E. Gaviola, A. Jablonski, G. Weber contribute to the advancement in the field of fluorescence. In the past three decades, there has been remarkable growth in the field of fluorescence in biomedical field. The fluorescence field in biomedical science was revolutionized by Richard Haugland, creator of the company, Molecular probes (currently a part Thermo fisher Scientific) for using organic fluorophores in human genome project.

2. The Fluorescence phenomena

Over the past few decades, fluorescence spectroscopy has become a valuable tool in biomedical research. It is a dominant technology, expanding to different branches in research, for example, biotechnology, genetics and medical diagnosis. The widespread use of fluorescence technology is mainly due to its high sensitivity and ease of use. This reason led to its extensive use in molecular and cellular imaging, which is very useful in determining numerous cellular processes, including localization of intracellular molecules even at the single molecule level.

Fluorescence is a phenomenon which occurs when a fluorophore absorbs light (energy) at a specific wavelength (corresponding to the transition energy behavior) and emits at a longer

wavelength. The emission of the light occurs from electronically excited singlet state of the molecule. In the singlet state, spins are completely antiparallel and thus the total spin is S=0. Excited electrons from the singlet excited state decays quickly back to the ground state yielding fluorescence. This phenomena leads to rapid rate of emission in fluorescence that is typically in the range of a few nanoseconds. However, electrons from the excited state can sometime go to the triplet state (forbidden transition) giving rise to phosphorescence which has lifetimes on the order of milliseconds. The scheme below depicts the absorption, fluorescence and phosphorescence process on a Jablonski diagram first published in Nature in year 1933 and describe the photophysical processes which occur when molecules absorb light [11]. Jablonski diagram is often used to demonstrate various molecular processes that occur during absorption and emission.

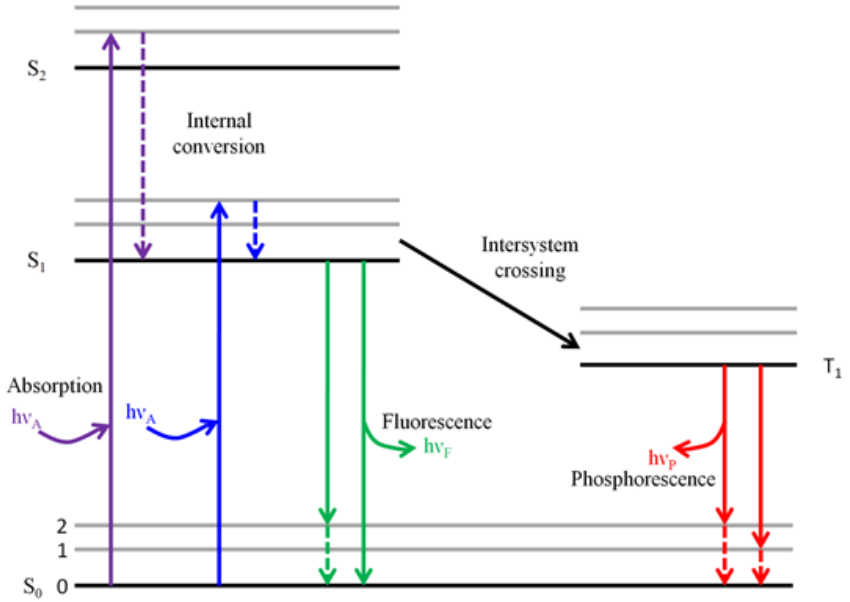

Figure 2: Jablonski diagram showing absorption, fluorescence and phosphorescence processes.

In this, diagram S0, S1 and S2 represents the singlet ground and first and second excited state. At each of these electronic states, electron can stay in any of the vibrational state. Generally, the energy of emission is lower than the energy of absorption as energy is lost during various

molecular processes. This leads to a red shift in the emission spectrum with a lesser energy. This phenomenon is called a Stokes shift. One of the various reason of stokes shift is internal conversion; energy loss can also by thermalization of extra vibrational energy, solvent effect, excited-state reaction, complex formation and energy transfer.

2.1. Fluorescence quantum yield

Radiative and non-radiative processes define how a molecule losses energy. Since only a small fraction of energy is dissipated back as fluorescence but mostly the energy is dissipated as heat. As shown in the Jablonski diagram, transition from S1 to S0 occurs with loss of energy. As a result, the number of photons emitted by a fluorophore is rarely equal to the number of photons absorbed by it [7,12,13]. This ratio of emitted photons to absorb is known as quantum yield and can be calculated by;

$$Q = \frac{\Gamma}{\Gamma + K_{nr}}$$

Where Γ is the Radiative decay rate and $K_{n\,r}$ is the non-radiative decay rate.

2.2. Fluorescence lifetime

An important and defining characteristic feature of a fluorescent material is its fluorescence lifetime. It a characteristic feature to each fluorophore and depends on various factors like molecular structure and the effect of external factors such as presence of quenchers, temperature and solvent polarity. It is a statistical process that tells us how long a fluorophore on average will stay in the excited state before it emits a photon and return to the ground state. The fluorescence lifetime is defined as the time it takes for the overall fluorescence intensity to decline 1/e of its initial intensity after the absorption of light. Similar to the quantum yield, the fluorescence

lifetime can be expressed as a function of radiative and non-radiative rate constant from the Jablonski diagram as shown in equation below

$$\tau = \frac{1}{\Gamma + K_{nr}}$$

Where τ is fluorescence lifetime, Γ is radiative decay and K_{nr} is the non-radiative decay rate. If the quantum yield of the fluorophore is 1, then the fluorescence lifetime of the fluorophore is known as natural lifetime and is given by:

$$\tau_n = \frac{1}{\Gamma}$$

If we assume that an initial amount of molecules N_0* are in the excited state, one can model the amount of molecules in the excited state as a function of time by the first order rate equation:

$$\frac{dN^*(t)}{dt} = -KN_0^*(t)$$

Where k is all decay rates (radiative and non-radiative). Integrating above equation with respect to time gives:

$$N^*(t) = N_0^* e^{-Kt}$$

We can also define the lifetime $\tau = 1/k$ so we are left with

$$N^*(t) = N_0^* e^{-t/\tau}$$

The fact that many typical organic fluorescent molecules have a lifetime in the range of 1-5 ns gives fluorescence spectroscopy an almost unparalleled advantage in detection of biological systems because all the biological processes occur in similar time scale. This can also allow the

molecule to interact with its environment during the time spent in its excited state and hence details about excited state interactions can be studied using fluorescence lifetime [14].

2.3. Fluorescence Anisotropy

Fluorescence anisotropy measures the rotational diffusion of a molecule by using polarized fluorescence signal from the molecule. Anisotropy measurements are typically used to measure the binding interaction between molecules. In biological sciences, fluorescence measurements are used for various purposes like measuring the size and shape of a molecule or proteins or more interestingly protein-protein interaction. The anisotropy is given as the ratio of fluorescence intensities and can be described as:

$$r = \frac{VV - VH}{VV + 2VH}$$

where VV is the fluorescence intensity with the polarizer aligned parallel to each other and VH with perpendicular orientation. The measured intensities at two different orientations of the polarizer will be different because the absorption probability depends on the angle between the electric vector and the absorption transition dipole moment of the absorbing molecule. During excitation of the fluorophore, the molecules are photoselected by the incident light. During the emission of light, the photon electric vector will be oriented along the molecules emission transition dipole moment. During the lifetime of the fluorophore, the photoselected population will rotate and therefore depolarize the emission. Depending on the environment and the lifetime of the fluorophore, the depolarization of light can be faster or slower. This can help in studying the dynamics of macromolecules in solutions. The Perrin equation relates the fluorescence lifetime of a fluorophore and the correlation time of the fluorophore to the observed anisotropy

and fundamental anisotropy. Fundamental anisotropy is the anisotropy measured in the absence of diffusion [15-20].

$$r = \frac{r_o}{1 + \frac{\tau}{\theta}}$$

Where r_0 is the fundamental anisotropy, τ is the fluorescence lifetime and θ is the correlation time for the rotational diffusion.

2.4. Fluorescence lifetime imaging (FLIM) microscopy

Fluorescence lifetime imaging produces an image based on the difference in the fluorescence lifetime (excited state decay rate) of the fluorescent sample. Thus it is a fluorescent imaging technique where the contrast on the image is based on the fluorescence lifetime of the individual fluorophore rather than its emission profile. The fluorescence lifetime depends on various environmental parameters such as pH, oxygen concentration, viscosity etc. It offers a unique method to study live or fixed cells because of its high sensitivity, specificity and versatility. The change in the lifetime of a fluorescent dye due to specific molecular interactions has several applications. If interaction of a fluorescent molecule with oxygen or its conjugation with a target molecule changes its fluorescence lifetime, then it can be seen as a contrast in the image in terms of different fluorescent lifetime [7,21-24].

FLIM techniques can be classified into time-domain and frequency domain. However in this section we will only discuss time-domain FLIM via time-correlated single photon counting (TCSPC) which is used in the later section of this dissertation. TCSPC-FLIM uses a multidimensional time-correlated counting process. Data recording is based on detecting single photon of fluorescence emission after each excitation and determining the arrival time of the

photon to the laser pulse and the position of the laser beam. From these parameters, a photon distribution over the spatial coordinates, x, y and the times of the photons (t) is build up. This results in the generation of a three-dimensional data array that represents the pixels of the two-dimensional scan, with each pixel containing photons in a large number of time channels for consecutive times after the excitation pulses [13,25].

3. Use of fluorophore in biology

Fluorescence without doubt is one of the most important tools in biology. The use of fluorescence has allowed us to sequence genome, study protein interactions, and study protein localization and kinetics [26-28]. Fluorescent dyes like Indocyanine green is an FDA approved contrast agent and has been used in diagnostics and surgical procedures. It had been used to image liver function and as a contrast for angiogram [29-31]. Fluorescence provides biologists the opportunities to study intracellular structures in more detail which was unattainable by more classic microscopy techniques like bright and dark field microscopy. With the inception of fluorescent protein, cell biologists can now monitor the intracellular environment, in real time without the addition of exogenous fluorophores [32,33]. The investigation of many fundamental processes occurring at biomolecular level requires tools for fast, sensitive and reproducible detection. One of the best methods to study biomolecular interactions is the use of photoluminescence with functional labels and dyes. Fluorescence-based detection is the most common method for biosensing because of its high sensitivity, selectivity and ease of use. The development of novel luminescent materials with unique fluorescent properties paves new roles for fluorescence based detection, imaging and sensing of biomolecules. Fluorescence spectroscopy and microscopy is widely used in various areas of biology and medicine, including proteomics and genomics studies, pharmaceutical screening, diagnostics, drug delivery and

medical imaging (like in-vivo imaging of cancer) [34,35]. Usually the molecules of interest in biomedical research are non-fluorescent and require the use of extrinsic fluorophores. The most common use of fluorophores in biology is in immunology, probing proteins and labeling antibodies. These small fluorescent dyes are indispensable tools in chemical biology, being ubiquitous as biomolecular labels and cellular stains.

4. Fluorophores

Fluorophores are the molecules which re-emits energy upon excitation by a light source. Developments in chemistry, physics, biology, and engineering have encouraged interest in dyes and fluorophores to study localization, trafficking or expression of biomolecules in live cells. Due to its widespread use in biology, fluorophores have become very useful in biotechnology and medicine. Fluorescent probes are widely used in biomedical science as it provides high sensitivity in detection with minimum perturbation to system under consideration. The use of fluorophores in protein biochemistry started with the synthesis of dansyl chloride in 1953 by Gregorio Weber. For his dissertation work, he also introduced fluorescence of flavins, ANS and TNS. Dr. Weber's work in predicting the intrinsic protein fluorescence and the first spectral resolution of their emission has allowed the use of the three known fluorescent aromatic amino acids (Tryptophan, Tyrosine and Phenylalanine) in protein dynamics studies [12,36].

Fluorophores can be broadly classified into two categories; intrinsic and extrinsic fluorophores. Intrinsic fluorophores are the chemical entities which are present in a cell and have fluorescent properties which include aromatic amino acids, flavins and flavoproteins. Extrinsic fluorophores are those that are added to the sample to provide them fluorescence properties. The indole group of tryptophan residue is the dominant source of UV absorption and emission in proteins. The emission of tryptophan is highly sensitive to its environment, and is often used to study protein

conformation change. Typical lifetimes of aromatic amino acids are in the range of few ns with tryptophan at 3.1 ns, tyrosine at 3.6 ns and phenylalanine at 6.8 ns.

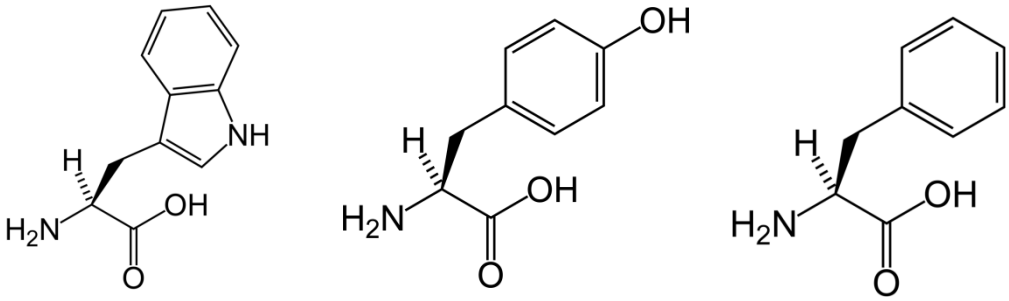

Tryptophan **Tyrosine** **Phenylalanine**

Figure 3: Chemical structure of three aromatic amino acids.

Enzyme cofactor like NADH is highly fluorescent, with absorption and emission maxima at 360nm and 460nm. Riboflavin, FMN, and FAD absorb light in the visible region around 450 nm and emission at 525 nm. Lifetimes for FMN and FAD are 4.7 and 2.3 ns. There is a great deal of interest in the use of fluorescence from tissue. The best characterized fluorescence from tissue is from the structural protein collagen and elastin. However, extrinsic fluorophores are mainly used for biomedical applications because of their superior photophysical properties and ease of application as most of the biological samples are not fluorescent by themselves. For example, DNA and lipids are devoid of fluorescence and requires the use of extrinsic fluorophores. Even in case of proteins, it is desirable to label them with a fluorophore that has excitation and emission wavelength longer than the aromatic amino acid [7,13]. Today fluorescein and rhodamine and their derivatives are the most commonly used fluorophores in biology. Fluorescein was first discovered by a German organic chemist, Adolf Van Bayer in 1871, much before the discovery of dansyl, but was not put in use in biology until recently [37].

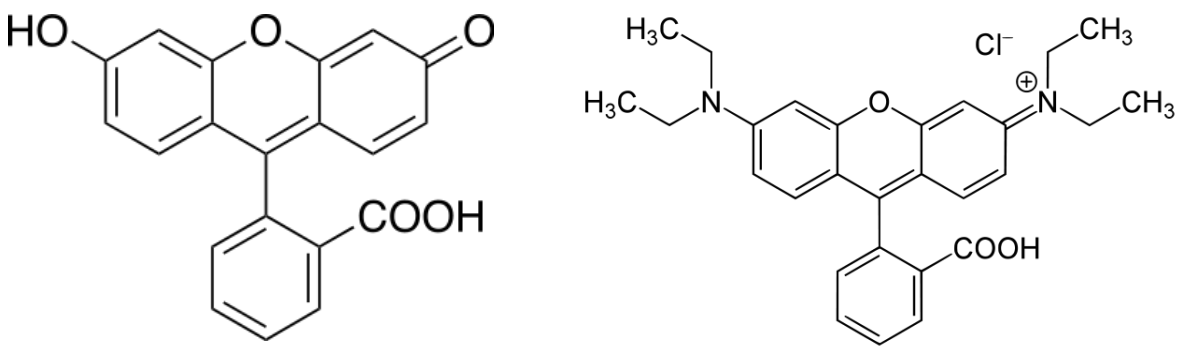

Fluorescein **Rhodamine B**

Figure 4: Chemical structure of fluorescein and Rhodamine B.

The advantage of using these dyes is their wide/narrow emission range of 510-620 nm and high extinction coefficient near 89,000$M^{-1}cm^{-1}$. BODIPY dyes later replaced fluorescein and rhodamine. BODIPY dyes have high fluorescence quantum yield, insensitivity to solvent polarity and pH, narrow emission bandwidth and greater photo-stability than fluorescein [38]. On the other hand, dyes like prodan and acrylodan are sensitive to polarity and show large spectral shifts at the membrane phase-transition temperature [39]. Apart from these dyes, dyes like ANS, TNS and 1,6-diphenyl1-1,3,5-hexatriene (DPH) that interact non-covalently with proteins and membrane are also widely used in biochemical studies [40-42]. The most recent dyes available for bioimaging is Green fluorescent protein discovered in 1979. This discovery led to noble prize in 2008 to Osamu Shimomura, Martin Chalfie, and Rogen Tsien [43]. However, the main problem associated with fluorescent proteins is the inability of their use in polarization studies apart from a shorter shelf life and difficult synthetic method.

Quantum dots are one of the newest additions to fluorophores. Although they were discovered in 1981, they did not find application application as a probe until 2002 when Quantum Dot Corporation of Hayward, CA started selling them to biologists. Quantum dots when compared to organic dyes are photostable and do no bleach at all. However, their main disadvantage is their large size which can produce perturbation in biological samples. Also, they are cytotoxic and photoblink when excited [44,45]. Lanthanides (europium and terbium) are another class of inorganic fluorophores. Lanthanides display line emission with very long fluorescence lifetime in the range of few milliseconds. Their major applications are as fluorescent substitutes for calcium and as a donor in FRET experiments. They are of limited use because of their low extinction coefficient and often need a chelator to excite them indirectly [13,46]. Another new class of fluorescent nanomaterials includes nanodiamonds, nanoruby and noble metal nanoclusters. Early reports on fluorescent nanodiamond came around 1997. The fluorescence from these nanodiamonds can be ascribed to the point defects (Nitrogen atoms) in crystal lattice called N-V centers. These vacancies are generated by proton, electron or ion bombardment in the presence of nitrogen [47,48]. Nanoruby is a recent type of fluorescent nanoprobe. This consists of Cr doped aluminum oxide (Al2O3), where replacement of Al by Cr is the reason for the luminescence. It shows zero photon line (ZPLs) at around 694 and 692 nm. Edmonds et al. reported its synthesis and use as a cellular probe for background free detection [49]. Noble metal fluorescent probes are amongst the newest class of fluorescent probes. These are organic ligand protected metal (Au, Ag, Cu, Pt) clusters which are less than 2 nm in size. The metal core consist of few atoms of a particular metal capped by an organic ligand. Nanoclusters bridge the gap between the behavior of metal atoms and metal nanoparticles [50-52]. Even with the emergence of different types of novel fluorescent probes, organic fluorophores are the most widely used fluorophore in several biomedical

research. Due to their small size, large extinction coefficient and ease of functionalization, it is really convenient to use organic fluorophores for different biomedical applications. Currently fluorophores with long fluorescence lifetime are attracting interest of biochemists for analytical and imaging purposes as their wavelength of excitation shifts towards longer wavelength thereby decreasing the autofluorescence from biological samples. In 1856, C.H.G Williams synthesized the first cyanine dye which emits in the blue region of the electromagnetic spectrum [53]. The fluorescence lifetimes of most red emitting organic probes is under 4 nanoseconds, which is a limiting factor in studying interactions and conformational dynamics of macromolecules. In addition, the nanosecond background autofluorescence is a significant interference during fluorescence measurements in cellular environment. Poly-aromatics such as pyrene are among few long-lived organic fluorescent probes available. Unfortunately these probes can only be excited in UV and near-UV (typically less than 350 nm) region of the spectrum, where the autofluorescence and cellular material absorption is also very strong. Therefore, red fluorescence emission with longer lifetimes will be immensely helpful. The new class of fluorophore with three oxygen bridges was originally synthesized by Martin and Smith in 1964. Just 15 years ago, Bo.W. Laursen and others dedicated attention to the development of this interesting class of fluorophores with long fluorescence lifetime >20 ns and emission in 520-600 nm. Azaoxa-triangulenium fluorophores ADOTA and DAOTA are red emitting small organic molecules with high quantum yield, long fluorescence lifetime and high limiting anisotropy. In aqueous environment, ADOTA and DAOTA absorption and emission maxima are respectively 540 nm and 556 nm, and 556 nm and 589 nm. Their emission extends beyond 700 nm. Both probes have the limiting anisotropy between 0.36–0.38 at their absorption peak. In both protic and aprotic solvents, their lifetimes are around 20 ns, making them among the longest-lived red emitting

organic fluorophores. The azaoxa-triangulenium probes, which absorb and emit in red are a sub-group of triangulenium structures in which oxygen is replaced by nitrogen and the three aromatic rings are bonded to a central carbon atom bearing a positive charge. They are either similar or smaller when compared to other red fluorophores. Their emissive properties, dictated by the oscillator strength of the primary transition, are unique, as the long 50 ns radiative lifetime does not result in extensive quenching of the emissive state. Consequently, the azaoxa-triangulenium dyes have high quantum yields, long fluorescence lifetimes and high limiting anisotropy [54-59].

The work described in this dissertation deals with the characterization and application of azadioxatriangulenium (ADOTA) fluorophore for biomedical sensing. As a proof of concept, for their applications in biomedical science, this fluorophore was used for the detection and imaging of enzyme hyaluronidase. The enzyme hyaluronidase is upregulated in various types of cancer. Hence, developing a probe that can sense and image hyaluronidase activity in biological samples will be beneficial. Initially a probe was developed for the detection of hyaluronidase using hyaluronic acid as the template labeled with fluorescein and rhodamine as the FRET pair. After that a similar probe using ADOTA fluorophore was synthesized. This probe was further characterized and used in sensing and imaging of hyaluronidase activity in biological samples. Physiological importance of hyaluronidase and hyaluronic acid are discussed in detail in the later section of this dissertation. The work in this dissertation has been divided into four parts.

Project 1: Synthesis and characterization of biosensor for the detection of hyaluronidase activity using fluorescein and rhodamine (HA-FRET)

Project 2: Characterization of azadioxatriangulenium fluorophore in polyvinyl alcohol (PVA) film and silica thin films

Project 3: Synthesis, characterization, and application of the biosensor developed using azadioxatriangulenium fluorophore (HA-ADOTA) for the detection of hyaluronidase activity

Project 4: Application of HA-ADOTA as a fluorescence lifetime-based imaging agent for the detection of hyaluronidase activity in cancer cells.

References

1. Peatross J, Ware M. *Physics of light and optics.* Brigham Young University, Department of Physics; 2011.

2. Hunger K. *Industrial dyes: Chemistry, properties, applications.* John Wiley & Sons; 2007.

3. Judd DB, Wyszecki G. Color in business, science, and industry. . 1975.

4. Mahnke FH. *Color, environment, and human response: An interdisciplinary understanding of color and its use as a beneficial element in the design of the architectural environment.* John Wiley & Sons; 1996.

5. Mason WT. *Fluorescent and luminescent probes for biological activity: A practical guide to technology for quantitative real-time analysis.* Academic Press; 1999.

6. Sabnis RW. *Handbook of biological dyes and stains: Synthesis and industrial applications.* John Wiley & Sons; 2010.

7. Valeur B, Berberan-Santos MN. *Molecular fluorescence: Principles and applications.* John Wiley & Sons; 2012.

8. Stokes GG. On the change of refrangibility of light. *Philosophical Transactions of the Royal Society of London*. 1852;142:463-562.

9. Brewster D. XIX. on the colours of natural bodies. *Trans R Soc Edinb*. 1834;12(02):538-545.

10. Valeur B, Berberan-Santos MN. A brief history of fluorescence and phosphorescence before the emergence of quantum theory. *J Chem Educ*. 2011;88(6):731-738.

11. Jaboski A. Efficiency of anti-stokes fluorescence in dye s. *Nature*. 1933;131(839-840):21.

12. Jameson DM. *Introduction to fluorescence.* Taylor & Francis; 2014.

13. Lakowicz JR. *Principles of fluorescence spectroscopy.* Springer Science & Business Media; 2013.

14. Berezin MY, Achilefu S. Fluorescence lifetime measurements and biological imaging. *Chem Rev*. 2010;110(5):2641-2684.

15. Lea WA, Simeonov A. Fluorescence polarization assays in small molecule screening. *Expert opinion on drug discovery*. 2011;6(1):17-32.

16. Cross AJ, Fleming GR. Analysis of time-resolved fluorescence anisotropy decays. *Biophys J*. 1984;46(1):45-56. doi: S0006-3495(84)83997-1 [pii].

17. Lakowicz JR, Cherek H, Kuśba J, Gryczynski I, Johnson ML. Review of fluorescence anisotropy decay analysis by frequency-domain fluorescence spectroscopy. *J Fluoresc*. 1993;3(2):103-116.

18. Kawski A. Fluorescence anisotropy: Theory and applications of rotational depolarization. *Crit Rev Anal Chem*. 1993;23(6):459-529.

19. Owicki JC. Fluorescence polarization and anisotropy in high throughput screening: Perspectives and primer. *Journal of Biomolecular Screening*. 2000;5(5):297-306.

20. Gradinaru CC, Marushchak DO, Samim M, Krull UJ. Fluorescence anisotropy: From single molecules to live cells. *Analyst*. 2010;135(3):452-459.

21. Szmacinski H, Lakowicz JR, Johnson ML. [30] fluorescence lifetime imaging microscopy: Homodyne technique using high-speed gated image intensifier. *Meth Enzymol*. 1994;240:723-748.

22. Draaijer A, Sanders R, Gerritsen H. Fluorescence lifetime imaging, a new tool in confocal microscopy. In: *Handbook of biological confocal microscopy.* Springer; 1995:491-505.

23. Herman B, Wang X, Wodnicki P, et al. Fluorescence lifetime imaging microscopy. *Applied fluorescence in chemistry, biology and medicine*. 1999:491-507.

24. Gadella TW, Jovin TM, Clegg RM. Fluorescence lifetime imaging microscopy (FLIM): Spatial resolution of microstructures on the nanosecond time scale. *Biophys Chem*. 1993;48(2):221-239.

25. Becker W. Fluorescence lifetime imaging–techniques and applications. *J Microsc*. 2012;247(2):119-136.

26. Walter M, Chaban C, Schütze K, et al. Visualization of protein interactions in living plant cells using bimolecular fluorescence complementation. *The Plant Journal*. 2004;40(3):428-438.

27. Giepmans BN, Adams SR, Ellisman MH, Tsien RY. The fluorescent toolbox for assessing protein location and function. *Science*. 2006;312(5771):217-224. doi: 312/5771/217 [pii].

28. Shendure J, Porreca GJ, Reppas NB, et al. Accurate multiplex polony sequencing of an evolved bacterial genome. *Science*. 2005;309(5741):1728-1732. doi: 1117389 [pii].

29. Ogawa M, Kosaka N, Choyke PL, Kobayashi H. In vivo molecular imaging of cancer with a quenching near-infrared fluorescent probe using conjugates of monoclonal antibodies and indocyanine green. *Cancer Res*. 2009;69(4):1268-1272. doi: 10.1158/0008-5472.CAN-08-3116 [doi].

30. Schaafsma BE, Mieog JSD, Hutteman M, et al. The clinical use of indocyanine green as a near-infrared fluorescent contrast agent for image-guided oncologic surgery. *J Surg Oncol*. 2011;104(3):323-332.

31. Ntziachristos V, Yodh AG, Schnall M, Chance B. Concurrent MRI and diffuse optical tomography of breast after indocyanine green enhancement. *Proc Natl Acad Sci U S A*. 2000;97(6):2767-2772. doi: 10.1073/pnas.040570597 [doi].

32. Betzig E, Patterson GH, Sougrat R, et al. Imaging intracellular fluorescent proteins at nanometer resolution. *Science*. 2006;313(5793):1642-1645. doi: 1127344 [pii].

33. Tavare JM, Fletcher LM, Welsh GI. Using green fluorescent protein to study intracellular signalling. *J Endocrinol*. 2001;170(2):297-306. doi: JOE04285 [pii].

34. Udenfriend S. *Fluorescence assay in biology and medicine.* Vol 2. Academic Press; 2014.

35. Rettig W, Strehmel B, Schrader S, Seifert H. *Applied fluorescence in chemistry, biology and medicine.* Springer Science & Business Media; 2012.

36. Jameson D. The seminal contributions of gregorio weber to modern fluorescence spectroscopy. In: *New trends in fluorescence spectroscopy.* Springer; 2001:35-58.

37. Huisgen R. Adolf von baeyer's scientific achievements—a legacy. *Angewandte Chemie International Edition in English*. 1986;25(4):297-311.

38. Loudet A, Burgess K. BODIPY dyes and their derivatives: Syntheses and spectroscopic properties. *Chem Rev*. 2007;107(11):4891-4932.

39. Parasassi T, Krasnowska EK, Bagatolli L, Gratton E. Laurdan and prodan as polarity-sensitive fluorescent membrane probes. *J Fluoresc*. 1998;8(4):365-373.

40. Davila H, Cohen L, Salzberg B, Shrivastav B. Changes in ANS and TNS fluorescence in giant axons fromLoligo. *J Membr Biol*. 1974;15(1):29-46.

41. Edelman GM, McClure WO. Fluorescent probes and the conformation of proteins. *Acc Chem Res*. 1968;1(3):65-70.

42. Gasymov OK, Glasgow BJ. ANS fluorescence: Potential to augment the identification of the external binding sites of proteins. *Biochimica et Biophysica Acta (BBA)-Proteins and Proteomics*. 2007;1774(3):403-411.

43. Shimomura O. Structure of the chromophore of aequorea green fluorescent protein. *FEBS Lett*. 1979;104(2):220-222.

44. Bourzac K. Quantum dots go on display. *Nature*. 2013;493(7432):283. doi: 10.1038/493283a [doi].

45. Klostranec JM, Chan WC. Quantum dots in biological and biomedical research: Recent progress and present challenges. *Adv Mater*. 2006;18(15):1953-1964.

46. Yuan J, Wang G. Lanthanide complex-based fluorescence label for time-resolved fluorescence bioassay. *J Fluoresc*. 2005;15(4):559-568.

47. Chang Y, Lee H, Chen K, et al. Mass production and dynamic imaging of fluorescent nanodiamonds. *Nature nanotechnology*. 2008;3(5):284-288.

48. Kompan M, Terukov E, Gordeev S, Zhukov S, Nikolaev YA. Photoluminescence spectra of ultradisperse diamond. *Physics of the Solid State*. 1997;39(12):1928-1929.

49. Edmonds AM, Sobhan MA, Sreenivasan VK, et al. Nano-Ruby: A promising fluorescent probe for Background-Free cellular imaging. *Particle & Particle Systems Characterization*. 2013;30(6):506-513.

50. Xavier PL, Chaudhari K, Baksi A, Pradeep T. Protein-protected luminescent noble metal quantum clusters: An emerging trend in atomic cluster nanoscience. *Nano Rev*. 2012;3(3).

51. Yuan X, Luo Z, Yu Y, Yao Q, Xie J. Luminescent noble metal nanoclusters as an emerging optical probe for sensor development. *Chemistry–An Asian Journal*. 2013;8(5):858-871.

52. Raut S, Chib R, Rich R, Shumilov D, Gryczynski Z, Gryczynski I. Polarization properties of fluorescent BSA protected au 25 nanoclusters. *Nanoscale*. 2013;5(8):3441-3446.

53. Hamer FM. *The chemistry of heterocyclic compounds, the cyanine dyes and related compounds*. Vol 18. John Wiley & Sons; 2009.

54. Laursen BW, Krebs FC, Nielsen MF, Bechgaard K, Christensen JB, Harrit N. 2, 6, 10-tris (dialkylamino) trioxatriangulenium ions. synthesis, structure, and properties of exceptionally stable carbenium ions. *J Am Chem Soc*. 1998;120(47):12255-12263.

55. Laursen BW, Krebs FC. Synthesis of a triazatriangulenium salt. *Angewandte Chemie*. 2000;112(19):3574-3576.

56. Maliwal BP, Fudala R, Raut S, et al. Long-lived bright red emitting azaoxa-triangulenium fluorophores. *PLoS One*. 2013;8(5):e63043.

57. Rich RM, Stankowska DL, Maliwal BP, et al. Elimination of autofluorescence background from fluorescence tissue images by use of time-gated detection and the AzaDiOxaTriAngulenium (ADOTA) fluorophore. *Analytical and bioanalytical chemistry*. 2013;405(6):2065-2075.

58. Thyrhaug E, Sørensen TJ, Gryczynski I, Gryczynski Z, Laursen BW. Polarization and symmetry of electronic transitions in long fluorescence lifetime triangulenium dyes. *The Journal of Physical Chemistry A*. 2013;117(10):2160-2168.

59. W Laursen B, C Krebs F. Synthesis, structure, and properties of azatriangulenium salts. *Chemistry–A European Journal*. 2001;7(8):1773-1783.

Chapter 2

Hyaluronic acid, hyaluronidase and methods of detection of hyaluronidase: an overview

1. Hyaluronic acid

Hyaluronic acid (HA), also called as hyaluronan was first isolated from bovine vitreous humor by Meyer and Palmer in 1934 [1]. It is a linear polysaccharide consisting of repeating disaccharide composed of N-acetylglucosamine and glucuronic acid, which are connected by a linked via alternating β-1,4 and β-1,3 glycosidic bond. Hyaluronic acid is a member of the glycosaminoglycans (GAGs), which are composed of repeating disaccharide of uronic acid and amino sugar. But compared to other GAGs like chondroitin, keratin, chondroitin sulfate, and heparin, all the GAGs are synthesized by resident Golgi enzymes, except hyaluronan which is synthesized at the inner surface of plasma membrane and then extruded out. Hyaluronan is produced by all vertebrates as a major component of extracellular matrix. In mammals, the highest levels can be found in umbilical cord, synovial fluid, skin, and vitreous humor. Increased concentrations of hyaluronic acid are found in the matrix produced by the cumulus cells around the oocyte. The overall amount of hyaluronic acid in a 70 kg individual is approximately 15gm [2].

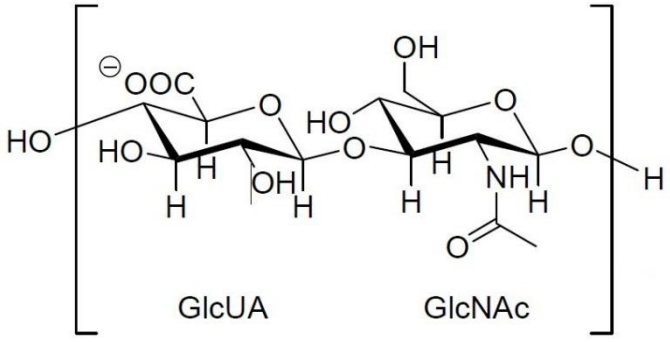

Figure 1: Chemical structure of hyaluronic acid.

Biosynthesis of hyaluronic acid are regulated by a class of integral membrane proteins called hyaluronan synthases of which vertebrates have three types: HAS1, HAS 2, and HAS 3. The active site of these transmembrane enzymes protrudes from the inner face to the plasma membrane and hyaluronic acid is extruded during synthesis through the cell membrane into the extracellular surface. The synthesized hyaluronic acid stays in contact with the plasma membrane via interaction with the cell surface receptor like CD44, RHAMM, LYVE-1, TLR-4 or by the membrane anchored hyaluronidase Hyal-2 [3]. The degradation of the hyaluronic acid was suggested by Csoka et al. First, higher molecular weight HA is degraded into small fragments of 20 kDa by the membrane bound Hyal-2. After internalization of the fragments further degradation occurs in the acidic surrounding of lysosomes with the help of Hyal-1 and two exoglycosidases called β-N-acetylglucosaminidase and β-glucuronidase. Finally the oligosaccharides are able to diffuse out of the lysosome, which is used again for the synthesis of hyaluronic acid. One third of the hyaluronic acid present in human body are metabolized and reproduced every day. In addition to the enzymatic degradation, it is also degraded under physiological conditions by reactive oxygen species like the hydroxyl radical [4].

Inside the body, hyaluronic acid serves various several functions. It functions as a lubricant, shock absorber, regulates water homeostasis and functions as an important structure-forming molecule, especially in joints and vitreous humor, and provide structural integrity to the skin. Furthermore, it is involved in embryological development and general processes like migration, proliferation, adhesion and differentiation of cells, immune surveillance, inflammation, wound healing, angiogenesis, and tumor progression. High molecular weight hyaluronan is anti-angiogenic and anti-inflammatory, whereas smaller hyaluronan fragments are angiogenic and inflammatory [2-16].

2. Hyaluronidase

The hyaluronidases were first discovered by Duran and Reynals in the extract of mammalian testis and were identified as "spreading factor" due to its ability to facilitate the diffusion of vaccines, dyes and toxins [17]. The term hyaluronidase was introduced by Meyer in the 1940. Hyaluronidase are found throughout the animal kingdom and can be isolated from a large number of organs like liver, kidney, testis, spleen, uterus and placenta, or from the venoms of animals like spiders, bees, wasp and scorpions [18,19].

In mammals, testicular hyaluronidase is present in the sperm acrosome for the fertilization of the ovum [20]. A few decades ago, a connection between hyaluronidase and cancer was established [21-23]. Hyaluronidases are a class of enzyme that degrades hyaluronic acid (HA). Hyaluronidase also degrades chondroitin sulfate and chondroitin at a slower rate. Six hyaluronidase genes are present in human genome and these occur in two linked triplicates HYAL-1,-1 and -3 genes are clustered in the chromosome 3p21.3 locus, whereas HYAL-4,HYAP-P1 and PH-20 resides in chromosome 7q31.3 [15,24,25]. Among the six mammalian hyaluronidases, HYAL-1 is the major tumor-derived hyaluronidase and is expressed by a variety of tumor cells. HYAL-1 was initially purified from the urine of patients with high-grade bladder cancer and has been shown to be expressed in the epithelial cells of bladder and prostate tumor and in head and neck squamous cell carcinoma [26]. Various test for the detection of hyaluronidase were established in the past decades. Using the hyaluronidase test, Lokeshwar et al. found that the levels of hyaluronidase are elevated in prostate cancer compared to normal prostate cells. This was the first study that links elevated hyaluronidase levels to tumor progression [27]. In that study, the levels of hyaluronidase were found to be elevated 3-7 –fold in high-grade prostate cancer when compared to low-grade prostate cancer tissues. Hyaluronidases levels are also elevated in high-grade bladder tumor

tissue, and in urine of patients with high-grade bladder cancer. These studies have established a link between hyaluronidase levels and extent of tumor invasion and metastasis [28-30]. In addition to genitourinary tumors, hyaluronidase levels are elevated in head and neck squamous cell carcinoma, breast tumors, and glioma cells [2,31-35]. Patients with head and neck squamous cell carcinomas have elevated levels of hyaluronidase in their saliva. Taken together, hyaluronidase expression appears to be elevated in many carcinomas and the expression correlates with tumor invasiveness.

3. Application of hyaluronic acid and hyaluronidase

The viscoelasticity and high biocompatibility make hyaluronic acid suitable for various medical applications. It is used in surgical procedures to support regenerative processes of surgical wounds. It also promotes corneal, tendon, bone, nasal mucosal, and diabetic foot ulcer wound healing. It is also used in the treatment of osteoarthritis as it is found to suppress cartilage degeneration, protect the surface of cartilage and even reduce pain perception. Hyaluronic acid can also be used in drug delivery where it enhances the partitioning of drug like diclofenac and ibuprofen into human skin and also enhances its retention in the epidermis. The hydrogel based on cross-linked or otherwise chemically modified hyaluronic acid are used to design biomaterial for soft tissue engineering applications. The application of HA leads to diminished tissue destruction after subcutaneous and intramuscular injection of fluid [7,36,37]. The clinical applications of hyaluronidase are based on the spreading effect of the enzyme. It can be used to increase the speed of absorption, to promote resorption of excess fluid and increase the effect of local anesthesia, and to diminish tissue destruction after subcutaneous and intramuscular injection of fluids. There is widespread application of hyaluronidase in fields like

ophthalmology, internal medicine, oncology, orthopedic, dermatology and gynecology. Hyaluronidase was also investigated as an additive to chemotherapeutic drugs [11,38-42].

4. Detection of hyaluronidase

Since the discovery of hyaluronidase by Duran and Reynals, various methods for the detection of hyaluronidase activity have been developed. Due to its role in various pathological conditions like cancer, a sensitive method to its activity is of utmost importance. Various methods for the detection of hyaluronidase activity are based on spectrophotometric, radiochemical, fluorogenic, enzymoimmunological, chemical physiocochemical and zymographic analysis are known. Various early developed assay methods lack sensitivity and/or the procedure is very long and cumbersome. Details about various methods of detection reported in the literature are

4.1. Turbidimetric assay

Turbidimetric detection depends on the observation that hyaluronic acid of high molecular mass forms precipitate with diluted acidified serum, whereas depolymerized hyaluronic acid remain clear under the same condition [43]. The average molecular mass where turbidity is reported to disappear is 6-8 KDa [44]. Other turbidimetric methods are based on the formation of insoluble complexes between high molecular mass hyaluronic acid and quaternary ammonium salt. A method by Di Ferrante utilized the formation of insoluble complexes between cetyltrimethylammounim bromide (CTAB) and the residual high molecular weight complexes after incubation with enzyme to determine hyaluronidase activity by quantification of the resulting turbidity using photometric detection at 600 nm[45,46]. In the turbidimetric assay hyaluronidase activity is expressed in turbidity reduction units (TRU): 1 TRU is defined as the amount of enzyme which will reduce the turbidity produced by 0.2mg of HA to that produced by 0.1mg of HA within 30 min under specified conditions. In 1957 an “International Standard for

Hyaluronidase" was established: tablets were prepared from lyophilized bovine testicular hyaluronidase blended with lactose, and their activity was assayed turbidimetrically. On the basis of this examination the International Unit (IU) of hyaluronidase was defined as the activity of 0.1mg of the international standard preparation, which is almost equal to 1 TR [6].

4.2. Viscosity-based detection

Viscosity-based detection of hyaluronidase activity was introduced by Mayer et al. [12] and Madinaveitia et al.[47]. This method is based upon detection of the reduction in viscosity of solution of hyaluronic acid, induced by hyaluronidase. In this experiment, 1U hyaluronidase is defined as the amount of enzyme required to reduce the viscosity of hyaluronic acid to half the initial viscosity. However, half viscosity reduction time was found to be dependent on the initial viscosity of hyaluronic acid solution, which indeed depends on the molecular mass of the hyaluronic acid used.

4.3. Colorimetric assay- Morgan Elson assay

This method is based on the reaction of the N-acetyl-D-glucosamine at the reducing ends of hyaluronic acid and its fragments with Ehrlich's reagent (p-dimethylaminobenzaldehyde).The reaction forms a red color product that can be measured photometrically at 586 nm [48-50]. The structure of the red product dye was postulated by Muckenschnabel in 1998 using HPLC-MS [51].

4.4. Zymographic analysis

This method allows visualization of enzyme activity following electrophoretic fractionation, which has been used for quantitative analysis of hyaluronidase. Zymographic analysis was carried out on a variety of solid support like agar, acrylamide or cellulose acetate membrane [52]. Herd et al. described the electrophoresis on cellulose acetate membrane. After electrophoresis,

the membrane is overlaid with a second membrane saturated with hyaluronic acid and incubated at 37^{o}C for 30 minutes. After treating the overlay membrane with alcian blue, the hyaluronidase activity is seen as white band in a blue background [53]. Fiszer-szafarz incorporated hyaluronic acid into polyacrylamide gels before electrophoresis; and the hyaluronidase activity is indicated by pink bands in a blue background [54].

4.5. Indirect enzymoimmunological assays

In this method, hyaluronectin, a hyaluronic acid acid-binding proteoglycan is used as a probe for the detection of hyaluronidase activity. Microplates coated with hyaluronic acid and are left at 4^{o} C overnight prior to rinsing with diluted water. Hyaluronidase containing sample is added to the wells and incubated at 37^{o} C for up to 24 hours. After incubation, the wells are rinsed and incubated with hyaluronectin immune complex conjugated with alkaline phosphatase. The hyaluronidase activity is measured by a decrease in the absorbance measured at 405 nm [52,55].

4.6. Radiochemical assay

The principle of the radiochemical method was described by Coulson and Girkin in 1975. The principal behind this assay is that cetylpyridinium chloride precipitates the high molecular weight hyaluronic acid, but not the smaller polysaccharide obtained by the digestion of hyaluronidase. In this procedure, hyaluronic acid is partially deacetylated using hydrazine and then reacetylated in the presence of [^{3}H] acetic anhydride. The radioactivity of the undigested substrate, precipitated with cetylpyridinium chloride is compared with the radioactivity of the blanks to get the hyaluronidase activity [52,56].

An alternative approach was described by Hotez et al. in which after incubation of the ^{3}H acetic anhydride labeled hyaluronic acid with hyaluronidase, the degraded substrate is applied to a

polyacrylamide gel, fixed and prepared for autoradiography. The hyaluronidase activity is observed as a decrease in the size of labeled hyaluronic acid [52,57].

4.7. UV spectroscopy based

Benchetrit et al. developed a sensitive method for the detection of hyaluronidase based on the shift in maximal absorbance after interaction of anionic mucopolysaccharides with a carbocyanine dye. Hyaluronidase activity is studied by a decrease in the absorbance of hyaluronic acid-dye complex. This method is useful for the detection and quantification of purified hyaluronidase, but it is not reliable for detection of activity in crude preparations where other substances may interfere. A modification of this procedure was described by Homer et al., and Turner et al.[52,58-60].

4.8. Fluorescence based detection method

Various fluorescence based methods have been reported in the literature for the detection of hyaluronidase as they are really sensitive, easy to use and less time consuming. All the fluorescence based methods depend on labeling of hyaluronic acid either via covalent bond formation or interaction of oppositely charged species. Nakamura et al. in 1990 reported a simple and sensitive hyaluronidase assay using pyridylaminohyaluronate as a substrate. In this method the reducing terminal of hyaluronate was labeled with 2-aminopyridine. Then the substrate is incubated for one hour. Following incubation, four volumes of ethanol were added and centrifuged. Supernatant containing the degradation product of hyaluronidase digestion was used to measure hyaluronidase activity by measuring emission at 400nm following a 320 nm excitation [61]. Lingling et al. suggested a cationic charged water-soluble polyfluorenes containing 2,1,3,-benzothiadiazole (BT) units. In the presence of oppositely charged hyaluronan, energy transfer from fluorine units to BT was observed, followed by a shift in the emission color from

blue to green. In the presence of hyaluronidase, hyaluronan is cleaved into fragments and recovery in blue emission from polyfluorenes was observed [62]. Zhang et al. developed a novel fluorescent substrate by labeling hyaluronic acid with fluorescein amine and rhodamine forming a classic FRET pair. In the presence of hyaluronidase, cleavage of hyaluronan disrupts the FRET resulting in loss of fluorescein quenching. Recovery of fluorescein signal was used as the detection method [63]. Murai et al. reported a fluorescence polarization method for detection of hyaluronidase by labeling hyaluronic acid with Alexa Fluor 488 (AF-HA). The change in the fluorescence polarization after enzymatic reaction at 519 nm was used as the detection mechanism [64]. Fudala et al. reported a steady-state ratiometric sensing method of hyaluronidase detection by labeling hyaluronic acid with fluorescein and rhodamine (HA-FRET). The change in the fluorescence emission intensity ratio of fluorescein to rhodamine, before and after enzymatic cleavage by hyaluronidase was used as the sensing system [65]. Chib et al. in 2013 used the same probe for detecting hyaluronidase activity in synthetic urine via a change in the fluorescence lifetime of the donor molecule (fluorescein) before and after reaction with enzyme hyaluronidase [66]. Fudala et al. also reported another probe for the detection of hyaluronidase by heavy labeling of hyaluronic acid with fluorescein. Heavy labeled hyaluronic acid has a short fluorescence lifetime and a weak fluorescence emission. In the presence of hyaluronidase, hyaluronic acid was cleaved reducing energy migration between fluorescein molecules resulting in the increase fluorescence lifetime and emission signal [67]. Wang et al. reported two kinds of fluorescent hyaluronan analog, using NIR dye for hyaluronidase detection. One probe serves as an imaging agent and the other used as a biosensitive contrast agent [68]. Rich et al. detected hyaluronidase activity using fluorescence correlation spectroscopy (FCS) by using fluorescein labeled hyaluronic acid. In the presence of hyaluronidase, increased diffusion rate of hyaluronic

acid fragments was used to study hyaluronidase activity [69]. Song et al. suggests a gold nanoparticle functionalized with cresyl violet and porphyrin with hyaluronic acid for the detection of hyaluronidase activity and used it as a cell imaging agent and at the same time used for phototherapy [70]. Chang et al. reported a one-step facile synthesis of hyaluronic acid functionalized fluorescent gold nanoprobe to detect hyaluronidase in urine sample. FITC labeled hyaluronic acid (FITC-HA) was conjugated with gold nanoparticle to form FITC-HA-AuNP FRET nanoprobe for the detection of hyaluronidase [71]. Xie et al. reported a ratiometric sensing method based on both aggregation-induced emission and aggregation-induced quenching. Negatively charged hyaluronic acid was labeled with positively charged tetraphenylethylene (TPE-$2N^+$) and anthracene derivative (AN-N^+) forming aggregates of a compound resulting in formation of nanoparticles. The aggregation caused quenching of anthracene unit (ems: 474) whereas, it leads to fluorescence enhancement of tetraphenylethylene (ems: 474 nm). In the presence of hyaluronidase, the emission of AN-N^+ was restored and TPE-$2N^+$ was suppressed forming a ratiometric sensor for the detection of hyaluronidase [72].

Wang et al. reported an upconversion luminescence nanoprobe for the detection of hyaluronidase by coupling hyaluronic acid-bearing upconversion fluorescent nanoparticle (HA-UCNPs) with poly(m-phenylenediamine) (PMPD) nanosphere via covalent linkage. The nanoprobe alone exhibits an extremely low background signal owing to the effective fluorescence quenching by electron-rich PMPD and the near-infrared excitation characteristic (λ_{ex}=980 nm) of HA-UCNPs; upon reaction with hyaluronidase, however, a more than 31-fold fluorescence enhancement is produced. This nanoprobe was excited at 960 nm and the emission was observed at 545 nm in the presence of hyaluronidase [73]. Liu et al. shows the application of amino functionalized fluorescent carbon nanodots for the detection of hyaluronidase. Carbon nanodots were

conjugated with negatively charged hyaluronan stabilized gold nanoparticle leading to energy transfer. Hyaluronidase degrades hyaluronan and breaks the surface energy transfer [74]. Hu et al. reported a ratiometric fluorescent probe based on hyaluronan induced formation of red-light emitting excimers containing a positively charged pyrene analog (N-py). Excimers of N-py emits red light, however in the presence of hyaluronidase, hydrolysis of hyaluronic acids into small fragments leads to disassembly of excimers into monomers. The emission ration from excimer-monomer transition was used to sense hyaluronidase activity [75].

References

1. Meyer K, Palmer JW. The polysaccharide of the vitreous humor. *J Biol Chem*. 1934;107(3):629-634.

2. Stern R. *Hyaluronan in cancer biology.* Academic Press; 2009.

3. Stern R. Hyaluronan metabolism: A major paradox in cancer biology. *Pathologie Biologie*. 2005;53(7):372-382.

4. Stern R. Hyaluronan catabolism: A new metabolic pathway. *Eur J Cell Biol*. 2004;83(7):317-325.

5. Dietrich A, Tanczos E, Vanscheidt W, Schöpf E, Simon J. High CD44 surface expression on primary tumours of malignant melanoma correlates with increased metastatic risk and reduced survival. *Eur J Cancer*. 1997;33(6):926-930.

6. El-Safory NS, Fazary AE, Lee C. Hyaluronidases, a group of glycosidases: Current and future perspectives. *Carbohydr Polym*. 2010;81(2):165-181.

7. Fraser J, Laurent T, Laurent U. Hyaluronan: Its nature, distribution, functions and turnover. *J Intern Med*. 1997;242(1):27-33.

8. Girish K, Kemparaju K. The magic glue hyaluronan and its eraser hyaluronidase: A biological overview. *Life Sci*. 2007;80(21):1921-1943.

9. Josefsson A, Adamo H, Hammarsten P, et al. Prostate cancer increases hyaluronan in surrounding nonmalignant stroma, and this response is associated with tumor growth and an unfavorable outcome. *The American journal of pathology*. 2011;179(4):1961-1968.

10. Laurent TC, Fraser JR. Hyaluronan. *FASEB J*. 1992;6(7):2397-2404.

11. Menzel E, Farr C. Hyaluronidase and its substrate hyaluronan: Biochemistry, biological activities and therapeutic uses. *Cancer Lett*. 1998;131(1):3-11.

12. Meyer K. The biological significance of hyaluronic acid and hyaluronidase. *Physiol Rev*. 1947;27(3):335-359.

13. Necas J, Bartosikova L, Brauner P, Kolar J. Hyaluronic acid (hyaluronan): A review. *Vet Med*. 2008;53(8):397-411.

14. Simpson MA, Lokeshwar VB. Hyaluronan and hyaluronidase in genitourinary tumors. *Front Biosci*. 2008;13:5664-5680. doi: 3108 [pii].

15. Stern R, Asari AA, Sugahara KN. Hyaluronan fragments: An information-rich system. *Eur J Cell Biol*. 2006;85(8):699-715.

16. Toole BP. Hyaluronan promotes the malignant phenotype. *Glycobiology*. 2002;12(3):37R-42R.

17. Meyer K, Hobby GL, Chaffee E, Dawson MH. Relationship between "Spreading factor" and hyaluronidase. *Exp Biol Med*. 1940;44(1):294-296.

18. Kreil G. Hyaluronidases—a group of neglected enzymes. *Protein Science*. 1995;4(9):1666-1669.

19. Csóka TB, Frost GI, Wong T, Stern R. Purification and microsequencing of hyaluronidase isozymes from human urine. *FEBS Lett*. 1997;417(3):307-310.

20. Gould S, Bernstein M. The localisation of bovine sperm hyaluronidases. *Differentiation*. 1975;3(1-3):123-132.

21. Lokeshwar VB, Young MJ, Goudarzi G, et al. Identification of bladder tumor-derived hyaluronidase: Its similarity to HYAL1. *Cancer Res*. 1999;59(17):4464-4470.

22. Lokeshwar VB, Cerwinka WH, Lokeshwar BL. HYAL1 hyaluronidase: A molecular determinant of bladder tumor growth and invasion. *Cancer Res*. 2005;65(6):2243-2250. doi: 65/6/2243 [pii].

23. Simpson MA. Concurrent expression of hyaluronan biosynthetic and processing enzymes promotes growth and vascularization of prostate tumors in mice. *The American journal of pathology*. 2006;169(1):247-257.

24. Csoka AB, Frost GI, Stern R. The six hyaluronidase-like genes in the human and mouse genomes. *Matrix Biology*. 2001;20(8):499-508.

25. Stern R, Jedrzejas MJ. Hyaluronidases: Their genomics, structures, and mechanisms of action. *Chem Rev*. 2006;106(3):818-839.

26. Franzmann EJ, Schroeder GL, Goodwin WJ, Weed DT, Fisher P, Lokeshwar VB. Expression of tumor markers hyaluronic acid and hyaluronidase (HYAL1) in head and neck tumors. *International Journal of Cancer*. 2003;106(3):438-445.

27. Lokeshwar VB, Lokeshwar BL, Pham HT, Block NL. Association of elevated levels of hyaluronidase, a matrix-degrading enzyme, with prostate cancer progression. *Cancer Res*. 1996;56(3):651-657.

28. HAUTMANN SH, LOKESHWAR VB, SCHROEDER GL, et al. Elevated tissue expression of hyaluronic acid and hyaluronidase validates the HA-HAase urine test for bladder cancer. *J Urol*. 2001;165(6):2068-2074.

29. Pham HT, Block NL, Lokeshwar VB. Tumor-derived hyaluronidase: A diagnostic urine marker for high-grade bladder cancer. *Cancer Res*. 1997;57(4):778-783.

30. Schroeder GL, Lorenzo-Gomez M, Hautmann SH, et al. A side by side comparison of cytology and biomarkers for bladder cancer detection. *J Urol*. 2004;172(3):1123-1126.

31. Bertrand P, Girard N, Duval C, et al. Increased hyaluronidase levels in breast tumor metastases. *International journal of cancer*. 1997;73(3):327-331.

32. Madan A, Yu K, Dhurandhar N, Cullinane C, Pang Y, Beech D. Association of hyaluronidase and breast adenocarcinoma invasiveness. *Oncol Rep*. 1999;6(3):607-616.

33. Godin DA, Fitzpatrick PC, Scandurro AB, et al. PH-20: A novel tumor marker for laryngeal cancer. *Archives of Otolaryngology–Head & Neck Surgery*. 2000;126(3):402-404.

34. Delpech B, Laquerriere A, Maingonnat C, Bertrand P, Freger P. Hyaluronidase is more elevated in human brain metastases than in primary brain tumours. *Anticancer Res*. 2002;22(4):2423-2427.

35. Junker N, Latini S, Petersen LN, Kristjansen PE. Expression and regulation patterns of hyaluronidases in small cell lung cancer and glioma lines. *Oncol Rep*. 2003;10(3):609-616.

36. Lee JY, Spicer AP. Hyaluronan: A multifunctional, megaDalton, stealth molecule. *Curr Opin Cell Biol*. 2000;12(5):581-586.

37. Wieland JA, Houchin-Ray TL, Shea LD. Non-viral vector delivery from PEG-hyaluronic acid hydrogels. *J Controlled Release*. 2007;120(3):233-241.

38. Frost GI, Csóka T, Stern R, 山形貞子. The hyaluronidases: A chemical, biological and clinical overview.: A chemical, biological and clinical overview. *Trends in glycoscience and glycotechnology*. 1996;8(44):419-434.

39. Farr C, Menzel J, Seeberger J, Schweigle B. Clinical pharmacology and possible applications of hyaluronidase with reference to hylase "dessau". *Wien Med Wochenschr*. 1997;147(15):347-355.

40. Bertelli G, Dini D, Forno G, et al. Hyaluronidase as an antidote to extravasation ofVinca alkaloids: Clinical results. *J Cancer Res Clin Oncol*. 1994;120(8):505-506.

41. Few BJ. Hyaluronidase for treating intravenous extravasations. *MCN: The American Journal of Maternal/Child Nursing*. 1987;12(1):23.

42. Spickenreither M. *Inhibitors of bacterial and mammalian hyaluronidases: design, synthesis and structure-activity relationships with focus on human enzymes*. 2008.

43. Kass EH, Seastone CV. The role of the mucoid polysaccharide (hyaluronic acid) in the virulence of group a hemolytic streptococci. *J Exp Med*. 1944;79(3):319-330.

44. RAPPORT MM, MEYER K, LINKER A. Correlation of reductimetric and turbidimetric methods for hyaluronidase assay. *J Biol Chem*. 1950;186(2):615-623.

45. DI FERRANTE N. Turbidimetric measurement of acid mucopolysaccharides and hyaluronidase activity. *J Biol Chem*. 1956;220(1):303-306.

46. Scott J. The reaction of long-chain quaternary ammonium salts with acidic polysaccharides. *Chem Ind*. 1955(7):168-169.

47. Madinaveitia J, Quibell TH. Studies on diffusing factors: The action of testicular extracts on the viscosity of vitreous humour preparations. *Biochem J*. 1940;34(4):625-631.

48. Elson LA, Morgan WT. A colorimetric method for the determination of glucosamine and chondrosamine. *Biochem J*. 1933;27(6):1824-1828.

49. Vercruysse KP, Lauwers AR, Demeester JM. Kinetic investigation of the action of hyaluronidase on hyaluronan using the morgan-elson and neocuproine assays. *Biochem J*. 1995;310 (Pt 1)(Pt 1):55-59.

50. Takahashi T, Ikegami-Kawai M, Okuda R, Suzuki K. A fluorimetric Morgan–Elson assay method for hyaluronidase activity. *Anal Biochem*. 2003;322(2):257-263.

51. Muckenschnabel I, Bernhardt G, Spruss T, Dietl B, Buschauer A. Quantitation of hyaluronidases by the Morgan–Elson reaction: Comparison of the enzyme activities in the plasma of tumor patients and healthy volunteers. *Cancer Lett*. 1998;131(1):13-20.

52. Hynes WL, Ferretti JJ. [48] assays for hyaluronidase activity. *Meth Enzymol*. 1994;235:606-616.

53. Herd JK, Tschida J, Motycka L. The detection of hyaluronidase on electrophoresis membranes. *Anal Biochem*. 1974;61(1):133-143.

54. Fiszer-Szafarz B. Hyaluronidase polymorphism detected by polyacrylamide gel electrophoresis. application to hyaluronidases from bacteria, slime molds, bee and snake venoms, bovine testes, rat liver lysosomes, and human serum. *Anal Biochem*. 1984;143(1):76-81.

55. Delpech B, Bertrand P, Chauzy C. An indirect enzymoimmunological assay for hyaluronidase. *J Immunol Methods*. 1987;104(1-2):223-229.

56. Coulson C, Girkin R. A rapid assay method for hyaluronidase. *Anal Biochem*. 1975;65(1):427-434.

57. Hotez PJ, Narasimhan S, Haggerty J, et al. Hyaluronidase from infective ancylostoma hookworm larvae and its possible function as a virulence factor in tissue invasion and in cutaneous larva migrans. *Infect Immun*. 1992;60(3):1018-1023.

58. Benchetrit LC, Pahuja SL, Gray ED, Edstrom RD. A sensitive method for the assay of hyaluronidase activity. *Anal Biochem*. 1977;79(1):431-437.

59. Homer K, Denbow L, Beighton D. Spectrophotometric method for the assay of glycosaminoglycans and glycosaminoglycan-depolymerizing enzymes. *Anal Biochem*. 1993;214(2):435-441.

60. Turner RE, Cowman MK. Cationic dye binding by hyaluronate fragments: Dependence on hyaluronate chain length. *Arch Biochem Biophys*. 1985;237(1):253-260.

61. Nakamura T, Majima M, Kubo K, Takagaki K, Tamura S, Endo M. Hyaluronidase assay using fluorogenic hyaluronate as a substrate. *Anal Biochem*. 1990;191(1):21-24.

62. An L, Liu L, Wang S. Cationic conjugated polymers for homogeneous and sensitive fluorescence detection of hyaluronidase. *Science in China Series B: Chemistry*. 2009;52(6):827-832.

63. Zhang L, Mummert ME. Development of a fluorescent substrate to measure hyaluronidase activity. *Anal Biochem*. 2008;379(1):80-85.

64. Murai T, Kawashima H. A simple assay for hyaluronidase activity using fluorescence polarization. *Biochem Biophys Res Commun*. 2008;376(3):620-624.

65. Fudala R, Mummert ME, Gryczynski Z, Gryczynski I. Fluorescence detection of hyaluronidase. *Journal of Photochemistry and Photobiology B: Biology*. 2011;104(3):473-477.

66. Chib R, Raut S, Fudala R, et al. FRET based ratio-metric sensing of hyaluronidase in synthetic urine as a biomarker for bladder and prostate cancer. *Curr Pharm Biotechnol*. 2013;14(4):470-474. doi: CPB-EPUB-20130109-1 [pii].

67. Fudala R, Mummert ME, Gryczynski Z, Rich R, Borejdo J, Gryczynski I. Lifetime-based sensing of the hyaluronidase using fluorescein labeled hyaluronic acid. *Journal of Photochemistry and Photobiology B: Biology*. 2012;106:69-73.

68. Wang W, Cameron AG, Ke S. Developing fluorescent hyaluronan analogs for hyaluronan studies. *Molecules*. 2012;17(2):1520-1534.

69. Rich RM, Mummert M, Foldes-Papp Z, et al. Detection of hyaluronidase activity using fluorescein labeled hyaluronic acid and fluorescence correlation spectroscopy. *Journal of Photochemistry and Photobiology B: Biology*. 2012;116:7-12.

70. Song Y, Wang Z, Li L, Shi W, Li X, Ma H. Gold nanoparticles functionalized with cresyl violet and porphyrin via hyaluronic acid for targeted cell imaging and phototherapy. *Chemical Communications*. 2014;50(99):15696-15698.

71. Cheng D, Han W, Yang K, Song Y, Jiang M, Song E. One-step facile synthesis of hyaluronic acid functionalized fluorescent gold nanoprobes sensitive to hyaluronidase in urine specimen from bladder cancer patients. *Talanta*. 2014;130:408-414.

72. Xie H, Zeng F, Wu S. Ratiometric fluorescent biosensor for hyaluronidase with hyaluronan as both nanoparticle scaffold and substrate for enzymatic reaction. *Biomacromolecules*. 2014;15(9):3383-3389.

73. Wang Z, Li X, Song Y, Li L, Shi W, Ma H. An upconversion luminescence nanoprobe for the ultrasensitive detection of hyaluronidase. *Anal Chem*. 2015;87(11):5816-5823.

74. Liu S, Zhao N, Cheng Z, Liu H. Amino-functionalized green fluorescent carbon dots as surface energy transfer biosensors for hyaluronidase. *Nanoscale*. 2015;7(15):6836-6842.

75. Hu Q, Zeng F, Wu S. A ratiometric fluorescent probe for hyaluronidase detection via hyaluronan-induced formation of red-light emitting excimers. *Biosensors and Bioelectronics*. 2016;79:776-783.

Chapter 3

FRET based ratiometric sensing of hyaluronidase using a dual labeled probe

Abstract

Elevated hyaluronidase levels are found in the urine of patients suffering from bladder and prostate cancer. Hence, hyaluronidase can be considered as an important biomarker for the detection of these cancers. In this report, we have used a FRET based ratiometric sensing approach to detect the level of hyaluronidase in synthetic urine. To synthesize this probe, we have labeled hyaluronic acid with a FRET pair in which fluorescein is the donor and rhodamine is the acceptor (HA-FRET). We monitor the cleavage of this HA-FRET probe with different concentrations of hyaluronidase in synthetic urine via change in fluorescence emission and fluorescence lifetime of the donor molecules. The extent to which FRET is released depends on the concentration of hyaluronidase in the system.

1. Introduction

Bladder and prostate cancer are among the most frequently diagnosed types of cancers worldwide. In the US alone, a total of 75,510 new cases of bladder cancer and 241,740 new cases of prostate cancer are estimated in year 2012 [1]. Therefore, it is necessary to develop a simple, ergonomic and noninvasive diagnostic technique, which can detect cancer at an early stage, so that proper therapeutic measures can be taken. An increased hyaluronidase level in the urine of patients with bladder cancer has been identified as a promising biomarker for bladder cancer [2,3]. Studies by the Lokeshwar group have shown that there is usually a 2.5- 6.5 fold increase in hyaluronidase levels in patients with bladder cancer in comparison to healthy individuals. Hyaluronidase levels greater than 10mU/mg indicate a higher grade cancer [4].

Therefore estimating the level of hyaluronidase in urine can help in accurately predicting the progression of bladder and prostate cancer.

Hyaluronidase is an endoglycosidase that catalyzes hyaluronic acid (HA) depolymerization via cleavage of the β-N-acetyl- D-glucosaminidic bonds [5] and it belongs to class hydrolase (EC3.2.1.35) [6]. Hyaluronic acid is associated with many biological processes such as cell adhesion, migration, and proliferation[7]. Hyaluronidase degrades HA into proangiogenic fragments which help in cancer progression and metastasis. The human genome contains six hyaluronidase like genes and these occur in two linked triplicates. Hyal1, Hyal2, Hyal3 are present on chromosome 3p21.3, and another two genes (Hyal4 and PH- 20/SPAM1) and one pseudogene (HyalP1) are present on chromosome 7q31.3 5. HYAL-1 was initially purified from the urine of patients with high-grade bladder cancer. It is overexpressed by the epithelial cells of the bladder and prostate tumor and is known to promote tumor growth, invasion and angiogenesis [8,9].

In our previous study by Fudala et al., they have developed a fluorescence based probe for the detection of hyaluronidase activity. To develop this probe, they have labeled hyaluronic acid with fluorescein and rhodamine B, which is a classic FRET pair where, fluorescein is the green donor fluorophore and rhodamine B is the red acceptor fluorophore. The excitation energy is transferred from the fluorescein moiety to the rhodamine B moiety resulting in the quenching of fluorescein molecules. Hyaluronic acid is the substrate for the enzyme hyaluronidase and the cleavage of this probe by hyaluronidase results in the release of FRET. They have shown the application of hyaluronic acid labeled with fluorescein and rhodamine (HA-FRET) in the detection of hyaluronidase activity in PBS at pH 6. As it is know from the literature, that the higher levels of hyaluronidase are present in the urine of patients suffering from bladder cancer,

we wanted to simulate a similar environment by using synthetic urine and adding different concentrations of hyaluronidase to it. We wanted to test if the same probe (HA-FRET) developed by Fudala et al. can be used reproducibly for the detection of hyaluronidase in synthetic urine containing different salts and hydrogen ion concentration (pH) as fluorescence is sensitive to the salt concentrations and the pH values. In this experiment we have used synthetic urine (pH 7.83) containing different salts of monovalent and divalent ions which mimic the salt concentrations present in human urine.

Fluorescence emission intensity measurements at a single wavelength are based on probe concentration and could lead to experimental variation due to differences in probe preparations. Collection of emission intensity at one wavelength can be tempered due to various reasons like fluctuation in the excitation intensity, emission collection efficiency, change in focal point, etc. This problem can be resolved using ratiometric sensing in which spectrum for each sample was recorded and release of FRET was compared in terms of ratio of fluorescein to rhodamine emission intensity. This is more sensitive than measuring only either donor or acceptor as it reduces undesirable experimental errors [10,11].

In our experiment, we have added HA-FRET probe into synthetic urine (pH 7.83) to prepare 2μM solution. To this solution, different concentrations of hyaluronidase was added. The change in fluorescence intensity ratio of fluorescein to rhodamine was measured for different amount of hyaluronidase as with the cleavage of HA-FRET probe by hyaluronidase, the ratio of fluorescein to rhodamine will change due to release of FRET. We also checked if this change in fluorescence intensity ratio is also accompanied by the change in the fluorescence lifetime of the donor molecule (fluorescein) as the fluorescence lifetime of the donor is also quenched in the presence of acceptor molecules in the close proximity.

2. Materials and methods

Sodium hyaluronate from bacterial fermentation was obtained from Acros Organics (Thermo Fisher Scientific, NJ, USA). Fluorescein amine, dimethyl sulfoxide (DMSO), guanidine hydrochloride, acetaldehyde, cyclohexyl isocyanide, Sephadex G-75, and bovine testes hyaluronidase (EC 3.2.1.35, type 1-S, 451 U/mg) were obtained from Sigma–Aldrich. Dulbecco's phosphate-buffered saline (PBS) was purchased from Invitrogen Life Technologies (Invitrogen Corporation, CA, and USA). Synthetic urine (pH 7.83) is obtained from Ricca chemical company (catalog number 8361-1), Slide-A-Lyser dialysis cassette (10,000 molecular weight cutoff) was purchased from Pierce Chemical (Thermo Fisher Scientific).

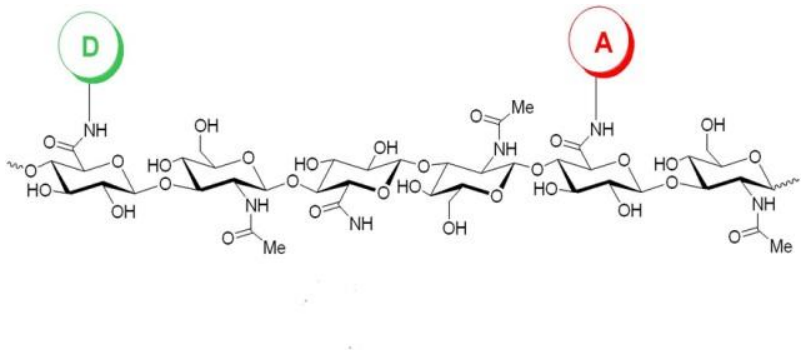

Scheme 1: HA-FRET molecule labeled with fluorescein as donor and rhodamine as acceptor.

2.1.Preparation of HA-FRET

The HA-FRET probe was prepared by the method mentioned in our previous paper [11]. In short, HA was covalently conjugated to fluorescein amine and rhodamine B using a condensation reaction. HA was dissolved to 1.25 mg/ml in dH2O. The HA solution was diluted 1:2 in DMSO, and fluorescein amine and rhodamine B amine (predissolved as a DMSO stock solution) was added to a final concentration of 5 mg/ml. Acetaldehyde and cyclohexyl isocyanide were added to 0.04% (v/v), and the reaction was allowed to proceed for 16 hr at 25ºC. Afterward, the solution was diluted 1:14 in ethanol/guanidine HCl (50 µL of 3 M guanidine HCl per 900 µL of 100% ethanol) and HA was allowed to precipitate overnight at -20ºC. The precipitate was then dissolved in 1ml of dH2O, followed by extensive dialysis against dH2O.

2.2.Fluorescence Measurement of Hyaluronan Hydrolysis

The HA–FRET probe was added to synthetic urine and incubated with different concentrations of hyaluronidase in synthetic urine at room temperature. The concentration of HA-FRET in final experiment setup was 2µM. The fluorescence emission spectra were collected using Cary Eclipse spectrofluorometer (Varian Inc., Australia) every 10 min for 90 minutes. Measurements were performed in 0.4X0.4 cm quartz cuvette using a 470 nm excitation source and emission was scanned from 500 nm to 700 nm using a 495 nm long pass filter on the emission side. Each spectrum is a convolution of the emission of donor and acceptor emission.

2.3.Deconvolution of HA-FRET Spectra

The respective emission due to the donor and acceptor alone was deconvoluted to obtain individual spectrum of donor and acceptor. All spectra were deconvoluted using the MATHCAD software. This program was designed to resolve a spectrum consisting of up to three constituent fluorophores which are assumed to combine linearly based on experimental fluorophores

reference spectra and the utilization of an algorithm for least squares minimization to produce corresponding unmixed spectra in graph form with error provided in minimal least squares values for flexibility in analysis. This will provide us the corrected intensity of fluorescein and rhodamine in our sample. For the deconvolution, reference spectra of fluorescein, rhodamine and synthetic urine were collected. The reference spectrum of fluorescein was obtained from hyaluronan labeled with fluorescein only (HA-FL) excited at 470 nm. The emission from rhodamine alone was measured by exciting our HA-FRET probe at 520 nm which will only excite the acceptor molecule.

2.4.Lifetime Measurement of HA-FRET Probe

Fluorescence lifetime measurements were done using a FluoTime 200 fluorometer (PicoQuant, GmbH, Berlin, Germany). This time–resolved instrument is equipped with an ultrafast detector, a Hamamatsu R3809U-50 microchannel plate photomultiplier (MCP). A 470 nm picosecond pulsed laser diode was used as the excitation source and the intensity decay was collected under magic angle conditions using and using a 495 nm long pass filter on the emission side to eliminate scattered excitation light. The intensity decay was analyzed with FluoFit, version 5.0 software (PicoQuant, GmbH) using exponential reconvolution procedure using nonlinear regression (multiexponential deconvolution model). In case of multiexponential analysis, the fluorescence decay was analyzed using

$I(t)= \sum \alpha_i \exp(-t/\tau_i)$

where, I(t) is the fluorescence intensity at time t and α_i is the preexponential factor representing the fractional contribution to the time-resolved decay of the component with the lifetime τ_i ($\sum \alpha_i = 1$). The amplitude average lifetime was calculated as $(\tau) = \sum_i \alpha_i \tau_i$.

3. Results and discussion

Scheme 1 shows the schematic representation of HA-FRET. The HA-FRET was obtained by labeling hyaluronic acid with fluorescein and rhodamine. In Figure 1, the emission profile of HA-FRET incubated with 35 U/ml of hyaluronidase is shown. It can be observed from figure 1, that the HA-FRET probe shows emission profile of rhodamine also when the probe is excited using a 470 nm excitation wavelength, where rhodamine cannot be excited. This proves the presence of efficient FRET in our system. Due to the presence of efficient FRET in our system, the emission intensity and the fluorescence lifetime of the donor (fluorescein) is quenched.

In our experiment, we measured the fluorescence emission spectra of the HA - FRET probe in the absence and presence (10, 35, and 100 U/ml) of hyaluronidase every 10 minutes for 90 minutes. As it can be seen from figure 1, after 90 minutes of enzymatic activity, we observed a huge increase in the fluorescence intensity at 520 nm (peak emission of fluorescein). It can also be seen from figure 1, that the measured spectra are convolution of fluorescein and rhodamine emission. Therefore, the emission spectra for all the concentrations of enzyme were deconvoluted. Figure 2A shows the normalized emission spectrum of fluorescein and rhodamine alone. We also checked the emission intensity of synthetic urine sample using a 470 nm excitation light. Figure 2 B shows that the emission intensity of synthetic urine is almost negligible compared to the fluorescence intensity of the HA - FRET probe under similar conditions. Figure 2c shows the resolved emission spectrum of HA-FRET using MATHCAD software, where the measured spectrum is shown in black color, corrected emission intensity of donor in green, and corrected intensity of acceptor in red. It had been our observation that the measured intensity of acceptor is higher compared to its corrected intensity. Hence, the emission spectrum of HA-FRET has to be deconvoluted to obtain correct emission intensities. After

resolving each spectrum for all enzyme concentrations, their intensity ratio at 520 nm to 590 nm was calculated. From the figure 3, it can be seen that in the absence of hyaluronidase, there is no change in the intensity ratio of HA-FRET probe. This shows that the synthesized HA-FRET probe is quite stable and didn't show any fluctuations at room temperature.

The time-dependent fluorescence intensity measurements show that the emission intensity ratio increases with increasing enzyme concentration and time. It can also be seen from the figure 3 that the emission intensity ratio almost reaches a plateau after 60 minutes of reaction. Hence, we took 60 minutes as the end point for our experiment. Using the intensity ratios at 60 minutes for all enzyme concentrations, calibration curve was made. Figure 4 shows the intensity ratio as a function of enzyme concentration. The curve was fitted using an exponential model. This calibration curve can be used to determine hyaluronidase concentration in an unknown sample.

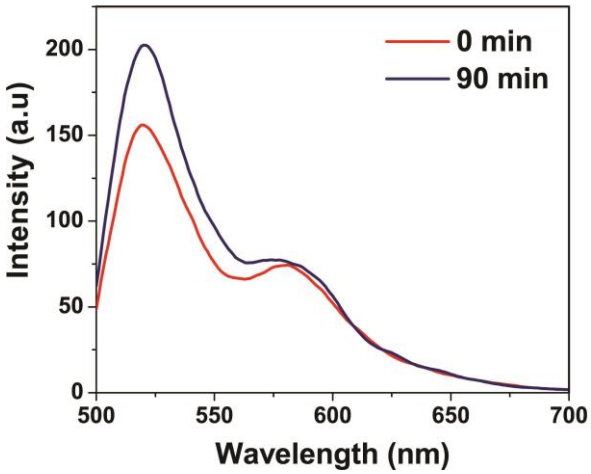

Figure 1: Difference in the emission intensity of HA-FRET probe incubated with 35 U/mL of hyaluronidase for 90 min. A 470 nm excitation light was used and experiment was carried out at room temperature in synthetic urine (pH 7.83).

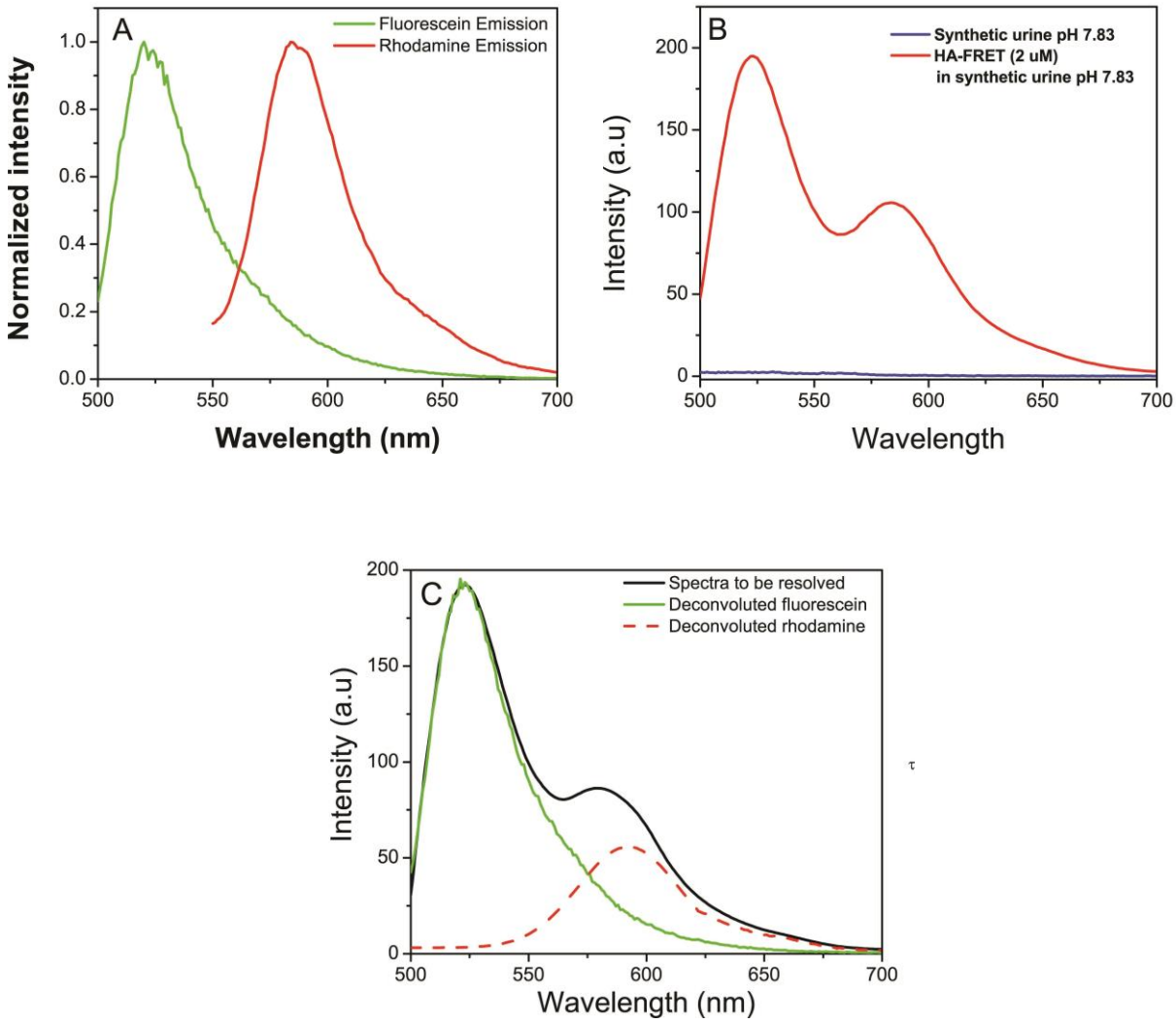

Figure 2. (**A**) normalized emission spectrum of fluorescein (from HA-FRET labeled with fluorescein only. Exc 470 nm) and rhodamine (from HA-FRET by exciting at longer wavelength. Exc 520 nm) in synthetic urine pH 7.83 at RT (**B**) Emission spectra from 2 μM HA-FRET and background signal from synthetic urine. (**C**) Shows example of how the HA-FRET spectrum was resolved into its components using MATHCAD based program written in our laboratory.

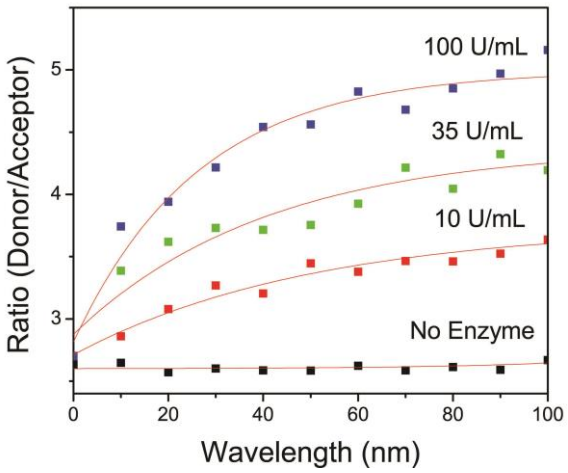

Figure 3: Time dependant fluorescence intensity ratio (green/red emission) of HA-FRET probe in the presence and absence of HAase and exponential fits (red lines) to data. Concentration of HAFRET sample was 2 uM in each case. The excitation was 470 nm and experiment was done at RT in synthetic urine pH 7.83.

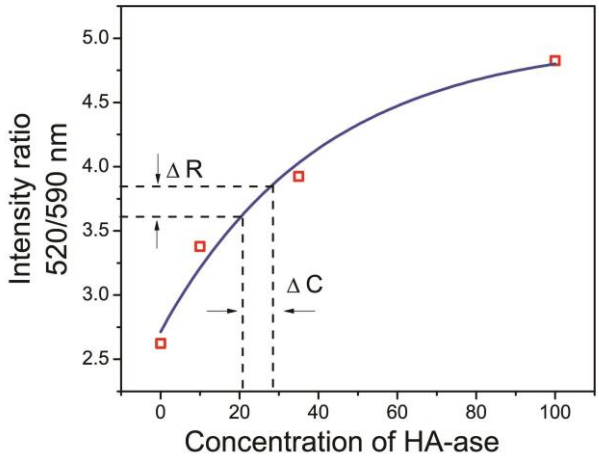

Figure 4: Intensity ratio (green/red emission) of HA-FRET as function of hyaluronidase concentration at 60 min and exponential fit (blue line. If $\Delta R = 3.72 \pm 0.12$ then $\Delta C = 24.5 \pm 3.5$.

We also checked, if the observed emission intensity changes are also accompanied by the change in the fluorescence lifetime of the donor molecule (fluorescein), as it should be quenched in an intact HA-FRET molecule due to the presence of acceptor in a close proximity. Figure 5 shows the fluorescence intensity decay of the HA - FRET probe in the absence and presence (35 U/ml) of hyaluronidase. It can be seen from figure 5, that the fluorescence lifetime of the fluorescein quenched in intact HA-FRET probe and shows an amplitude weighted fluorescence lifetime of 1.89 ns. However, in the presence of hyaluronidase, when the probe is cleaved, an increase in fluorescence lifetime was observed. After 90 minutes of enzyme activity with 35 U/ml of enzyme, a fluorescence lifetime of 3.24 ns was observed. This change in fluorescence lifetime, before and after enzymatic cleavage shows that fluorescein molecule was indeed quenched in the HA-FRET probe. The fluorescence intensity decay of the HA - FRET probe in the presence of different concentrations (10, 35 and 100 U/ml) of hyaluronidase was also measured and the measured fluorescence lifetime after 90 minutes of enzyme activity is given in Table 1.

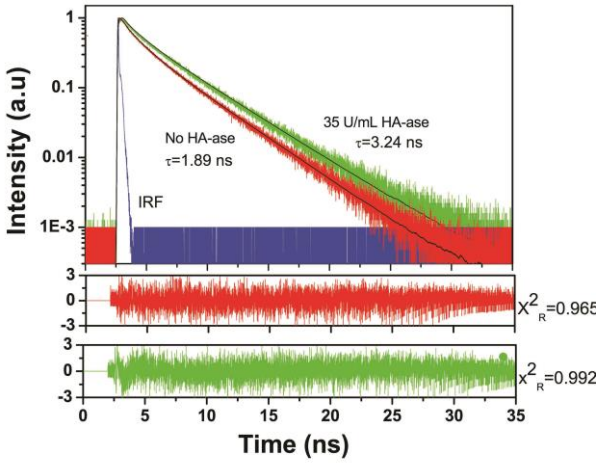

Figure 5: Fluorescence intensity decays of 2 uM HA-FRET (donor) in synthetic urine incubated with 35U/mL of HA-ase enzyme for 90 minutes. Excitation used was 470 nm laser. Donor

emission was observed at 520 nm using a 495 long pass filter before detector. Decays were fitted using multi-exponential function and chi square values were used to access the goodness of fit.

Table 1: Time resolved fluorescence intensity decay parameters for the donor in HA- FRET with different concentration of hyaluronidase at room temperature.

	No Enzyme	**10 U/ml**	**35U/ml**	**100U/ml**
τ1 (ns)	3.65	4.04	4.14	4.19
τ2(ns)	1.35	0.79	0.62	0.49
τ3(ns)	0.21	-	-	-
α1	0.74	0.92	0.95	0.96
α2	0.22	0.08	0.05	0.03
α3	0.035	-	-	-
$<\tau>$ i)	1.89	3.01	3.24	3.48
$\bar{\tau}$ ii)	3.02	3.77	3.97	4.1
X^2_R iii)	0.965	0.966	0.992	0.938

τ 1, τ 2 and τ 3 are different lifetime and α1, α2 and α3 are components of fluorescence lifetime in nanoseconds.

i) $< \tau >= \sum_i \alpha_i \tau_i$

ii) $\bar{\tau} = \sum_i f_i \tau_i$, Where, $f_i = \frac{\alpha_i \tau_i}{\sum_i \alpha_i \tau_i}$

iii) χ^2_R = goodness of fit.

4. **Conclusions**

By using HA-FRET probe, it is possible to check hyaluronidase activity by fluorescence intensity changes and fluorescence lifetime changes. In summary, we have successfully developed a hyaluronidase sensor by labeling hyaluronic acid with a FRET pair. This probe serves as an intensity-based ratiometric sensor and fluorescence lifetime based sensor of hyaluronidase. Intact HA-FRET showed a quenched fluorescence emission and fluorescence lifetime of the donor molecule (fluorescein). Cleavage of HA-FRET probe by hyaluronidase results in increase emission intensity and fluorescence lifetime of the donor molecule. In future, this probe can also be used to check hyaluronidase activity in urine samples of patients suffering from bladder cancer.

References

1. Siege R, Naishadham D, Jemal A. Cancer statistics, 2012. *cancer journal for clinician*. 2012;62:10.

2. Lokeshwar VB, Lokeshwar BL, Pham HT, Block NL. Association of elevated levels of hyaluronidase, a matrix-degrading enzyme, with prostate cancer progression. *Cancer Res*. 1996;56(3):651-657.

3. Konety BR, Getzenberg RH. Urine based markers of urological malignancy. *J Urol*. 2001;165(2):600-611. doi: 10.1097/00005392-200102000-00081.

4. Lokeshwar VB, Block NL. HA-HAase urine test. A sensitive and specific method for detecting bladder cancer and evaluating its grade. *Urol Clin North Am*. 2000;27(1):53-61.

5. Csoka AB, Frost GI, Stern R. The six hyaluronidase-like genes in the human and mouse genomes. *Matrix Biol*. 2001;20(8):499-508.

6. Stern R, Jedrzejas MJ. Hyaluronidases: Their genomics, structures, and mechanisms of action. *Chem Rev*. 2006;106(3):818-839. doi: 10.1021/cr050247k.

7. Lee JY, Spicer AP. Hyaluronan: A multifunctional, megaDalton, stealth molecule. *Curr Opin Cell Biol*. 2000;12(5):581-586.

8. Benitez A, Yates TJ, Lopez LE, Cerwinka WH, Bakkar A, Lokeshwar VB. Targeting hyaluronidase for cancer therapy: Antitumor activity of sulfated hyaluronic acid in prostate cancer cells. *Cancer Res*. 2011;71(12):4085-4095. doi: 10.1158/0008-5472.CAN-10-4610 [doi].

9. Lin G, Stern R. Plasma hyaluronidase (hyal-1) promotes tumor cell cycling. *Cancer Lett*. 2001;163(1):95-101.

10. Ma C, Zeng F, Wu G, Wu S. A nanoparticle-supported fluorescence resonance energy transfer system formed via layer-by-layer approach as a ratiometric sensor for mercury ions in water. *Anal Chim Acta*. 2012;734:69-78.

11. Fudala R, Mummert ME, Gryczynski Z, Gryczynski I. Fluorescence detection of hyaluronidase. *J Photochem Photobiol B*. 2011;104(3):473-477. doi: 10.1016/j.jphotobiol.2011.06.003.

Chapter 4

Azadioxatriangulenium (ADOTA) fluorophore in PVA and silica thin films

Abstract

A cationic azadioxatriangulenium dye was entrapped in silica thin films obtained by the sol-gel process and in poly (vinyl) alcohol (PVA) thin films. Azadioxatriangulenium is a red emitting fluorophore with a long fluorescence lifetime of ~20 ns. The fluorescent properties of azadioxatriangulenium in silica thin films and PVA films were studied by means of steady-state and time resolved fluorescence techniques. We have found that the azadioxatriangulenium entrapped in silica thin film has a wider fluorescence lifetime distribution (Lorentzian distribution), lower fluorescence efficiencies, shorter lifetimes compared to Azadioxatriangulenium in a PVA film. The local environment of azadioxatriangulenium molecules in the silica thin film is rich with water and ethanol, which creates the possibility of forming excited state aggregates due to high concentration of dye within a small confined area. In contrast to the PVA matrices, the porous silica films allow restricted rotations of Azadioxatriangulenium molecules, which result in faster and complex fluorescence anisotropy decays suggesting energy migration among dye molecules.

1. Introduction

Over the past decade, the synthesis and characterization of hybrid materials based on silica, in which organic dyes were entrapped has attained considerable attention [1,2]. The use of semiconductor materials for entrapment of the organic fluorophores has been and will remain a very important way to obtain new materials for different applications, including, functional

materials in optoelectronic devices, optical sensors [3], optical components like solid state tunable lasers [4] and highly luminescent materials in medicine [5,6].

The initial investigation of entrapping optically active organic molecules with the sol-gel process was performed by Avnir et al. [7] in which they studied the fluorescence properties of rhodamine 6G in different stages of sol-gel development. Since then, various photoactive dyes have been incorporated and studied in the matrices obtained by the sol-gel process [8-10]. Moreover, new hybrid materials provide a great subject of extensive research in materials chemistry [11-13]. To obtain new hybrid materials, an efficient sol-gel process is used which combines the remarkable properties of inorganic and organic materials in a controlled way [14-18]. In particular, because of the good mixing of the starting compounds, it creates the possibility to obtain a homogenous hybrid material at relatively low temperatures [19]. During the Sol-gel process, the host molecules are already present in the precursor solution and the conditions of the reactions are mild, therefore the optical properties of the fluorophore remain intact [20,21]. Also the entrapment of organic fluorophores in a gel matrix provides better protection of the molecule and higher stability than the free molecules in liquid media [22]. At the same time, silicon dioxide (SiO2) is well-known as a material with good optical quality, thermal stability, mechanical strength and photochemical stability. Another property of silica, which makes it a good candidate as a host matrix for incorporation of organic fluorophores is the ability to modify the surface by amines, thiols and other coupling agents [23,24]. On the other hand, organic dyes incorporated into silica matrix, sometimes afford more interesting luminescence properties due to strong host-guest interactions. Therefore, preparation of new hybrid materials based on silica in which organic fluorophores are entrapped is suitable for the design of highly luminescent materials.

In the present study, we have introduced an azadioxatriangulenium dye into a silica thin film obtained by the sol-gel process and into a PVA film [25-28]; specifically the acid derivative N-(u-butanoic acid)-azatriangulenium tetrafluoroborate (ADOTA); the molecular structure can be seen in Scheme 1. ADOTA belongs to the class of azaoxa-triangulenium fluorophores which are planar and rigid in structure. Furthermore, ADOTA in water emits in the red region around 560 nm with a fluorescence lifetime of ~20 ns, which makes it the longest orange/red emitting organic fluorophore [29,30].

The spectroscopic properties of the material presented are discussed in this paper. In particular, we compared the absorption, fluorescence emission, steady state anisotropy, time resolved anisotropy and fluorescence lifetime of ADOTA in thin layers of silica and in a PVA film. The use of PVA provides a more rigid environment compared to silica matrix and hence the photophysical properties of the ADOTA can be studied in two different semi-solid matrices. In addition, the photophysical characterization of ADOTA in a heterogeneous environment can be efficiently studied over time by using time resolved fluorescence spectroscopy.

2. Material and Methods

All the starting materials for the preparation of silica thin films were of analytical grade. Tetramethoxysilane Si(OCH3)4 (TMOS) was purchased from Aldrich Co., methanol as a diluent and ammonia were purchased from POCH Company (Poland). Deionized (DI) water was obtained from a Hydrolab system. Polyvinyl alcohol (130, 000 MW) was purchased from Sigma Aldrich (Sigma Aldrich, St Louis, MO USA). N-(u-butanoic acid)-azatriangulenium tetrafluoroborate (ADOTA) was prepared as previously described [27,31].

2.1.Sample preparation and AFM measurements

ADOTA/silica thin films were obtained by the sol-gel spin coating method, summarized in Scheme 1. Firstly, tetramethoxysilane (TMOS) and methanol were mixed by vigorous stirring for 15 min. After several minutes (which is very important to reach homogeneity of the solution), ADOTA was dissolved in methanol and added to the precursor solution. In order to initiate the sol-gel process, an appropriate volume ofwaterwas added. The final molar ratio TMOS/water/methanol was 1:4:12, while the concentration of ADOTA in sol was 2X 10^{-3} M (a low concentration sample with an overall ADOTA concentration of $<10^{-6}$ M was also prepared). The films were distributed over a clean piece of a microscopic slide using the spin-coating technique after 15 min after mixing all of the components. Microscopic glasses were cleaned in a mixture of 33% H_2O_2 and H_2SO_4 in molar ratio 2:1 over 24 h and rinsed with deionized water.

The spin coating was done at 150 rpm for 60 s to disperse the sol. After that, the thin films were allowed to dry in air for 24 h. Moreover, to prepare ADOTA in PVA films, the ADOTA was mixed in PVA solution and spread onto a thin glass slide to evenly coat the slide using spin coating. Atomic Force Microscopy (AFM) micrographs were produced by using scanning atomic force microscopy on the NTEGRA Prima scanning probe microscope manufactured by NT-MDT (Moscow, Russia). Closed-loop feedback semi-contact mode has been used at rate 0.5 Hz. Scanning was controlled and images were analyzed with NOVA software by NT-MDT instrument manufacturer.

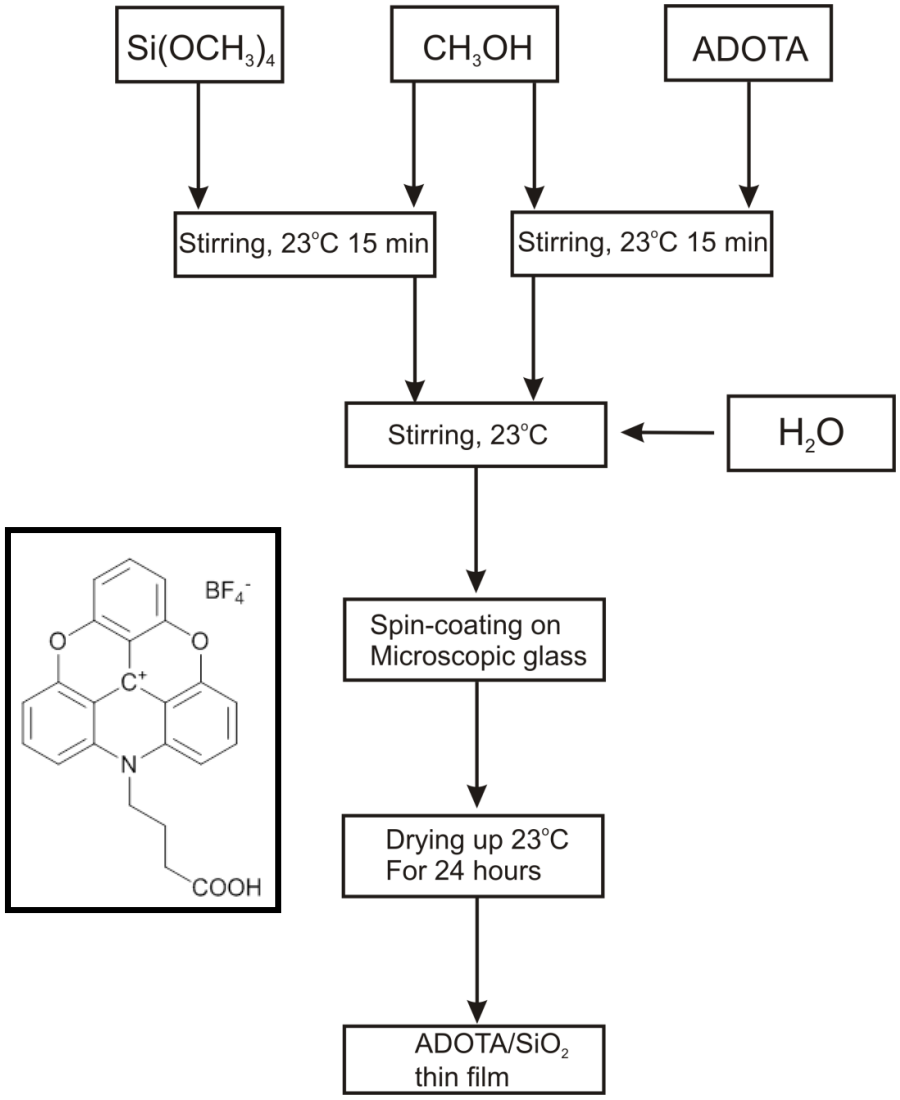

Scheme1. Flow chart of preparation of ADOTA doped silica thin films. Insert: molecular structure of N-(u-butanoic acid)-azatriangulenium tetrafluoroborate (ADOTA).

2.2.Absorption measurements

Absorption spectra were measured using a Cary 50 Bio UV-visible spectrophotometer (Varian Inc., Australia). Absorption spectra were scanned from 400 nm to 600 nm using bare glass slide as a baseline. Absorption spectra of silica thin films were corrected for the scattering by subtracting the scattering profile of silica thin films prepared without addition of the dye.

2.3.Steady-state fluorescence measurements

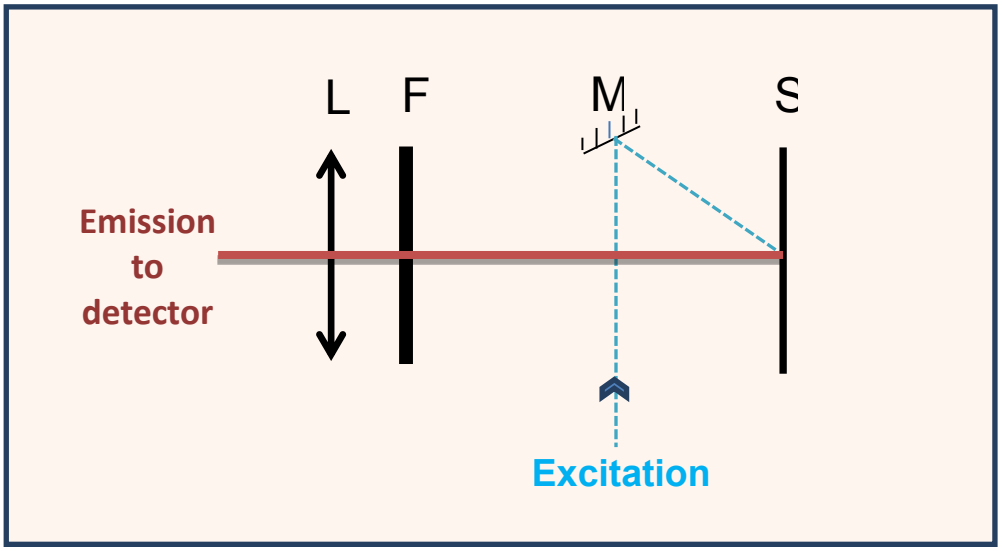

Scheme 2: Schematic of the front face arrangement used for steady state and time resolved fluorescence measurements. In this scheme, S represents the sample used for measurement, M is the mirror, F is long pass filter before detector, L is lens.

Steady-state fluorescence intensity measurements of all the samples were made using a Carry Eclipse spectrofluorometer (Varian Inc., Australia) by using the front face geometry as shown in Scheme 2. In Scheme 2, S represents the sample used for measurements, M is the mirror, F is a long pass filter before detector and L is the lens. The emission was scanned from 520 nm to 700 nm following a 470 nm excitation and using 495 nm long pass filter on the emission side. Steady-state excitation spectra were measured by observing the emission at 600 nm and

excitation was scanned from 400 nm to 560 nm using a 570 nm long pass filter on the emission side. Steady-state fluorescence anisotropy of all the samples were measured using a Carry Eclipse spectrofluorometer (Varian Inc., Australia), with manual polarizers on both the excitation and emission side. Emission anisotropy was measured following 470 nm excitation with a 495 nm long pass filter along the emission side and manually operated parallel and perpendicular polarizers. Anisotropy was calculated using the following formula:

$$r = \frac{I_{VV} - I_{VH}G}{I_{VV} + 2I_{VH}G}$$

where, IVV is the fluorescence intensity measured with the parallel polarizer orientation on the observation path, IVH is the fluorescence intensity at the perpendicular orientation of the polarizer on the emission side and G is the instrumental correction factor calculated by measuring the intensity in HV and HH polarizer orientation.

2.4.Fluorescence intensity decay

Fluorescence lifetimes of all the samples were measured using FluoTime 200 (PicoQuant, GmbH, Berlin, Germany) time resolved spectrofluorometer. This instrument contains a multichannel plate detector (Hamamatsu, Japan) and a 470 nm laser diode was used as the excitation source. The front face geometry as shown in Scheme 2 was used for these measurements as well. The fluorescence intensity decays were measured under magic angle conditions and data was analyzed with FluoFit version 4.5.3 software (PicoQuant GmbH, Berlin, Germany) using both the exponential reconvolution procedure using non-linear regression (multiexponential deconvolution model) and by the lifetime distribution model (Lorentzian model) [32]. In the case of multiexponential analysis, the fluorescence decay was analyzed using:

$$I(t) = \int_{-\infty}^{t} IRF(t') \sum_{i} \alpha_i e^{\frac{-t-t'}{\tau_i}}$$

where IRF (t') is the instrument response function at time t', α is the amplitude of the decay of the ith component at time t and τ_i is the lifetime of the ith component. In case of Lorentzian lifetime distribution, all the data were analyzed using the following equation

$$I(t) = \int_{-\infty}^{\infty} \rho(\tau) e^{-\frac{t}{\tau}} d_\tau$$

Where, $$\rho(\tau) = \sum_{i=1}^{n} \frac{A_i}{\pi} \frac{\frac{\Delta_{FWHM\,i}}{2}}{(\tau-\tau_i)^2+(\Delta_{FWHM\,i}/2)^2}$$

Where A_i is the amplitude of the i^{th} component, τ_i is the central lifetime value of the i^{th} distribution. The use of the continuous distribution ρ(τ) minimizes the number of floating parameters in the fitting algorithms.

2.5.Time resolved anisotropy measurements

Excitation used for time resolved anisotropy measurement was 470 nm while emission was observed at 560 nm and 620 nm with vertical and horizontal polarizer position on the emission side using appropriate filters on both excitation and emission side. Anisotropy decays were analyzed with the exponential fitting model in the FluoFit 4.5.3 program from Pico-Quant, Inc. (Germany) using the following equation:

$$r(t) = r_{INF} + \sum_{i=1}^{n} r_i\, e^{-\frac{t}{\Phi_i}}$$

Where, r_i is the anisotropy of the i^{th} component at time t and Φ_i is the rotational correlation time of the i^{th} component. The quality of the fit in lifetime and anisotropy decay analysis was judged by the quality of the residuals and χ^2 square value.

3. Results and discussion

3.1.AFM micrographs of silica thin films

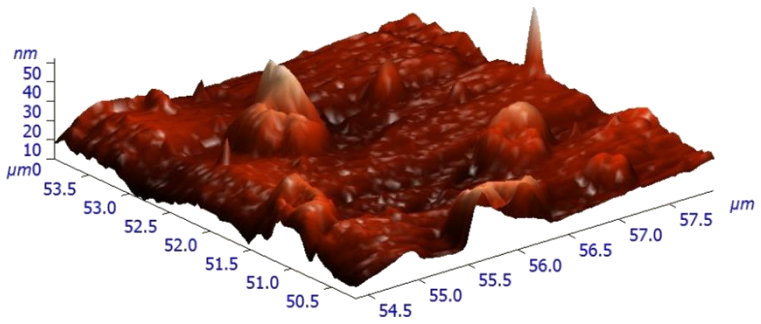

Figure 1: AFM showing the surface topography of the silica thin layer prepared by the sol gel process.

The surface topography of the silica thin film with N-(u-butanoic acid)-azatriangulenium tetrafluoroborate (ADOTA) was studied using the AFM technique as shown in Fig. 1. From this micrograph, we can observe that the surface of the porous silica is rough, with maximum particle size close to 50 nm. The ADOTA doped PVA films did not show any significant roughness. In order to check how dye is distributed in the prepared silica or PVA layers, confocal fluorescence images were taken and found that ADOTA dye is evenly distributed in all film on the scale of the optical resolution, about 400 nm (see Supplementary information, Fig. S2).

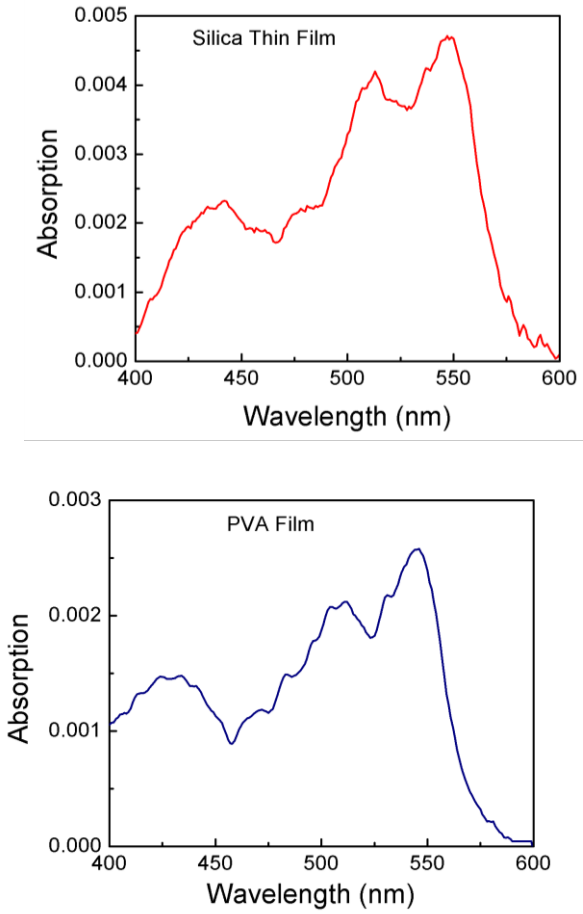

Figure 2: Top panel: absorption spectrum of N-(u-butanoic acid)-azatriangulenium tetrafluoroborate (ADOTA). in silica thin film. Bottom panel: absorption spectrum of ADOTA in PVA film.

3.2.Absorption spectra

Fig. 2 shows the absorption spectrum of ADOTA in silica thin films and in PVA films dried on a cover-glass. It can be seen from both the figures that the absorption spectra appears somewhat noisy. This is due to the small thickness/path-length (100e150 nm) and small absorptions recovered after correcting for the scattering arising in these samples. The absorption spectrum shape and peak absorption wavelengths did not change in the silica gel environment compared to the PVA film suggesting no significant perturbation in the immobilized ground state fluorophores population.

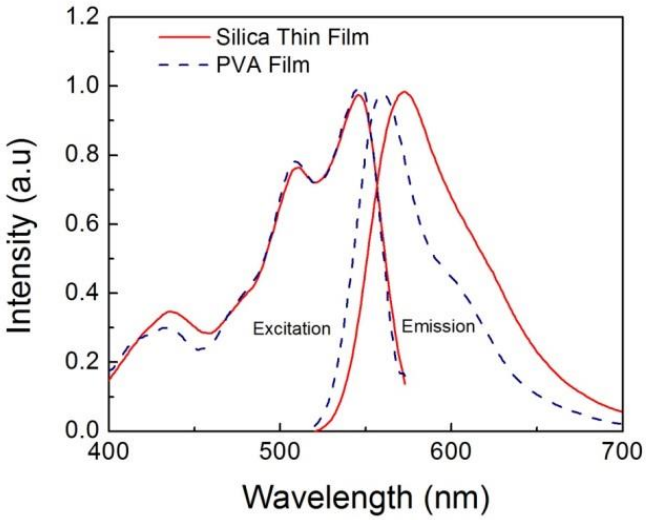

Figure 3: Normalized excitation and emission spectrum of *N*-(ω-butanoic acid)-azatriangulenium tetrafluoroborate (ADOTA) in silica thin film (red) and in PVA film (blue).

3.3.Steady state measurements

Fig. 3 shows the normalized excitation and emission spectra of ADOTA entrapped in a silica thin film (red) and a PVA film (blue). Similar to the absorption data, we did not see any significant change in the excitation spectrum of the dye entrapped within the two different environments. However, a ~15 nm red shift in the emission spectra was observed for the ADOTA in silica thin films. When we examined the emission spectra of a low concentration ADOTA in the silica layer we found that the emission spectrum was similar to the emission spectrum of ADOTA in PVA film. ADOTA in silica layer shows concentration dependent red shift in emission spectrum. Supplementary information shows all the emission spectra along with measured Full Width Half Maxima (FWHM, Supplementary Fig. S3). For high concentration of the dye in silica layer, the

spectrum is red shifted compared to low concentration along with an increase in the FWHM value, suggesting dye aggregation/ excimer formation. Although, we have already ruled out the possibility of ground state aggregation since there in no experimental evidence here in this case. However, we cannot rule out the possibility of excimer formation here as the dyes are packed very close to each other and do not require a significant diffusion to form aggregates in the excited state. The rapid formation of excimers is outside the measurement capabilities of our instrument and hence the rise time (negative exponent) cannot be observed. We ascribe the broadening of the emission spectrum from ADOTA in silica thin films to the heterogeneous environment and aggregation of dye molecules in the silica matrix. This is a very elaborate problem, because ADOTA entrapped in the pores of the matrix has a possibility to interact not only with itself but also with the surface of three-dimensional network. In the literature this problem is called as the "cage effect"[33]. In the present case, the local environment of the ADOTA molecule is rich with water and methanol. In other words, the cage is filled with solvent and this creates the possibility of forming heterogeneous environment within the confined area. Steady state anisotropy measurements gave us the overall idea of the mobility of the fluorophore molecules in a silica film and PVA matrix.

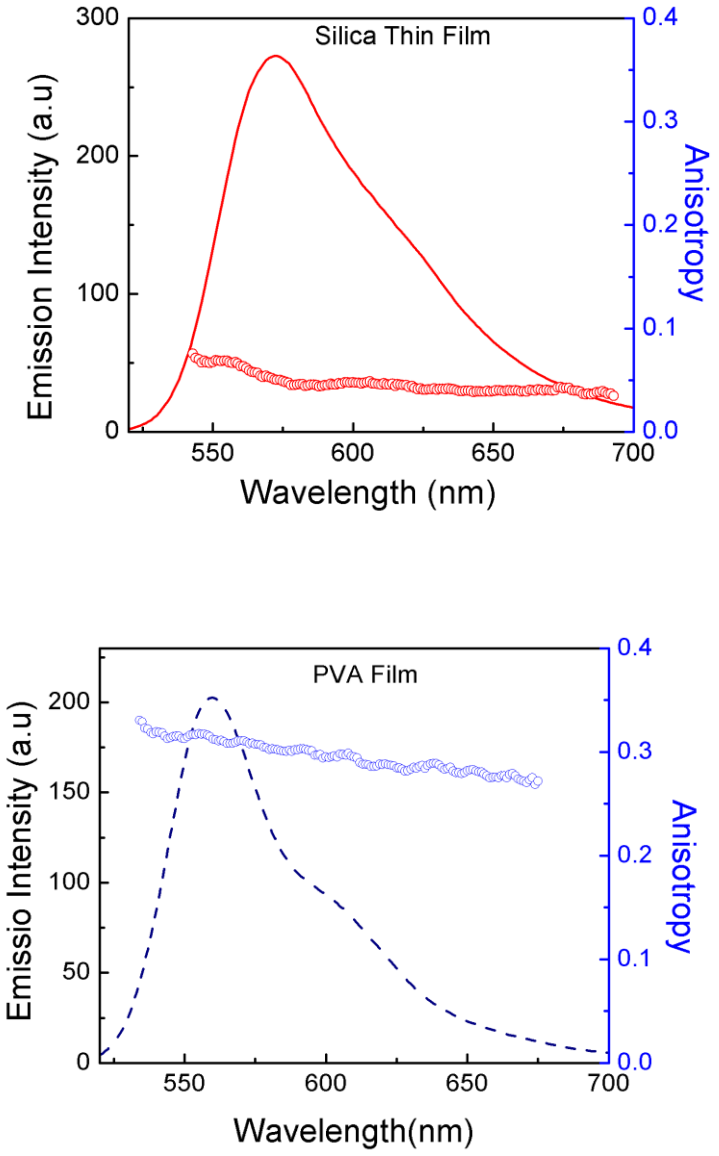

Figure 4:Top panel: fluorescence emission spectrum (red line) and anisotropy (blue circle) of *N*-(ω-butanoic acid)-azatriangulenium tetrafluoroborate (ADOTA) in silica thin film. Bottom panel: fluorescence emission spectrum (blue line) and anisotropy (blue circle) of ADOTA in PVA film.

The steady state anisotropy data are presented in Fig. 4. ADOTA entrapped in a PVA matrix showed high anisotropy reaching a value close to 0.3, thus suggesting a very rigid environment. On the other hand, ADOTA incorporated into silica thin film showed moderate anisotropy of 0.05. This suggests that the dyes are not rigidly linked to the matrix or that the anisotropy is lost due to energy transfer (HOMO-FRET) and that the pores are large on the molecular scale, making the silica matrix less rigid than PVA matrix.

These results were confirmed by blowing the argon on to silica film for 1 h and re-measuring the steady state anisotropy to exclude the possibility of rotational diffusion due to the hygroscopic nature of the silica film. Interestingly, the possibility of ADOTA being covalently linked to the matrices through the acid functional group is not explored and is a topic of further research in this area.

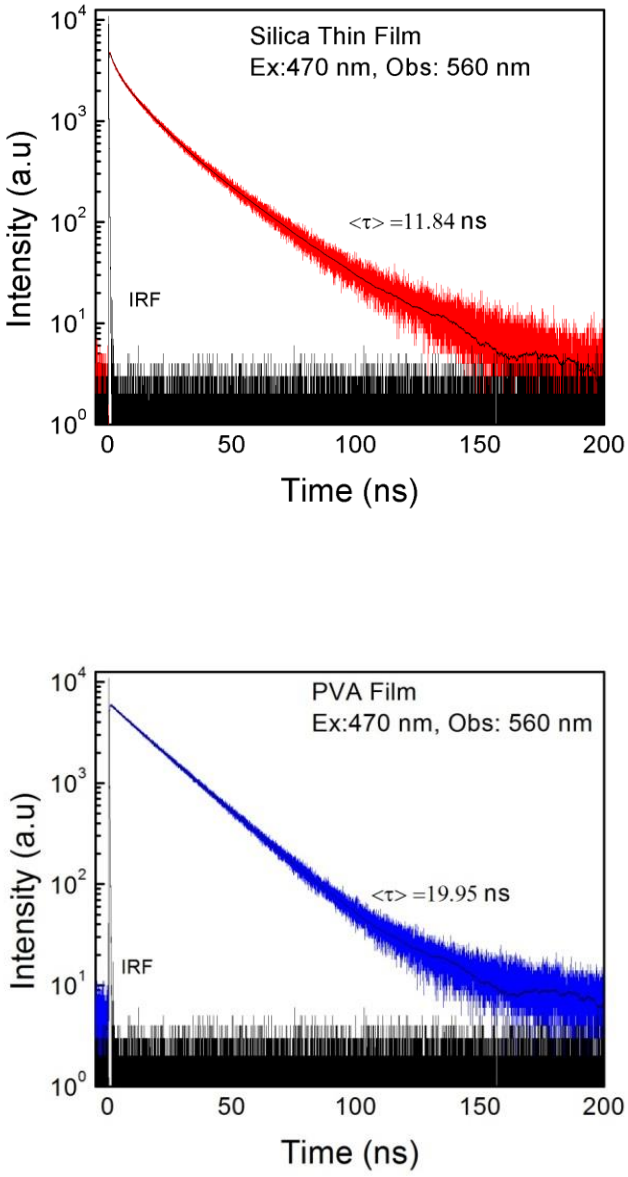

Figure 5: Top Panel: fluorescence intensity decay of *N*-(ω-butanoic acid)-azatriangulenium tetrafluoroborate (ADOTA) in silica thin film (Ex: 470nm, Obs: 560nm). Bottom panel: fluorescence intensity decay of ADOTA in PVA film (Ex: 470nm, Obs: 560nm).

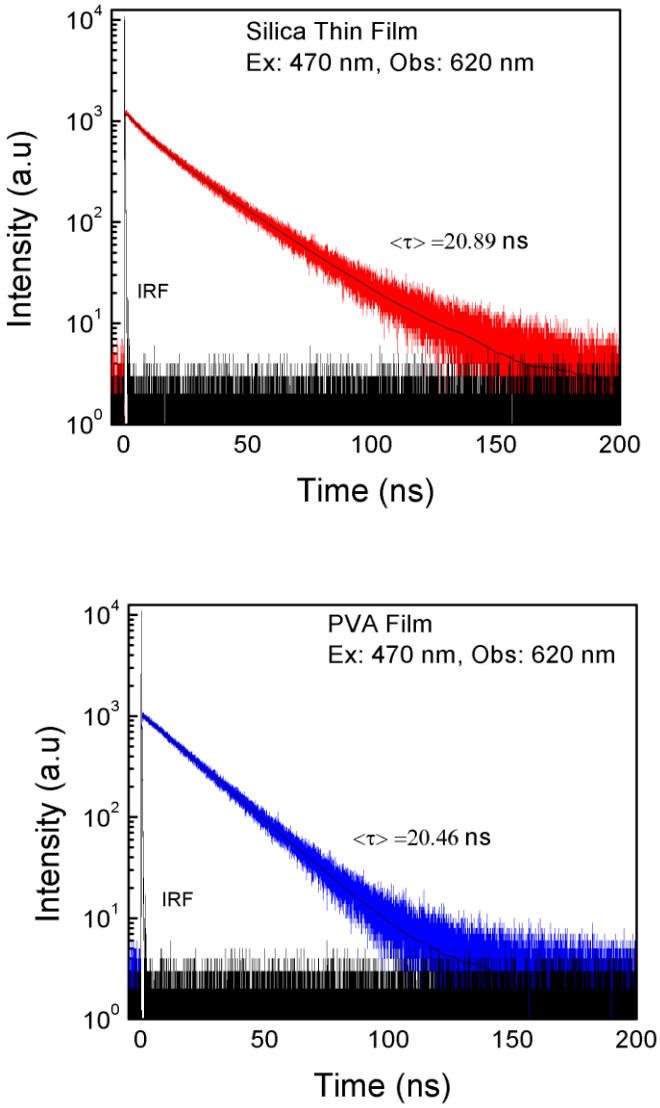

Figure 6: Top panel: fluorescence intensity decay of *N*-(ω-butanoic acid)-azatriangulenium tetrafluoroborate (ADOTA) in silica thin film (Ex: 470nm, Obs: 620nm). Bottom panel: fluorescence intensity decay of ADOTA in PVA film (Ex: 470nm, Obs: 620nm).

3.4.Time resolved intensity decay/fluorescence lifetime

The fluorescence lifetime of the ADOTA incorporated into a silica thin film was heterogeneous compared to fluorescence lifetime of the ADOTA incorporated into a PVA matrix. The lifetimes measured at 560 nm are shown in Fig. 5. The average lifetime was found to be ~12 ns in the silica matrix and ~20 ns in the PVA matrix. Three components are needed to fit the data at 560 nm for the silica thin film, whereas only two components are needed for the sample in the PVA film (Table 1). The shorter and heterogeneous nature of the decay in silica suggests different environments to which dye molecules are exposed to. Hence, we decided to measure the lifetimes at a longer wavelength (620 nm) which will further allow us to know more about the silica network environment. Fig. 6 shows the lifetime decays at 620 nm wavelength. One can see that the lifetime of ADOTA in the PVA matrix did not change significantly and stayed approximately 20 ns. However, the fluorescence lifetime of ADOTA (at 620 nm) incorporated into the silica matrix is significantly longer than the fluorescence lifetime measured at 560 nm. This could be due to the presence of the dye molecules in the confined space in the silica matrix. Stacking of dyes leads to the restricted motion and less vibrational/torsional losses and hence the longer lifetime at 620 nm observation. Table 1 shows the lifetime values from the data analyzed using multiexponential reconvolution model.

Sample	Observation (nm)	Lifetime (ns)			Amplitudes			Average lifetime (ns)		Chi square
		τ_1	τ_2	τ_3	α_1	α_2	α_3	τ_{AMP}	τ_{INT}	χ^2
ADOTA silica thin film	560	25.14	10.10	2.004	0.28	0.41	0.31	11.84	18.60	0.955
	620	26.98	9.33	_	0.65	0.35	_	20.89	20.24	0.892
ADOTA PVA film	560	21.01	13.42	_	0.86	0.14	_	19.95	20.30	0.997
	620	20.46	_	_	1	_	_	20.46	20.46	0.811

Where,

$$\tau_{AMP} = \sum_i \alpha_i \tau_i$$

$$\tau_{INT} = \sum_i f_i \tau_i$$

$$f_i = \frac{\alpha_i \tau_i}{\sum_i \alpha_i \tau_i}$$

Table 1: Analysis of *N*-(ω-butanoic acid)-azatriangulenium tetrafluoroborate (ADOTA) fluorescence intensity decay using multi-exponential model of in Silica thin film and PVA thin film.

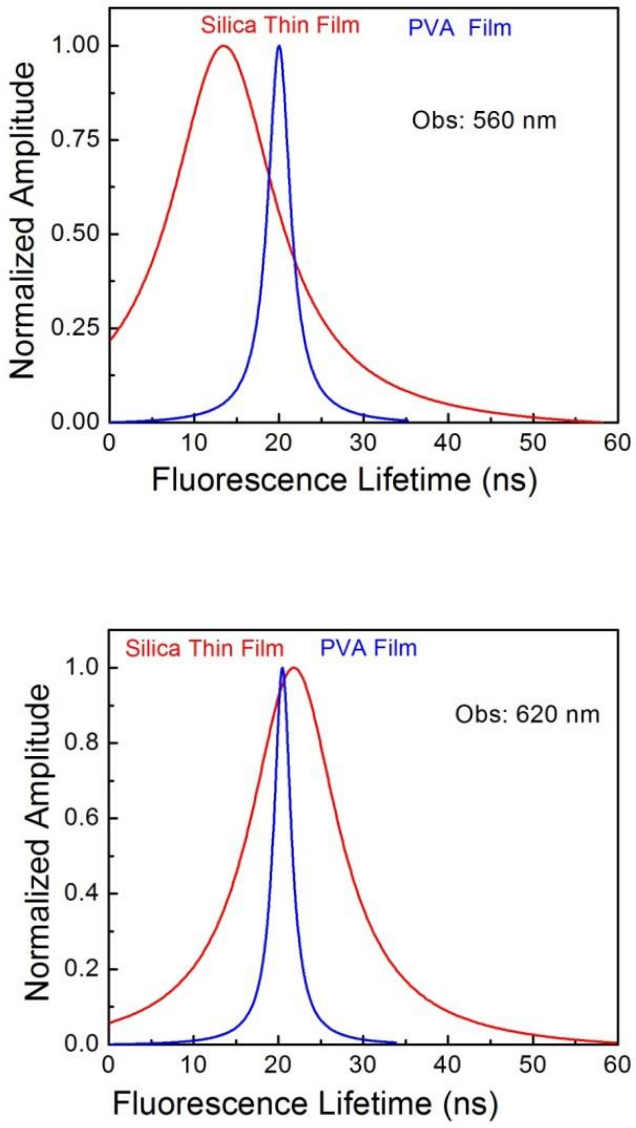

Figure 7- Lifetime distribution (Lorentzian Model) of *N*-(ω-butanoic acid)-azatriangulenium tetrafluoroborate (ADOTA) in silica thin film and PVA film. (Top Panel) This figure represents the fluorescence lifetime distribution when observed at 560 nm. (Bottom Panel) This figure represents fluorescence lifetime distribution observed at 620 nm. ADOTA is more heterogeneous at 560 nm (Silica Thin $Film_{FWHM}$ =15.05 ns, PVA $Film_{FWHM=}$3.22 ns) compared to observation at 620 nm (Silica Thin $Film_{FWHM}$ = 12.71ns, PVA $Film_{FWHM=}$2.45 ns)

We also analyzed the fluorescence intensity decays using a Lorentzian lifetime distribution model that takes into consideration the average number of emitting species in different environments. The FWHM values of the distribution shows the degree of distribution of the emitting molecules which are much higher in silica thin films than in the PVA films (Fig. 7). The Lorentzian distributions (Table 2) for ADOTA in PVA films are very narrow, about 3 ns at 560 nm observation, and about 2.45 ns at 620 nm observation, which suggests a very uniform environment and lack of interactions between fluorescent molecules. In contrast, the Lorentzian distributions in silica are very wide. In case of ADOTA in silica thin films, the FWHM value at 560 nm is about 15 ns and at 620 nm about 13 ns. These higher FWHM values show the broader distribution of the emitting molecules in silica thin films.

	Observation (nm)	Lifetime, τ (ns)	FWHM (ns)	Chi square(χ^2)
ADOTA silica thin film	560	13.5	15.1	0.98
	620	21.8	12.7	0.92
ADOTA PVA film	560	20	3.2	0.98
	620	20.4	2.45	0.93

Table 2: Lorentzian analysis of fluorescence intensity decays of *N*-(ω-butanoic acid)-azatriangulenium tetrafluoroborate (ADOTA).

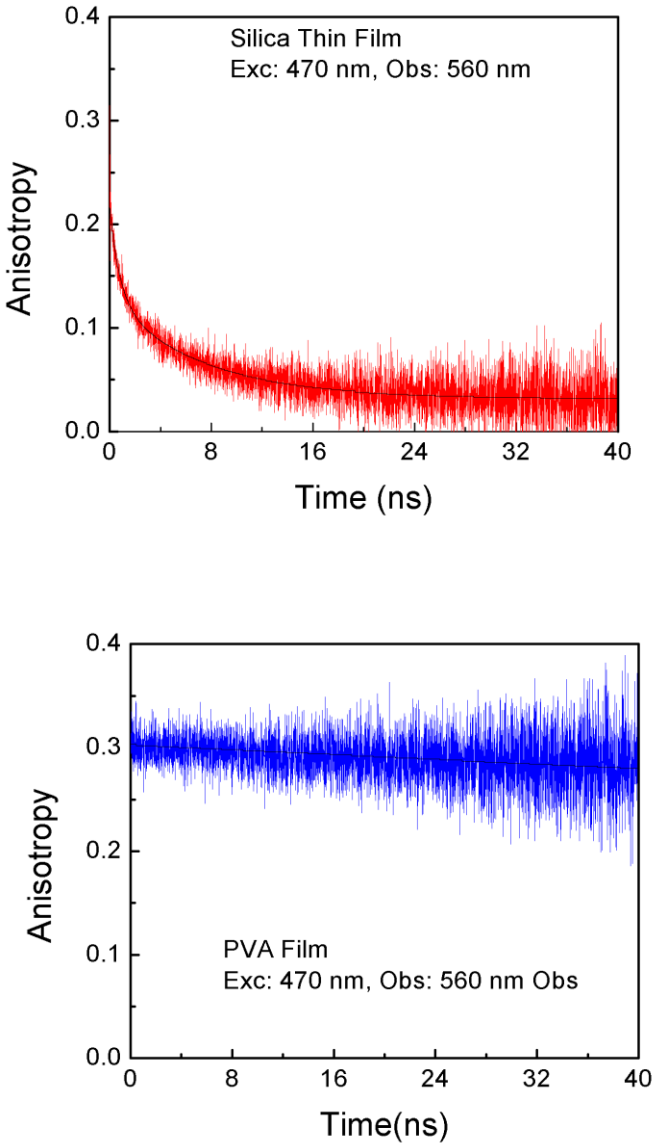

Figure 8: Top panel: Fluorescence anisotropy decay of *N*-(ω-butanoic acid)-azatriangulenium tetrafluoroborate (ADOTA) in silica thin film (Ex: 470nm, Obs: 560nm). Bottom panel: fluorescence anisotropy decay of ADOTA in PVA film (Ex: 470nm, Obs: 560nm).

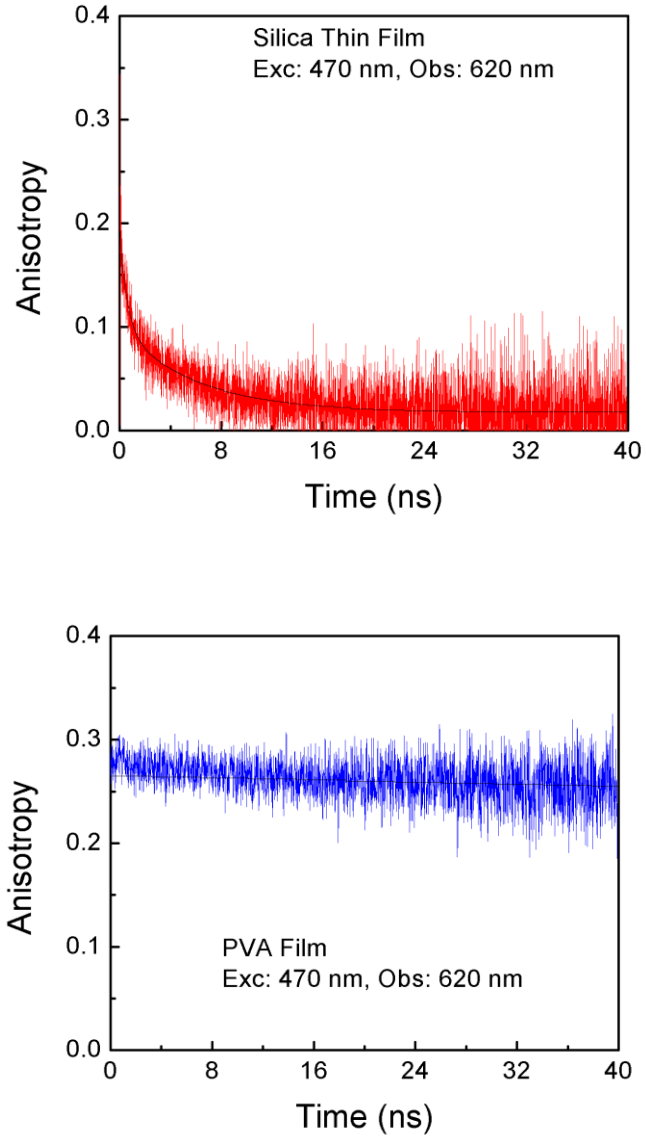

Figure 9: Top panel: Fluorescence anisotropy decay of *N*-(ω-butanoic acid)-azatriangulenium tetrafluoroborate (ADOTA) in silica thin film (Ex: 470nm, Obs: 620nm). Bottom panel: fluorescence anisotropy decay of ADOTA in PVA film (Ex: 470nm, Obs: 620nm).

Sample	Observation (nm)	Anisotropy			Correlation time (ns)	
		r_1	r_2	r_{INF}	Φ_1	Φ_2
ADOTA Silica thin film	560	0.088	0.095	0.03	0.81	7.37
	620	0.081	0.093	0.017	6.02	0.58
ADOTA PVA film	560	0.30	_	_	504.4	_
	620	0.26	_	_	1000	_

Table 3: Analysis of *N*-(ω-butanoic acid)-azatriangulenium tetrafluoroborate (ADOTA) anisotropy decay using multiexponential model of on Silica thin film and PVA film.

3.5.Time resolved anisotropy

Time resolved anisotropy measurements presented in Figs. 8 and 9 shows some interesting information. As expected in the case of the PVA matrix, initial anisotropy was high (0.3) with a very long correlation time (>500 ns) (correlation time >> fluorescence lifetime) at both observation wavelengths (560 and 620 nm). However, in case of silica gel matrix the recovered initial anisotropy values are 0.21 and 0.19 for 560 and 620 nm observation and the measured correlation times and rINF values are not significantly different (Table 3). The heterogeneous nature of the correlation times is due to the populations of the dyes in different types of matrix environment. Therefore, it will not be surprising if a part of the dye population is immobilized completely and a part of it has a moderate freedom than the others. It is suggested in the literature that the hydrogen bonding among silica mesh and the dye molecules undergoes reshuffling in excited state and it may give rise to such correlation times. Moreover, the estimated steady state anisotropy values at these wavelengths are 0.069 and 0.042. The drop in the initial recovered anisotropy, in case of anisotropy decay, and steady state anisotropy values suggests energy migration (if the dye molecules are sitting together below 40 A0 distances which is the approximate Forster distance for such homo-transfer and is a possibility we cannot ignore).

Although energy migration is a rapid process which takes place over the lifetime of the fluorophore despite having a relatively long fluorescence lifetime in both matrices.

4. Conclusions

In the present work, the organic fluorophore, N-(u-butanoic acid)-azatriangulenium tetrafluoroborate (ADOTA) was successfully incorporated into silica thin films by the sol-gel process as well as in PVA films. The PVA matrix was chosen to study fluorescence properties of ADOTA in a more rigid environment. Silica matrix provides an unusual environment for the entrapped fluorophores and affects the dye properties in many different ways. A red shift of 15 nm was observed in the emission spectra of ADOTA in silica thin film. In addition, the fluorescence lifetime of ADOTA at 560 nm observation in silica matrix was 12 ns compared to 20 ns in PVA film. However, when the wavelength of observation was placed at 620 nm, the fluorescence lifetimes of ADOTA entrapped in both the matrices are almost similar. The Lorentzian lifetime distribution shows the presence of broad distribution of the emitting species in silica thin layer compared to PVA film. To sum up, considering all the observations such as lower fluorescence efficiencies, shorter lifetimes and concentration dependent red shifted emission suggests aggregation of dye molecules in the excited state. Ultrafast spectroscopy experiments will further support our observations.

SUPPLEMENTARY INFORMATION

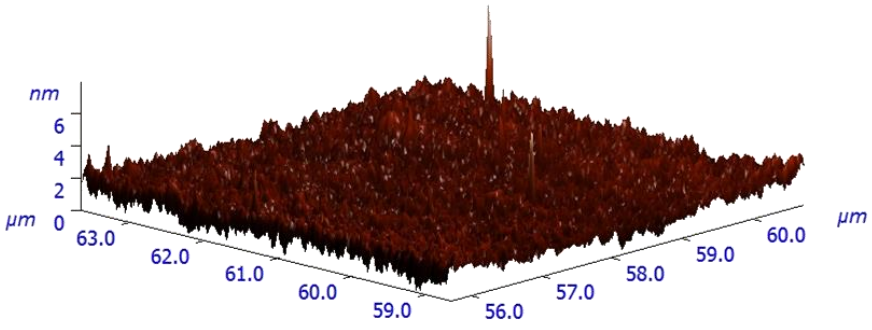

Figure S1- AFM Image of *N*-(ω-butanoic acid)-azatriangulenium tetrafluoroborate (ADOTA) in PVA film showing surface topography.

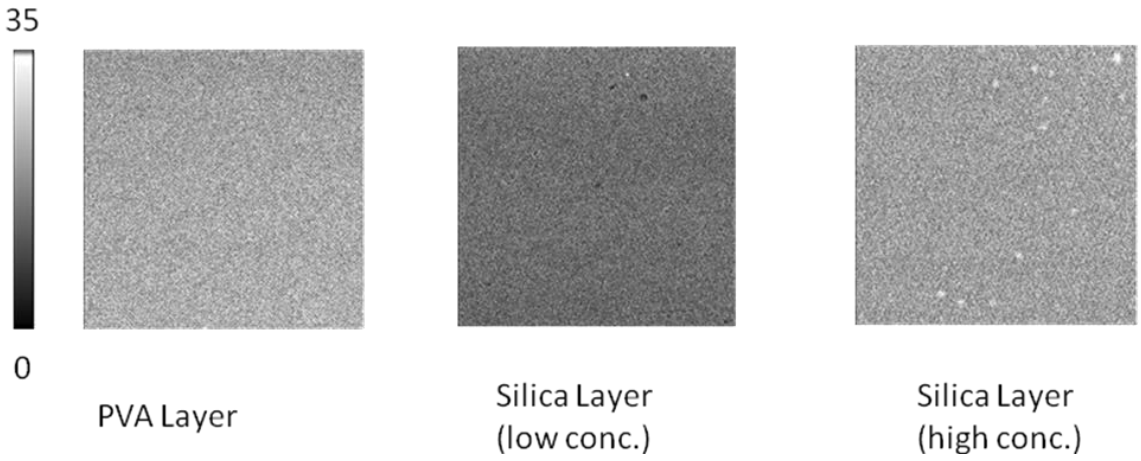

Figure S2- Uniform distribution of *N*-(ω-butanoic acid)-azatriangulenium tetrafluoroborate (ADOTA) in both PVA and Silica matrix shown by con-focal intensity image (Ex. 470nm).

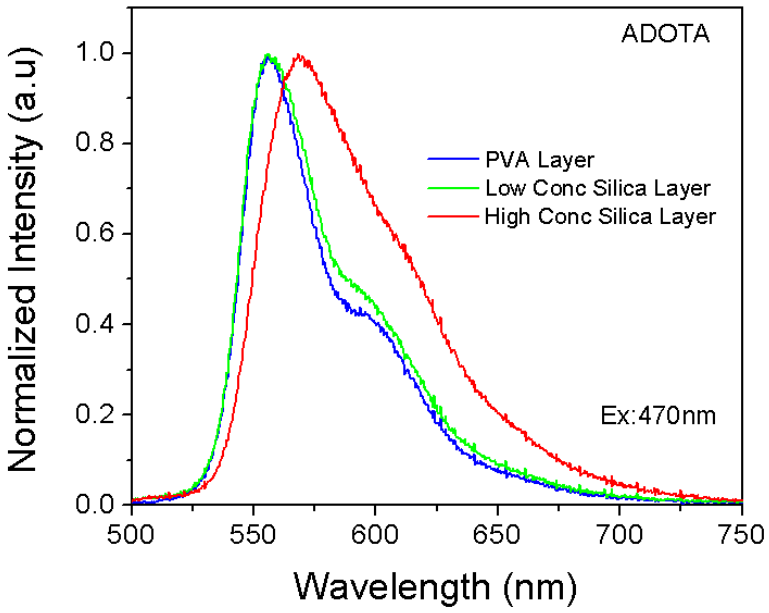

Sample	FWHM
PVA Layer	38 nm
Low Conc. Silica Layer	45 nm
High Conc. Silica Layer	69 nm

Figure S3- Emission spectra and FWHM of *N*-(ω-butanoic acid)-azatriangulenium tetrafluoroborate (ADOTA) in PVA and Silica layer

References

1. MacCraith BD, McDonagh C. Enhanced fluorescence sensing using sol-gel materials. *J Fluoresc*. 2002;12(3-4):333-342.

2. Wang X, Wolfbeis OS. Fiber-optic chemical sensors and biosensors (2008–2012). *Anal Chem*. 2012;85(2):487-508.

3. McDonagh C, Burke CS, MacCraith BD. Optical chemical sensors. *Chem Rev*. 2008;108(2):400-422.

4. Vannahme C, Leung MC, Richter F, Smith CL, Hermannsson PG, Kristensen A. Nanoimprinted distributed feedback lasers comprising TiO2 thin films: Design guidelines for high performance sensing. *Laser & Photonics Reviews*. 2013;7(6):1036-1042.

5. Reisfeld R. Spectroscopy and applications of molecules in glasses. *J Non Cryst Solids*. 1990;121(1):254-266.

6. Levy D. Sol-gel glasses for optics and electro-optics. *J Non Cryst Solids*. 1992;147:508-517.

7. Avnir D, Levy D, Reisfeld R. The nature of the silica cage as reflected by spectral changes and enhanced photostability of trapped rhodamine 6G. *J Phys Chem*. 1984;88(24):5956-5959.

8. Lewkowicz A, Bojarski P, Synak A, et al. Concentration-dependent fluorescence properties of rhodamine 6G in titanium dioxide and silicon dioxide nanolayers. *The Journal of Physical Chemistry C*. 2012;116(22):12304-12311.

9. Lewkowicz A, Synak A, Grobelna B, Kułak L, Bojarski P. Spectroscopic properties of rhodamine B entrapped in hybrid porous nanolayers at high dye concentration. *Chem Phys*. 2014.

10. Synak A, Bojarski P, Grobelna B, Kułak L, Lewkowicz A. Determination of local dye concentration in hybrid porous silica thin films. *The Journal of Physical Chemistry C*. 2013;117(21):11385-11392.

11. Livage J. Sol-gel processes. *Current Opinion in Solid State and Materials Science*. 1997;2(2):132-138.

12. Gomez-Romero P. Hybrid Organic±Inorganic MaterialsÐ in search of synergic activity*. *Adv Mater*. 2001;13(3):5.

13. Eremenko A, Smirnova N, Rusina O, et al. Photophysical properties of organic fluorescent probes on nanosized TIO< sub> 2/SIO< sub> 2 systems prepared by the sol–gel method. *J Mol Struct*. 2000;553(1):1-7.

14. Henglein A. Small-particle research: Physicochemical properties of extremely small colloidal metal and semiconductor particles. *Chem Rev*. 1989;89(8):1861-1873.

15. Spanhel L, Anderson MA. Synthesis of porous quantum-size cadmium sulfide membranes: Photoluminescence phase shift and demodulation measurements. *J Am Chem Soc*. 1990;112(6):2278-2284.

16. Spanhel L, Anderson MA. Semiconductor clusters in the sol-gel process: Quantized aggregation, gelation, and crystal growth in concentrated zinc oxide colloids. *J Am Chem Soc*. 1991;113(8):2826-2833.

17. Kamat PV. Photochemistry on nonreactive and reactive (semiconductor) surfaces. *Chem Rev*. 1993;93(1):267-300.

18. Liu X, Thomas J. Formation and photophysical properties of cadmium sulfide in zeolites with cages and channels. *Langmuir*. 1989;5(1):58-66.

19. Brinker CJ, Scherer GW. *Sol-gel science: The physics and chemistry of sol-gel processing.* Gulf Professional Publishing; 1990.

20. Wohlrab S, Hoppe R, Schulz-Ekloff G, Wöhrle D. Encapsulation of methylene blue into aluminophosphate family molecular sieves. *Zeolites*. 1992;12(7):862-865.

21. Knobbe ET, Dunn B, Fuqua PD, Nishida F. Laser behavior and photostability characteristics of organic dye doped silicate gel materials. *Appl Opt*. 1990;29(18):2729-2733.

22. Kim M, Seok S, Ahn B, Koo S, Paik S. Encapsulation of water-soluble dye in spherical sol-gel silica matrices. *J Sol Gel Sci Technol*. 2003;27(3):355-361.

23. Panitz J, Geiger F. Leaching of the anthraquinone dye solvent blue 59 incorporated into organically modified silica xerogels. *J Sol Gel Sci Technol*. 1998;13(1-3):473-477.

24. Tani T, Namikawa H, Arai K, Makishima A. Photochemical hole-burning study of 1, 4-dihydroxyanthraquinone doped in amorphous silica prepared by alcoholate method. *J Appl Phys*. 1985;58(9):3559-3565.

25. Laursen BW, Krebs FC. Synthesis of a triazatriangulenium salt. *Angewandte Chemie International Edition*. 2000;39(19):3432-3434.

26. W Laursen B, C Krebs F. Synthesis, structure, and properties of azatriangulenium salts. *Chemistry-A European Journal*. 2001;7(8):1773-1783.

27. Sørensen TJ, Thyrhaug E, Szabelski M, et al. Azadioxatriangulenium: A long fluorescence lifetime fluorophore for large biomolecule binding assay. *Methods and applications in fluorescence*. 2013;1(2):025001.

28. Sørensen TJ, Hildebrandt CB, Elm J, et al. Large area, soft crystalline thin films of N, N′, N″-trialkyltriazatriangulenium salts with homeotropic alignment of the discotic cores in a lamellar lattice. *Journal of Materials Chemistry*. 2012;22(11):4797-4805.

29. Thyrhaug E, Sørensen TJ, Gryczynski I, Gryczynski Z, Laursen BW. Polarization and symmetry of electronic transitions in long fluorescence lifetime triangulenium dyes. *The Journal of Physical Chemistry A*. 2013;117(10):2160-2168.

30. Dileesh S, Gopidas K. Photoinduced electron transfer in azatriangulenium salts. *J Photochem Photobiol A*. 2004;162(1):115-120.

31. Maliwal BP, Fudala R, Raut S, et al. Long-lived bright red emitting azaoxa-triangulenium fluorophores. *PloS one*. 2013;8(5):e63043.

32. Bharill S, Sarkar P, Ballin JD, Gryczynski I, Wilson GM, Gryczynski Z. Fluorescence intensity decays of 2-aminopurine solutions: Lifetime distribution approach. *Anal Biochem*. 2008;377(2):141-149.

33. Kaufman VR, Avnir D. Structural changes along the sol-gel-xerogel transition in silica as probed by pyrene excited-state emission. *Langmuir*. 1986;2(6):717-722.

Chapter 5

Azadioxatriangulenium (ADOTA) fluorophore for hyaluronidase sensing

Abstract

In this report, we have designed a rapid and sensitive, intensity-based ratiometric sensing as well as lifetime-based sensing probe for the detection of hyaluronidase activity. Hyaluronidase expression is known to be upregulated in various pathological conditions. We have developed a fluorescent probe by heavy labeling of hyaluronic acid with a new orange/red-emitting organic azadioxatriangulenium (ADOTA) fluorophore, which exhibits a long fluorescence lifetime (∼20 ns). The ADOTA fluorophore in water has a peak fluorescence lifetime of ∼20 ns and emission spectra centered at 560 nm. The heavily ADOTA-labeled hyaluronic acid (HAADOTA) shows a red shift in the peak emission wavelength (605 nm), a weak fluorescence signal, and a shorter fluorescence lifetime (∼4 ns) due to efficient self-quenching and formation of aggregates. In the presence of hyaluronidase, the brightness and fluorescence lifetime of the sample increase with a blue shift in the peak emission to its original wavelength at 560 nm. The ratio of the fluorescence intensity of the HA-ADOTA probe at 560 and 605 nm can be used as the sensing method for the detection of hyaluronidase. The cleavage of the hyaluronic acid macromolecule reduces the energy migration between ADOTA molecules, as well as the degree of self-quenching and aggregation. This probe can be efficiently used for both intensity-based ratiometric sensing as well as fluorescence lifetime-based sensing of hyaluronidase. The proposed method makes it a rapid and sensitive assay, useful for analyzing levels of hyaluronidase in relevant clinical samples like urine or plasma.

1. Introduction

Hyaluronidase is a family of endoglycosidase that catalyzes the depolymerization of hyaluronic acid (HA) via cleavage of β-N-acetyl-D-glucosaminidic bonds [1]. Hyaluronidase is known to be involved in various physiological and pathological conditions like fertilization, embryogenesis, inflammation, tumor growth, and wound healing [2-6]. Initially in the literature, it was described as a "spreading factor" which was found in the testicular extract of animal and humans. It was later characterized as hyaluronic acid-degrading enzyme and called hyaluronidase [5,7-9]. Recent studies have shown the role of hyaluronic acid and hyaluronidase with the differentiation, proliferation, migration, and angiogenesis of tumor cells [2,10,11]. HA is a linear, non-sulfated glycosaminoglycan composed of multiple subunits of D-glucuronic acid and N-acetylglucosamine. In humans, HA is known to maintain various important functions like cartilage integrity, osmotic balance, and homeostasis of water owing to its gel like properties [12-14]. An overexpression of hyaluronidase is associated in the literature with patients suffering from cancers, such as prostate cancer [15], bladder cancer [6], head and neck carcinoma [4], colon cancer, and malignant melanoma [5]. Therefore, it is of great interest to develop a simple, sensitive, and fast technique with which one can estimate the activity/level of hyaluronidase in biological samples.

Several methods have been reported in the literature for detecting hyaluronidase activity, which mainly depends on the degradation of hyaluronic acid by hyaluronidase. To measure hyaluronidase activity/level, there are several methods reported in the literature which includes turbidimetry [16], viscometry [17], ELISA-like assay [18,19], colorimetry [20], zymography [21,22], and fluorescence detection [23-32]. Methods like turbidimetry, colorimetry, and viscometry are not very sensitive and cannot detect the level of hyaluronidase at different time points of an experiment. Zymography is simple yet not very sensitive for quantitative measurements. ELISA-like assays

are sensitive and selective but do not allow real-time monitoring of hyaluronidase activity. However, fluorescence-based detection of hyaluronidase is a fast and sensitive method, useful for high-throughput screening, and has a real-time monitoring capability and their usefulness in biological samples makes it an ideal method for hyaluronidase detection.

Various novel fluorescence assays designed to detect hyaluronidase activity have been reported in the literature. These fluorescent probes have been designed for hyaluronidase detection by using hyaluronic acid as a template and labeling it with gold nanoparticles [23,33], organic fluorescent dyes [34,35], conjugated small molecules [36], and upconversion luminescence material [29]. Although these fluorescence-based methods have superior properties compared to previous methods in terms of sensitivity, they also have a few drawbacks. For example, gold nanoparticles precipitate in biological high salt environments [26,37]. Fluorescent probes developed using organic fluorophores are smaller in size compared to probes developed using quantum dots, nanodots, and noble metal nanoparticle as the luminescent material. Some fluorescent probes have a very short fluorescence lifetime and hence cannot be used for lifetime-based sensing or imaging, as the background of the biological sample interferes with the fluorescence signal of the probe and cannot be easily removed as the fluorescence intensity decay of background and probe is almost similar [27,34].

To make this probe, we heavily labeled hyaluronic acid with an azadioxatriangulenium (ADOTA) fluorophore. ADOTA is an orange/red-emitting organic fluorophore with peak emission centered at 560 nm and a fluorescence lifetime of 20 ns in aqueous solution. Our previous studies have shown that it is the only red-emitting organic fluorophore with a long fluorescence lifetime of 20 ns [38-47]. One major problem encountered using fluorescence detection methods in biological fluids, cells, and tissue is the presence of autofluorescence which reduces

the obtainable signal-to-noise ratio. As most biomolecules emit at higher energies, the autofluorescence level decreases towards the red/NIR region of the electromagnetic spectrum. Therefore, using a red-emitting fluorophore can help to overcome this issue.

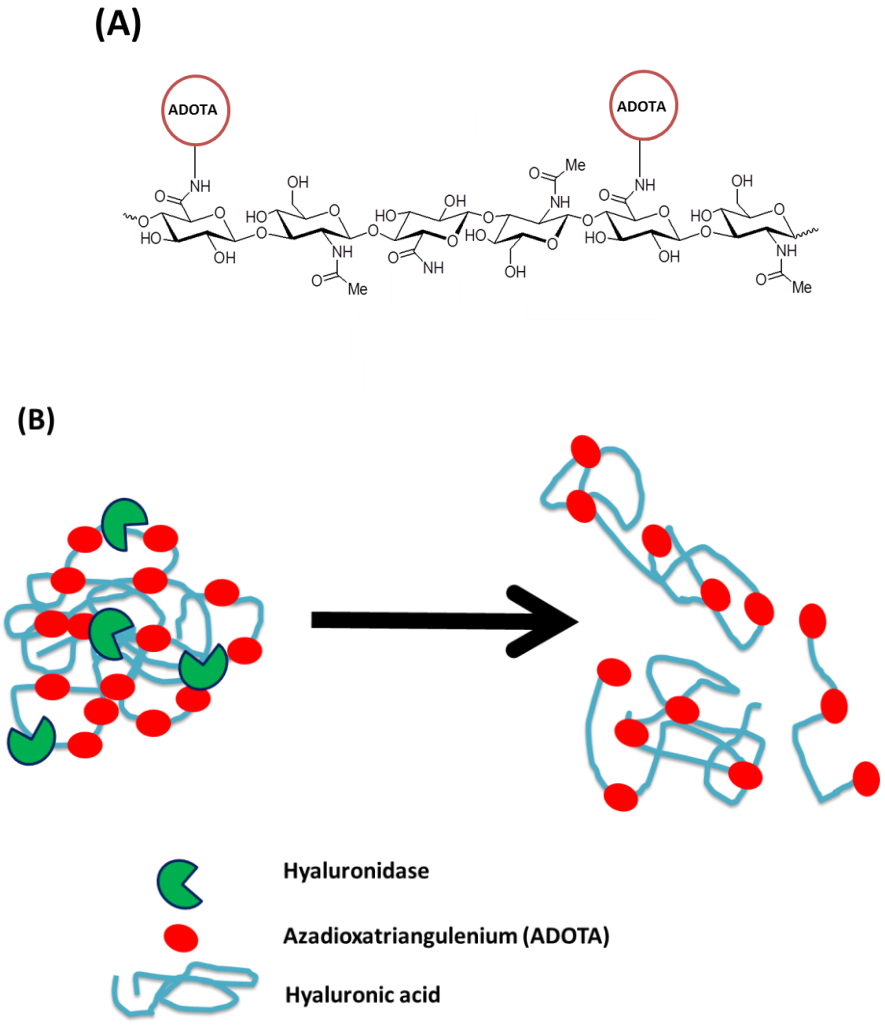

Scheme 1: Schematic representation for the assay system and its response to the enzyme hyaluronidase. (A) shows the covalent binding of ADOTA fluorophore to the COOH group of hyaluronic acid. (B) Shows the undigested HA-ADOTA probe and cleaved probe following enzymatic action

The goal of this study was to develop a rapid and sensitive ratiometric sensing probe for estimating hyaluronidase activity/ level. To achieve this goal, a simple strategy was used where we developed a probe using HA as template and labeled it with an orange/red-emitting organic fluorophore with a long fluorescence lifetime. The design of this probe was created by heavy labeling of HA with an aniline-substituted ADOTA fluorophore (Scheme 1) [48]. When a certain molar ratio of the fluorophore to hyaluronic acid is reached, fluorophores are close enough that dimers or higher order aggregates may form. The aggregated dyes display red shifted absorption and fluorescence as well as reduced fluorescence lifetime (4 ns). Even a small fraction of aggregates dominates the optical properties due to the close proximity of all dyes bound to HA and the resulting quenching of non-aggregated dyes via energy transfer to the red-shifted aggregates. The fluorescence intensity and fluorescence lifetime of the HA-ADOTA probe are thus significantly reduced compared to the non-aggregated ADOTA dye. The fluorescence signal will recover after the degradation of the probe by hyaluronidase, where the long hyaluronic acid chains of the HAADOTA probe are split into shorter fragments and the fluorophore molecules will move apart. It was observed from our previous observations that the aggregation of ADOTA fluorophore causes a red shift in the peak emission wavelength [39]. Similarly, heavy labeling of hyaluronic acid with ADOTA causes a shift in the peak emission wavelength of the probe to 605 nm. Once the hyaluronidase starts degrading this probe, the peak emission wavelength shifts back to its original position at 560 nm. This shift in emission wavelength after degradation of the probe provides a method to develop a ratiometric sensing probe, where the ratio of emission intensity of the digested to undigested probe can be used to calculate hyaluronidase activity/level. Some of the reported methods for the fluorescence detection utilize single fluorescence intensity as the sensing method. Collection of the signal at a fixed wavelength can

be tempered due to various reasons like fluctuation in the excitation intensity, emission collection efficiency, change in focal point, etc [49,50]. These problems can be overcome by ratiometric collection of signal at two different wavelengths. Ratiometric sensing acts in a self-calibrating way to minimize interfering factors while allowing for more accurate detection of analyte [51-53].

The activity/level of hyaluronidase can also be estimated using the change in the fluorescence lifetime of the biosensor as the aggregation in the undigested probe leads to a decrease in the fluorescence lifetime (4 ns). After cleavage of the biosensor by hyaluronidase, a recovery in the amplitude weighted fluorescence lifetime was observed (15 ns). This large difference in the fluorescence lifetime of the probe can be used for the detection of hyaluronidase. Here in this paper, we tested the HA-ADOTA probe in spiked PBS and we also used it to measure hyaluronidase activity/level in cell culture media from a prostate cancer cell line (DU-145) which is known to express higher levels of hyaluronidase [15,54].

2. Materials and methods

Sodium hyaluronate from bacterial fermentation was obtained from Acros Organics (Thermo Fisher Scientific, Fair Lawn, NJ). Dimethyl sulfoxide (DMSO), guanidine hydrochloride, acetaldehyde, cyclohexyl isocyanide, centricon filter (30,000 molecular cutoff), and bovine testis hyaluronidase (EC 3.2.1.35, type 1-S, 451 U/mg) were obtained from Sigma- Aldrich (Sigma-Aldrich, St. Louis, MO). Dulbecco's phosphate-buffered saline (PBS), fetal bovine serum (FBS), DMEM media, antibiotic, insulin, transferrin, and selenium (ITS) supplement, and Slide-A-Lyser dialysis cassettes (10, 000 molecular weight cutoff) were purchased from Thermo Fisher

Scientific (Waltham, MA). ELISA kit for hyaluronic acid was purchased from R&D Systems (Minneapolis, MN). DU-145 cells were purchased from ATCC (Manassas, VA). The ADOTA fluorophore (N-(4-aminophenyl)- azadioxatriangulenium tetrafluoroborate) was synthesized as described elsewhere [48]. All compounds, solvents, and materials were used as received; water was used directly from a Millipore (Billerica, MA) purification system.

2.1. Preparation of the active amine form of the azadioxatriangulenium (ADOTA-NH2) fluorophore

The ADOTA fluorophore with a reactive amine group was prepared according to previously published procedures [48]. Briefly, tris(2,6-dimethoxyphenyl)methylium tetrafluoroborate was reacted with p-aminoaniline and 2,6-lutidinein acetonitrile at ambient temperature for 90 min to form the respective acridinium salt. Subsequent twofold ring closure in molten pyridinium hydrochloride at 200 °C in 60 min provided the fluorescent ADOTA. Precipitation as the tetrafluoroborate salt and recrystallization from methanol yield the pure compound in excellent yield as dark crystals (Scheme 2).

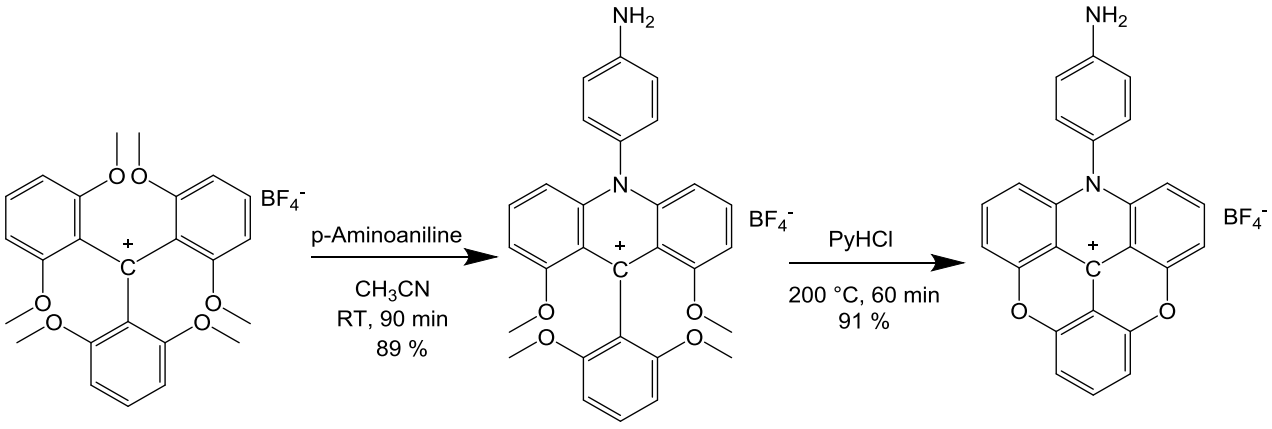

Scheme 2: Synthetic procedure for the preparation of p-aminophenyl-ADOTA BF_4

2.2. Preparation of HA-ADOTA probe

The starting material for the preparation of the reactive amine of the AzaDiOxaTriaAngulenium (ADOTA-phenyl-NH2) was prepared according to the above-described method (Scheme 2). HA was dissolved to 1.25 mg/mL in dH2O and then diluted 1:2 in DMSO. The ADOTA-NH2 was dissolved in DMSO and added to the HA solution for a final ADOTANH2 concentration of 25 mg/mL. Acetaldehyde and cyclohexyl isocyanide were added to 0.04 % (v/v), and the reaction was allowed to proceed for 48 h at 25 °C. Afterwards, the solution was diluted 1:14 in ethanol/ guanidine HCl (50 μL of 3 M guanidine HCl per 900 μL of 100 % ethanol) and the HA-ADOTA allowed to precipitate overnight at −20 °C. The precipitate was then dissolved in 1 mL of dH2O followed by extensive dialysis against dH2O. The concentration of HA in the probe was measured using ELISA kit for hyaluronic acid and was found to be 0.6 mg/mL.

2.3. Preparation of cell culture media

Concentrated cell culture media were prepared according to the method mentioned by Lokeshwar et al. with slight modifications [54]. DU-145 cells were plated in DMEM media containing 10 % FBS and 1 % antibiotic solution. After 70 % confluency, cells were washed three times with serum-free DMEM media. Cells were then incubated with serum-free DMEM media with ITS supplement. The serum-free media were collected after 72 h and concentrated ten times using 30,000 molecular cutoff centricon filter. Concentrated media from six culture

flasks were pooled together and used for analyzing hyaluronidase activity in the media.

3. Experimental section

3.1. Absorption measurements

Absorption spectra were measured using a Cary 50 Bio UV–visible spectrophotometer (Varian Inc., Australia). Absorption spectra were scanned from 350 to 620 nm in PBS at room temperature.

3.2. Steady-state fluorescence measurements of hyaluronan hydrolysis

The HA-ADOTA probe was incubated with different amount of hyaluronidase (0–100 U/mL) in PBS, pH 7.4, at room temperature. The fluorescence emission spectra were recorded every 10 min for 150 min for all the concentrations of the enzyme. Steady-state fluorescence intensity measurements of all the samples were made using a Carry Eclipse spectrofluorometer (Varian Inc., Australia) using a 10-mm × 4-mm quartz cuvette. The emission was scanned from 520 to 700 nm following a 470-nm excitation and using a 495-nm-long pass filter on the emission side. Steadystate excitation spectra were measured by observing the emission at 605 nm, and excitation was scanned from 400 to 600 nm using a 590-nm-long pass filter on the emission side.

3.3. Fluorescence intensity decay

Same amount of HA-ADOTA probe was added to PBS (pH 7.4) with varying amount of hyaluronidase (0–100 U/mL). The change in fluorescence lifetime was measured for all the concentrations of enzyme every 20 min for 160 min. Fluorescence lifetimes of all the samples were measured using FluoTime 200 (PicoQuant, GmbH, Berlin, Germany) time resolved spectrofluorometer. This instrument contains a multichannel plate detector (Hamamatsu, Japan), and a 470-nm laser diode was used as the excitation source. The fluorescence intensity decays

were measured under magic angle conditions (54.7°), and data was analyzed with FluoFit version 4.5.3 software (PicoQuantGmbH, Berlin, Germany) using the exponential reconvolution procedure using nonlinear regression (multiexponential deconvolution model). In the case of multiexponential analysis, the fluorescence decay was analyzed using:

$$I(t) = \sum_i \alpha_i \exp(-t/\tau_i)$$

where τi are the decay time and αi are the pre-exponential factors (amplitudes) of the individual components. Amplitude-weighted lifetime is given by:

$$\langle \tau \rangle = \sum_i \alpha_i \tau_i$$

For measuring fluorescence lifetime of HA-ADOTA in solution containing concentrated media from DU-145 cells, a confocal microscope equipped with time-correlated single photon counting (TCSPC) detector was used (MicroTime 200, PicoQuant, Germany). A 470-nm laser operating at 5 MHz repetition rate was used. Sample is prepared in a glass bottom petri dish, and laser excitation is used on Olympus 1X71 inverted microscope. The signal from the detector was routed into a PicoHarp 300 (PicoQuant, Germany) TCSPC module. Fluorescence lifetime was measured every 10 min for 150 min. All analyses were performed using SymPho Time, V.5.3.2 software from PicoQuant.

4. Results and discussion

Scheme 1 shows the schematic representation of HA-ADOTA probe. The HA-ADOTA probe obtained from heavy labeling of ADOTA fluorophore produces a low fluorescence signal and exhibit a short fluorescence lifetime resulting from aggregation and FRET between ADOTA molecules and aggregates. Nevertheless, the addition of hyaluronidase to the HAADOTA biosensor solution causes a strong fluorescence enhancement and an increase in the fluorescence lifetime, which is attributed to the specific cleavage of the hyaluronic acid template by hyaluronidase and the breakup of aggregates and spatial separation of fluorophores.

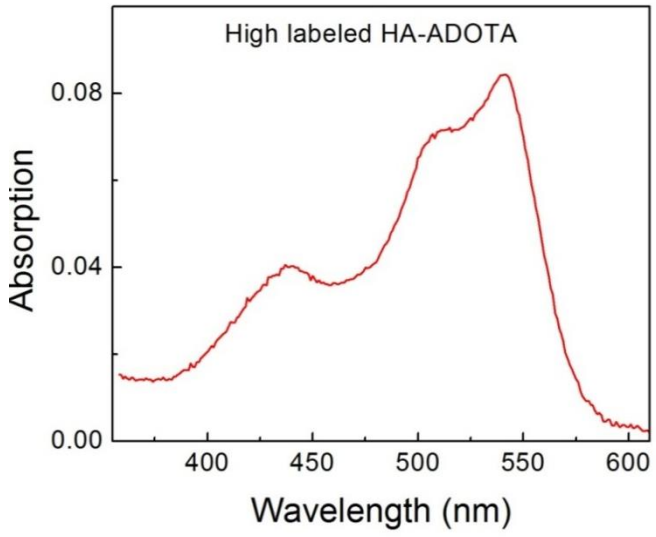

Figure 1: The absorption spectrum of HA-ADOTA probe in PBS (pH 7.4). The concentration of ADOTA in HA-ADOTA probe is 13.96 μM. HA-ADOTA probe in the assay system is 70 nM.

Figure 1 shows the absorption spectrum of HA-ADOTA probe in PBS solution at room temperature with the maximum absorption peak centered at 540 nm. A second transition is of lower oscillator strength with peak centered at 440 nm. As it can be seen from Fig. 1, even though the main absorption peak is centered at 540 nm, a 470-nm excitation is also enough to

excite the probe. Furthermore, a complete emission spectrum can be obtained when the probe is excited using a 470-nm excitation source. The concentration of the ADOTA in the stock HA-ADOTA is 13.96 μM. The probe was diluted 200 times in the assay system (70 nM). The normalized emission spectra of HA-ADOTA probe and free ADOTA fluorophore in PBS following a 470-nm excitation are shown in Fig. 2A. It can be seen from the graph that the emission spectra of free fluorophore are centered at 560 nm, whereas the peak emission of HA-ADOTA probe is centered at 605 nm. The 45-nm shift in the peak emission wavelength was obtained due to aggregation of the fluorophore molecules. This shift in the peak emission proves the efficient energy transfer between the ADOTA molecules and in fact shows the efficient design of this biosensor. The excitation spectra and emission spectra of HA-ADOTA probe before and after enzymatic cleavage with 100 U/mL of hyaluronidase are shown in Fig. 2B. It can be seen from Fig. 2B that the emission spectrum of the digested probe shifts back to its original peak emission wavelength of 560 nm, whereas the intact probe has a peak emission wavelength centered at 605 nm. This aggregation-induced shift in the emission wavelength allows for an efficient method to ratiometrically detect the enzyme activity by measuring the fluorescence intensity at two wavelengths, i.e. 560 and 605 nm. The ratiometric sensing provides a built-in self-calibration and higher accuracy in terms of quantitative analysis. We also observed a small change in the excitation spectra of HA-ADOTA probe before and after cleavage by hyaluronidase. The shift in the emission wavelength of the HA-ADOTA probe is also visible to the eye. Figure 2C shows the change in the color of the solution containing HA-ADOTA probe before and after enzymatic cleavage, when excited using a handheld blue laser. We also estimated the quantum yield of the ADOTA monomer and aggregates by mimicking the monomer/aggregate system in thin polyvinyl alcohol (PVA) films with low and high

concentration of ADOTA. The estimated quantum yield for monomer is 55 %, whereas the quantum yield for aggregate ADOTA system is less than 1 %. The details about quantum yield measurement are given in the Electronic Supplementary Material (ESM, Fig. S1).

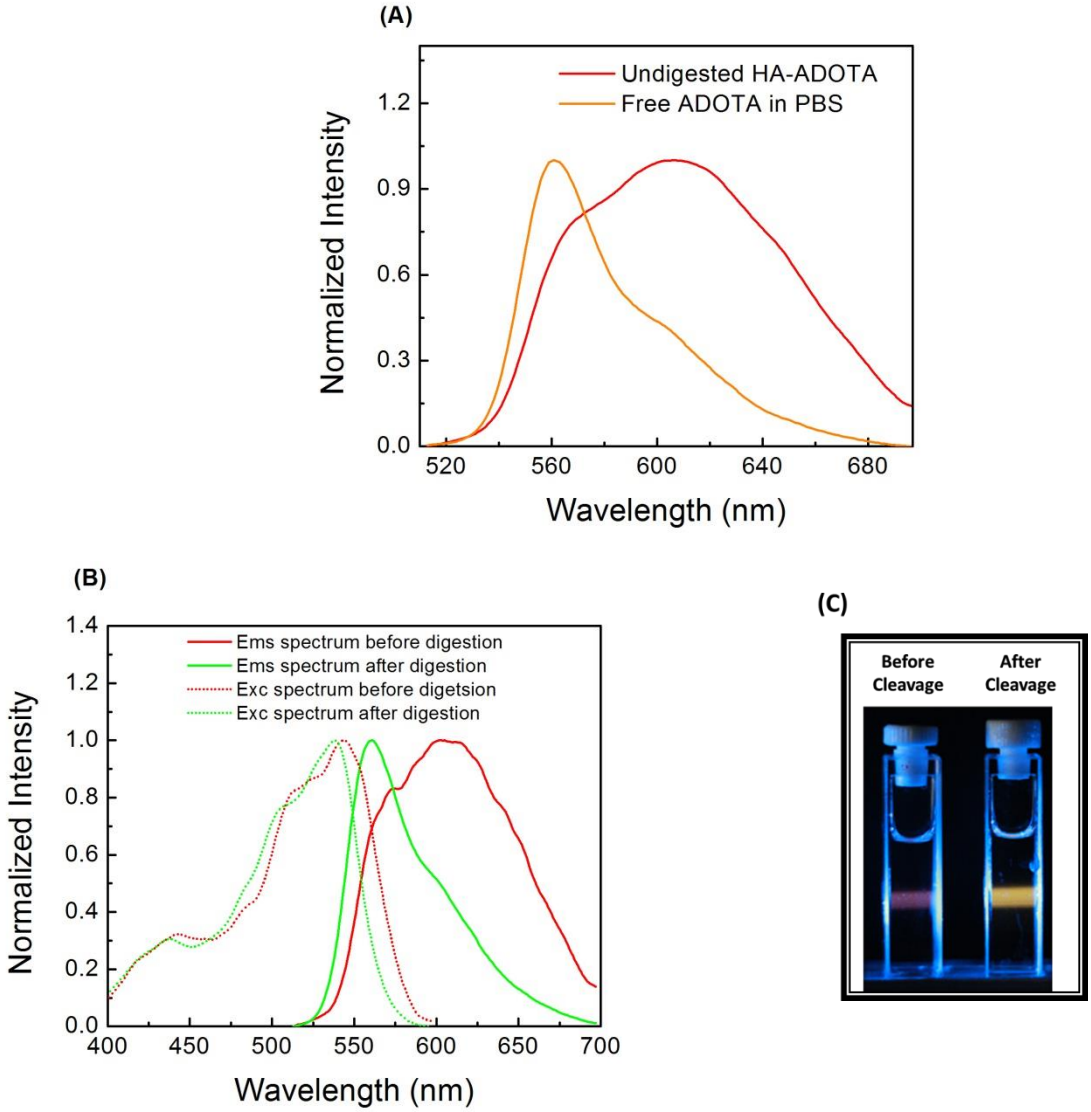

Figure 2 : (A)- Shows the normalized emission spectra of free ADOTA fluorophore in PBS (pH 7.4) and the emission spectra of HA-ADOTA probe (70nM ADOTA) in PBS (pH 7.4) when excited using a 470 nm light source. (B)- The excitation and emission spectra of heavily labeled HA-ADOTA (70 nM ADOTA) probe before and after enzymatic cleavage. The large spectral

overlap between excitation and emission spectra is responsible for an efficient excitation energy migration (HOMO-FRET) between ADOTA molecules. The energy migration between ADOTA molecules is responsible for the self-quenching process. (C)- Pictorial representation of the change in the color of HA-ADOTA solution before and after hyaluronidase cleavage.

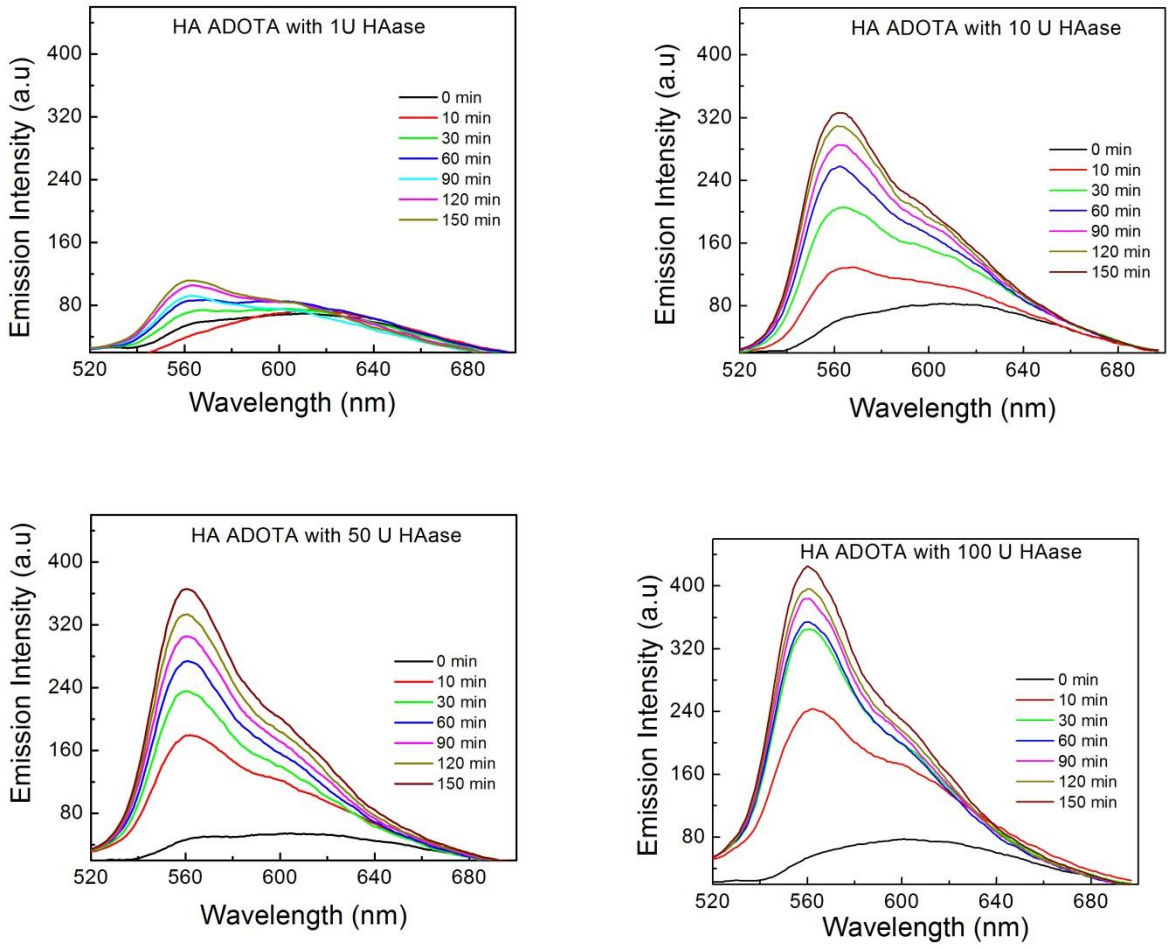

Figure 3: The change is fluorescence emission of HA-ADOTA probe (70 nM ADOTA, PBS pH7.4) after incubation with different amount of hyaluronidase enzyme. The fluorescence emission spectra was collected for 150 minutes. A 470 nm laser was used for the excitation and the experiments were performed in triplicate and a same increase in fluorescence intensity was observed.

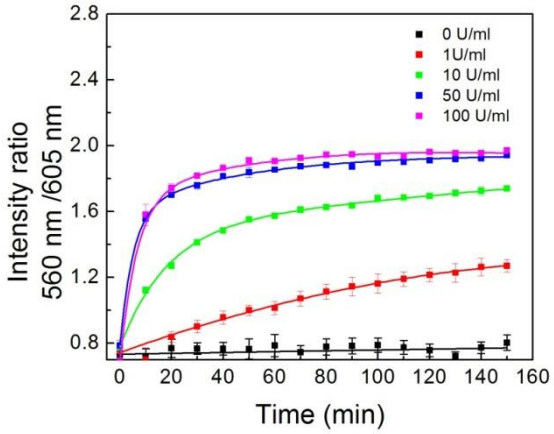

Figure 4: Change is the ratio of emission intensity (560nm/605nm) of the assay system (70 nm ADOTA) in PBS buffer (PBS 7.4) at room temperature vs reaction time in the presence of different amount hyaluronidase. A 470 nm laser was used for excitation and all the experiments were performed in triplicate.

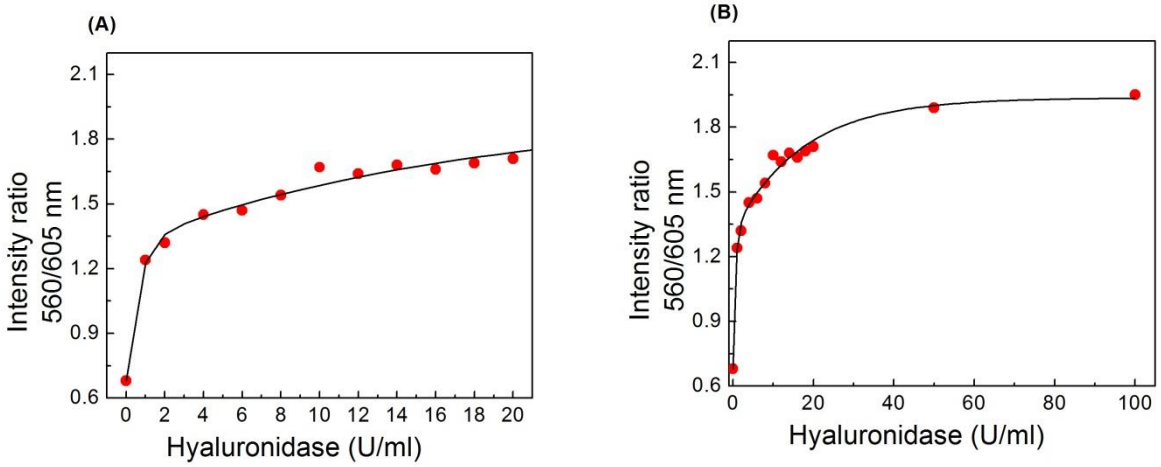

Figure 5: The calibration curve for the intensity ratio of HA-ADOTA (70 nM ADOTA) probe in PBS (pH 7.4) at 100 minute as a function of hyaluronidase level (A) 0-20 U/ml, (B) 0-100 U/ml.

4.1. Response of HA-ADOTA probe with hyaluronidase

As mentioned, the HA-ADOTA probe was synthesized by heavy labeling of hyaluronic acid with ADOTA fluorophore through covalent bond formation. To investigate the response of the biosensor towards hyaluronidase, the fluorescence response of HA-ADOTA probe to hyaluronidase at varying concentration was investigated by adding hyaluronidase to HA-ADOTA probe (70 nM ADOTA) in PBS (pH 7.4) at room temperature. Figure 3 shows the hyaluronidase concentration dependent change in the fluorescence intensity of the HA-ADOTA probe. The fluorescence intensity of the reaction system increases with increasing concentration of hyaluronidase from 0 to 100 U/mL of hyaluronidase. Even 1 U/mL of hyaluronidase was enough to increase the fluorescence intensity and causes the shift in the peak emission of the HA-ADOTA probe. In the case of 1 U/mL of hyaluronidase, the fluorescence intensity shows 1.7 times enhancement in the fluorescence signal, whereas, in the case of 100 U/mL of enzyme, 5.6 times enhancement in the fluorescence signal was observed. The emission intensity for different amount of hyaluronidase are drawn to the same scale so as to easily distinguish the change in the fluorescence enhancement with different amount of enzyme.

The kinetic assay of the enzymatic reaction was determined by measuring the time-dependent change in the fluorescence intensity of the HA-ADOTA probe in the absence and presence of hyaluronidase. We assessed the change in fluorescence intensity for all concentrations of enzyme every 10 min for 150 min and calculated the change in the intensity ratio using the fluorescence intensity at 560 and 605 nm as the observation points. From Fig. 4, it can be seen that in the absence of hyaluronidase, we did not notice any change in the ratio of fluorescence intensity, which proves the stability of HA-ADOTA probe. The time-dependent fluorescence intensity measurement shows that the emission intensity ratio at 560 and 605 nm gradually increases with

increasing amount of enzyme and time. It was also observed from Fig. 4 that the emission intensity ratio almost reaches a plateau after 80 min of reaction when the enzyme concentration was 50 U/mL or higher. To ensure the reaction was complete, we took 100 min as the end point in our experiment. Figure 5A represents the calibration curve obtained by measuring the change in the fluorescence intensity after 100 min as a function of hyaluronidase activity for enzyme within 0–20 U/mL, whereas Fig. 5B represents the entire region with 0–100 U/mL. Both the curves were fitted using exponential model ($Y= A_1*e^{(-X/t1)}+A_2*e^{(-X/t2)}+Y_o$, $R^2= 0.98$). Detail about the fitting method is given in the supplementary data. Using this standard curve, the level of hyaluronidase from an unknown sample can be easily determined.

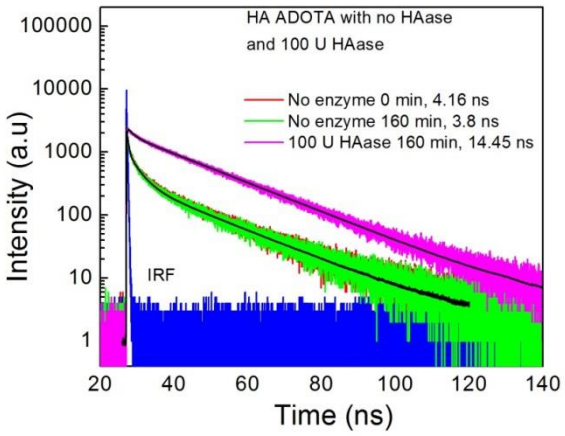

Figure 6: The fluorescence intensity decay of HA-ADOTA probe (70 nm ADOTA, 0.6mg/ml HA) in PBS (pH 7.4) in the absence and presence of hyaluronidase. In the prescence of enzyme, an increase in the fluorescence lifetime was observed. Without the enzyme at 0 min 3 components are needed to fit the data with amplitudes of 0.16, 0.53 and 0.31 with the lifetime of 18 ns, 0.41 ns and 3.23 ns. With 100U/ml of hyaluronidase at 160 minutes, the decay was fitted

using 2 coponents with amplitudes of 0.74 and 0.26 with lifetime of 18.85 ns and 1.83 ns. All fluorescence lifetime measurements were performed in triplicate.

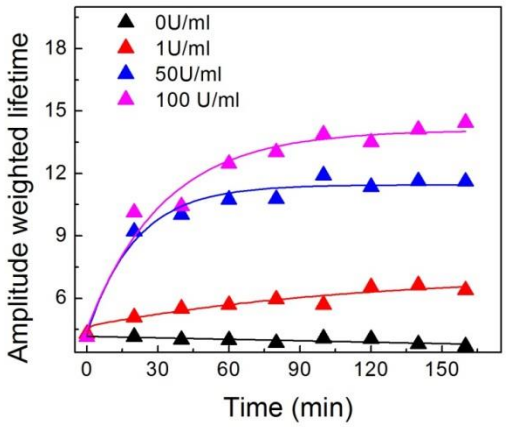

Figure 7: The time dependent change in the fluorescence lifetime of HA-ADOTA probe (70 nM ADOTA) in PBS (pH 7.4) in the absence and presence of hyaluronidase.

4.2. Fluorescence lifetime-based sensing of hyaluronidase

We also desired to determine if the observed spectral changes are as well accompanied by the change in the fluorescence lifetime of the HA-ADOTA probe. The fluorescence intensity decay measurements are presented in Fig. 6 for HA-ADOTA probe in PBS at room temperature. The emission of the HAADOTA probe is highly quenched in the absence of hyaluronidase and shows a heterogenous decay. Three exponentials are needed to fit the data, and an amplitude-weighted lifetime of 4 ns is determined as compared to 20 ns lifetime for free fluorophore in PBS. In the presence of hyaluronidase, the amplitude-weighted lifetime increases with the increasing amount of enzyme. Table 1 shows the detailed analysis of the intensity decay of HA-ADOTA probe with different concentrations of hyaluronidase (0, 1, 10, 50, and 100 U/mL). The recovered average amplitude-weighted lifetime of HA-ADOTA probe with 100 U/mL of hyaluronidase was 15 ns, and two components were needed to fit the decay with amplitudes of 0.74 and 0.26 and lifetime

of 18.85 and 1.83 ns. Figure 7 shows the change in the amplitude-weighted fluorescence lifetime of HA-ADOTA probe with different amounts of enzyme. It can be observed from the graph that with an increasing concentration of hyaluronidase and increasing time, an increase in the fluorescence lifetime is also observed. The time-resolved measurements demonstrate the generation of free unquenched ADOTA dyes ($\tau \sim 19$ ns) in the presence of hyaluronidase.

Hyaluronidase concentration	Time (min)								
	0	20	40	60	80	100	120	140	160
0U	4.16ns	4.16ns	4.02ns	4ns	3.86ns	4.08ns	4.05ns	3.8ns	3.8ns
1U	4.3ns	5.09ns	5.51ns	5.69ns	6.07ns	8.35ns	8.63ns	8.77ns	8.89ns
50U	4.16ns	9.22ns	10.03ns	10.75ns	10.78ns	11.91ns	11.36ns	11.64ns	11.62ns
100 U	4.16ns	10.13ns	10.44ns	12.47ns	13.03ns	13.88ns	13.5ns	14.11ns	14.45ns

Table1: Amplitude weighted lifetime of HA-ADOTA with different amount of hyaluronidase. Averaged amplitude weighted lifetime of HA-ADOTA probe was estimated every 20 minute of the enzymatic reaction**.**

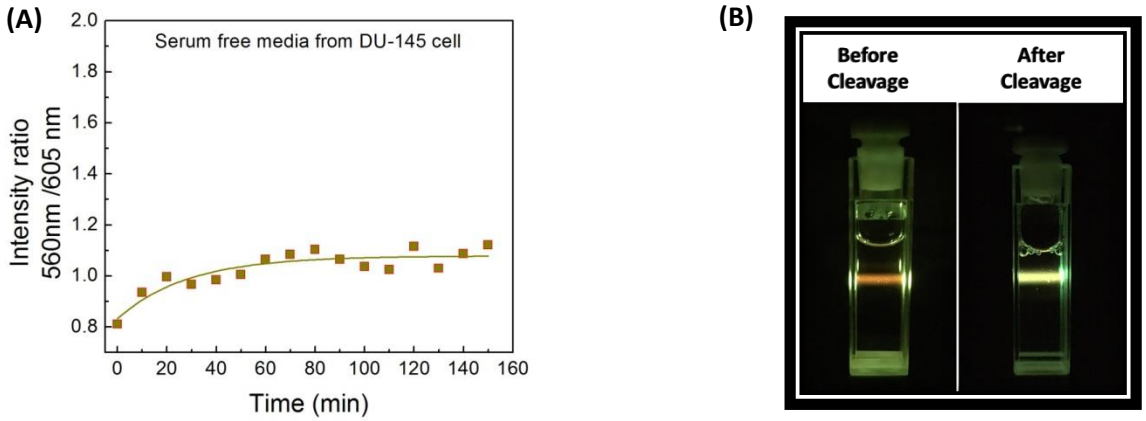

Figure 8: (A) Change is the ratio of emission intensity (560nm/605nm) from cell culture media as a function of change in time. A 470 nm excitation was used and the reaction was continued for 150 min at room temperature. All the experiments were performed in triplicate. (B) change in the colour of fluorescence emission of HA-ADOTA probe in culture media before and after enzymatic cleavage.

Time (min)	DU-145 media	DU-145 media with apigenin
Background	2.56 ns	2.07 ns
10	4.81 ns	2.8 ns
20	11.09 ns	4.3 ns
30	13.97 ns	5.1 ns
40	14.93 ns	4.14 ns
50	15.25 ns	5.28 ns
60	16.35 ns	3.48 ns
70	18.13 ns	4.56 ns
80	17.74 ns	5.24 ns
90	18.21 ns	4.03 ns
100	17.74 ns	3.85 ns
110	18 ns	4.28 ns
120	17.72 ns	4.3 ns
130	18.37 ns	4.12 ns
140	17.94 ns	4.78 ns
150	17.9 ns	4.87 ns

Table II: Amplitude weighted fluorescence lifetime of HA-ADOTA probe media collected from DU-145 cell line. Data also shows the effect of apigenin on the inhibition of hyaluronidase activity from culture

4.3. Estimating hyaluronidase activity in cell culture media

It has been previously reported that several prostate cancer cell lines overexpress hyaluronidase activity. DU-145 is one such cell line which is reported to have overexpression of hyaluronidase. To investigate the activity of hyaluronidase produced by DU-145 prostate cancer cell line, we measured enzyme activity in concentrated serum-free culture media using an HAADOTA probe. In a solution of 100 μL of concentrated media and PBS (pH 7.4), HA-ADOTA probe (70 nM ADOTA in assay system) was added (total volume 1000 μL). The change in fluorescence intensity ratio was calculated every 10 min for 150 min (Fig. 8). The intensity ratio at 100 min was used to estimate hyaluronidase level using the standard curve obtained from spiked PBS buffer solution (Fig. 5). The calculated hyaluronidase level was 5 U/mL. To confirm if the fluorescence enhancement was caused by hyaluronidase, the effect of apigenin (inhibitor of hyaluronidase) was also examined on the activity of hyaluronidase [5,55,56]. Stock solution (20 mM) of apigenin was prepared in DMSO. The final concentration of apigenin in experimental solution was 50 μM. It was observed that the apigenin inhibited the fluorescence enhancement of HA-ADOTA probe. To confirm our steady-state fluorescence intensity data, we also measured the change in the fluorescence lifetime of HA-ADOTA probe in the concentrated serum-free media. Of concentrated media with PBS and HA-ADOTA probe (100 μL total volume), 10 μL was added to a glass bottom petri dish. Fluorescence lifetime was measured using a time-resolved microscope (MicroTime 200, PicoQuant, Germany). The main advantage of using confocal microscope with TCSPC abilities can help us to focus exactly at the center of the media while simultaneously only needing a small volume of the biological sample. The measured amplitude-weighted fluorescence lifetime of the undigested probe was around 4.5 ns. However, after 150 min of enzymatic reaction in the concentrated culture media, a fluorescence lifetime of 18 ns was

measured. We also measured the effect of apigenin (hyaluronidase inhibitor) on the fluorescence lifetime of HA-ADOTA probe. Apigenin solution (50 μM) was prepared with 10 μL concentrated media and PBS (total volume= 100 μL). We found that the apigenin inhibited the activity of hyaluronidase and fluorescence lifetime of HAADOTA probe stayed constant (4.5 ns). These data suggest that the increase in fluorescence intensity and fluorescence lifetime indeed arises from the hyaluronidase activity. The amplitude-weighted fluorescence lifetime of HA-ADOTA probe in concentrated media with and without apigenin is given in Table 2.

5. Conclusions

In summary, we have successfully developed a biosensor for hyaluronidase using an orange/red-emitting organic ADOTA fluorophore with a long fluorescence lifetime. This probe serves as an intensity-based ratiometric sensor and fluorescence lifetime-based sensor of hyaluronidase. Moreover, due to ratiometric sensing ability, a higher sensitivity can be achieved. The change in color of the fluorescence emission of undigested (red) and digested (yellow) HA-ADOTA probe can also be observed by the naked eyes using an appropriate excitation. Compared to other biosensors developed over nanoparticles, the biosensor developed using organic fluorophore is much smaller in size. The large difference between the fluorescence lifetime of undigested and digested probe helps to easily quantify hyaluronidase level using fluorescence lifetime as detection parameter. Emission in the orange/red region where there is a long fluorescence lifetime makes this probe highly useful for biological samples which possess a large amount of autofluorescence. It is a widely understood phenomenon that the contribution of autofluorescence decreases in the orange/red region of the electromagnetic spectrum. We

successfully estimated the level of hyaluronidase in serum-free culture media of DU-145 prostate cancer cells. In conclusion, this HA-ADOTA biosensor can be easily used to measure hyaluronidase activity/level in complex pathological samples where the enzyme hyaluronidase is overexpressed.

Supplementary data

Quantum yield determination

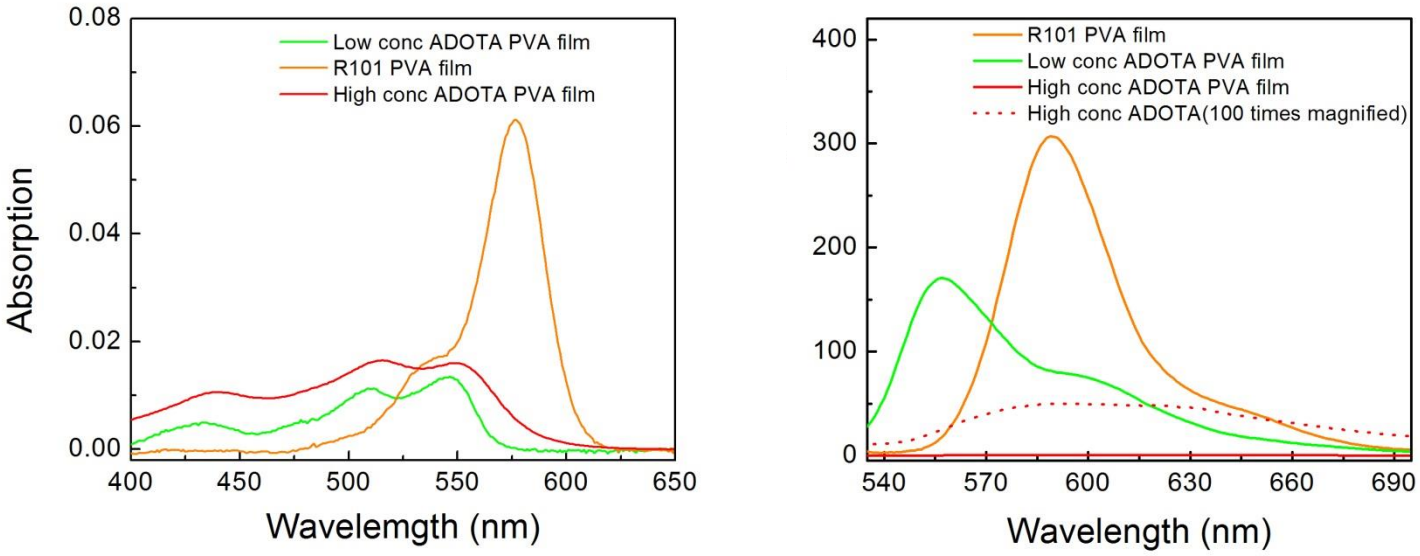

Figure S1: Left panel-Absorption spectra of low concentration of ADOTA, high concentration of ADOTA and low concentration of rhodamine 101 in thin PVA film. **Right panel**- Emission spectra of all three samples in PVA films.

It not possible to estimate the quantum yield (QY) of ADOTA aggregate in HA-ADOTA system as the system is not homogenous and hence true QY cannot be calculated. Also, the concentration we use in our system is very very low (70 nM ADOTA) and hence absorption spectra cannot be measured. To calculate the QY approximately, we mimic the monomer and aggregate system of ADOTA by incorporating low and high concentration in thin PVA films to represent monomer and aggregate system. Rhodamine 101 was used as a reference dye as it has a very high QY (almost 100%) and the emission spectra of rhodamine 101 is between the emission peak for monomer (560nm) and aggregate(605 nm). It can be seen from the absorption spectra

that the absorption spectrum of low concentration ADOTA PVA films intersect the rhodamine 101 absorption at 522 nm. Hence, we chose 522 nm as our excitation because at that wavelength the photons absorbed by both the samples will be equal. When excited at 522 nm, low concentration ADOTA PVA films has approximately half emission intensity compared to the rhodamine 101 film which shows that low concentration ADOTA film or monomer system has approximately 50% QY compared to rhodamine 101 system. Whereas, the high concentration ADOTA PVA film has a very very low emission intensity even when the absorption spectrum represents higher concentration. We corrected the emission spectrum of high concentration ADOTA PVA film for its excitation. The emission spectrum of high concentration film is multiplied 100 times to represent the shape of the spectrum in aggregated high concentration PVA film.

Fitting equation for Figure 5A and 5B

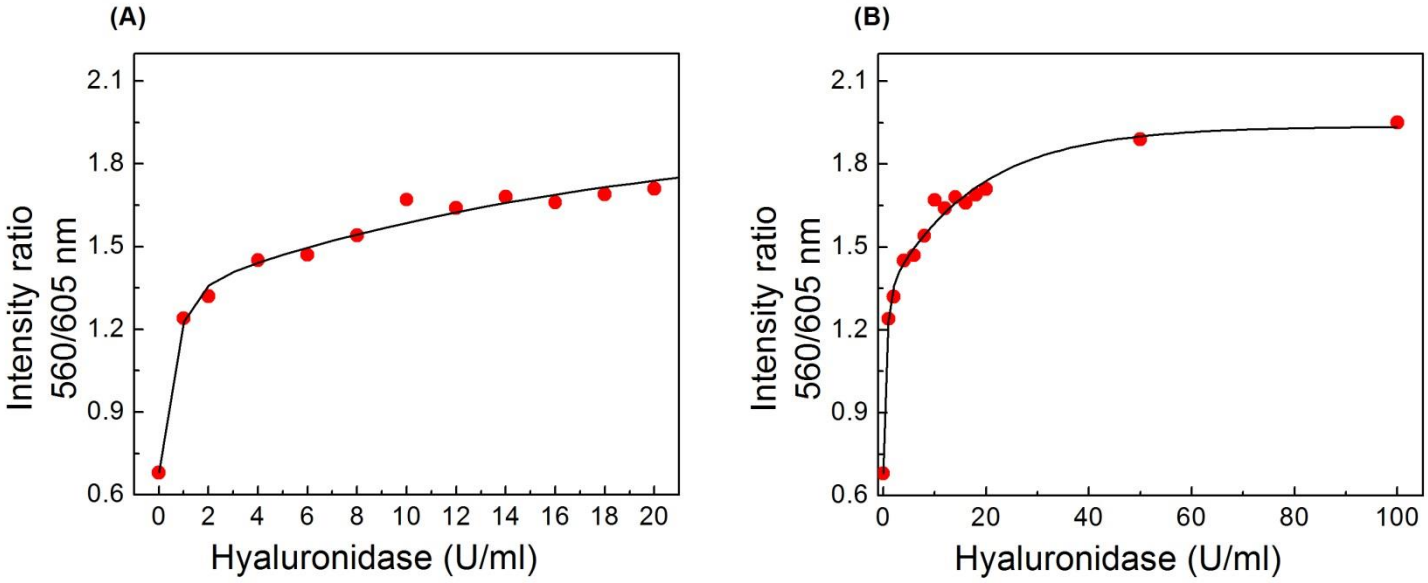

The data was fitted using multiexponential model (2 exponents) with R^2 of 0.98.

The equation used for figure is $Y= A_1*e^{(-X/t1)}+A_2*e^{(-X/t2)}+Y_o$

Where, A_1 and A_2 are amplitudes, t_1 and t_2 are constant and Y_o is offset

A_1=-0.6210, A_2 = -0.6310, t_1 = 17.338, t_2= 0.61, Y_o= 1.93

References

1. Stern R. Hyaluronidases in cancer biology. . 2008;18(4):275-280.

2. Chao KL, Muthukumar L, Herzberg O. Structure of human hyaluronidase-1, a hyaluronan hydrolyzing enzyme involved in tumor growth and angiogenesis. *Biochemistry (N Y)*. 2007;46(23):6911-6920.

3. Bollet AJ, Bonner WM, Nance JL. The presence of hyaluronidase in various mammalian tissues. *J Biol Chem*. 1963;238:3522-3527.

4. Franzmann EJ, Schroeder GL, Goodwin WJ, Weed DT, Fisher P, Lokeshwar VB. Expression of tumor markers hyaluronic acid and hyaluronidase (HYAL1) in head and neck tumors. *International journal of cancer*. 2003;106(3):438-445.

5. Liu D, Pearlman E, Diaconu E, et al. Expression of hyaluronidase by tumor cells induces angiogenesis in vivo. *Proc Natl Acad Sci U S A*. 1996;93(15):7832-7837.

6. Lokeshwar VB, Estrella V, Lopez L, et al. HYAL1-v1, an alternatively spliced variant of HYAL1 hyaluronidase: A negative regulator of bladder cancer. *Cancer Res*. 2006;66(23):11219-11227. doi: 66/23/11219 [pii].

7. Chain E, Duthie E. Identity of hyaluronidase and spreading factor. *Br J Exp Pathol*. 1940;21(6):324.

8. Hobby GL, Dawson MH, Meyer K, Chaffee E. The relationship between spreading factor and hyaluronidase. *J Exp Med*. 1941;73(1):109-123.

9. McCUTCHEON M, COMAN DR. Spreading factor in human carcinomas. *Cancer Res*. 1947;7(6):379-382.

10. Turley EA, Noble PW, Bourguignon LY. Signaling properties of hyaluronan receptors. *J Biol Chem*. 2002;277(7):4589-4592. doi: 10.1074/jbc.R100038200 [doi].

11. Girish K, Kemparaju K. The magic glue hyaluronan and its eraser hyaluronidase: A biological overview. *Life Sci*. 2007;80(21):1921-1943.

12. Stern R. Hyaluronan catabolism: A new metabolic pathway. *Eur J Cell Biol*. 2004;83(7):317-325.

13. Stern R. Hyaluronan metabolism: A major paradox in cancer biology. *Pathologie Biologie*. 2005;53(7):372-382.

14. Stern R, Asari AA, Sugahara KN. Hyaluronan fragments: An information-rich system. *Eur J Cell Biol*. 2006;85(8):699-715.

15. Lokeshwar VB, Rubinowicz D, Schroeder GL, et al. Stromal and epithelial expression of tumor markers hyaluronic acid and HYAL1 hyaluronidase in prostate cancer. *J Biol Chem*. 2001;276(15):11922-11932. doi: 10.1074/jbc.M008432200 [doi].

16. DORFMAN A, OTT ML. A turbidimetric method for the assay of hyaluronidase. *J Biol Chem*. 1948;172(2):367-375.

17. Knudsen P, Koefoed J. Viscometric determination of hyaluronidase activity in biological fluids. *Scand J Clin Lab Invest*. 1961;13(4):673-682.

18. Stern M, Stern R. An ELISA-like assay for hyaluronidase and hyaluronidase inhibitors. *Matrix*. 1992;12(5):397-403.

19. Pham HT, Block NL, Lokeshwar VB. Tumor-derived hyaluronidase: A diagnostic urine marker for high-grade bladder cancer. *Cancer Res*. 1997;57(4):778-783.

20. Bonner W, Cantey EY. Colorimetric method for determination of serum hyaluronidase activity. *Clinica Chimica Acta*. 1966;13(6):746-752.

21. Steiner B, Cruce D. A zymographic assay for detection of hyaluronidase activity on polyacrylamide gels and its application to enzymatic activity found in bacteria. *Anal Biochem*. 1992;200(2):405-410.

22. Podyma KA, Yamagata S, Sakata K, Yamagata T. Difference of hyaluronidase produced by human tumor cell lines with hyaluronidase present in human serum as revealed by zymography. *Biochem Biophys Res Commun*. 1997;241(2):446-452.

23. Cheng D, Han W, Yang K, Song Y, Jiang M, Song E. One-step facile synthesis of hyaluronic acid functionalized fluorescent gold nanoprobes sensitive to hyaluronidase in urine specimen from bladder cancer patients. *Talanta*. 2014;130:408-414.

24. Chib R, Raut S, Fudala R, et al. FRET based ratio-metric sensing of hyaluronidase in synthetic urine as a biomarker for bladder and prostate cancer. *Curr Pharm Biotechnol*. 2013;14(4):470-474. doi: CPB-EPUB-20130109-1 [pii].

25. Fudala R, Mummert ME, Gryczynski Z, Rich R, Borejdo J, Gryczynski I. Lifetime-based sensing of the hyaluronidase using fluorescein labeled hyaluronic acid. *Journal of Photochemistry and Photobiology B: Biology*. 2012;106:69-73.

26. Huang Y, Song C, Li H, et al. Cationic conjugated polymer/hyaluronan-doxorubicin complex for sensitive fluorescence detection of hyaluronidase and tumor-targeting drug delivery and imaging. *ACS applied materials & interfaces*. 2015.

27. Liu S, Zhao N, Cheng Z, Liu H. Amino-functionalized green fluorescent carbon dots as surface energy transfer biosensors for hyaluronidase. *Nanoscale*. 2015;7(15):6836-6842.

28. Murai T, Kawashima H. A simple assay for hyaluronidase activity using fluorescence polarization. *Biochem Biophys Res Commun*. 2008;376(3):620-624.

29. Wang Z, Li X, Song Y, Li L, Shi W, Ma H. An upconversion luminescence nanoprobe for the ultrasensitive detection of hyaluronidase. *Anal Chem*. 2015.

30. Rich RM, Mummert M, Foldes-Papp Z, et al. Detection of hyaluronidase activity using fluorescein labeled hyaluronic acid and fluorescence correlation spectroscopy. *Journal of Photochemistry and Photobiology B: Biology*. 2012;116:7-12.

31. Fudala R, Mummert ME, Gryczynski Z, Gryczynski I. Fluorescence detection of hyaluronidase. *Journal of Photochemistry and Photobiology B: Biology*. 2011;104(3):473-477.

32. Hu Q, Zeng F, Wu S. A ratiometric fluorescent probe for hyaluronidase detection via hyaluronan-induced formation of red-light emitting excimers. *Biosensors and Bioelectronics*. 2016;79:776-783.

33. Song Y, Wang Z, Li L, Shi W, Li X, Ma H. Gold nanoparticles functionalized with cresyl violet and porphyrin via hyaluronic acid for targeted cell imaging and phototherapy. *Chemical Communications*. 2014;50(99):15696-15698.

34. Wang W, Cameron AG, Ke S. Developing fluorescent hyaluronan analogs for hyaluronan studies. *Molecules*. 2012;17(2):1520-1534.

35. Zhang L, Mummert ME. Development of a fluorescent substrate to measure hyaluronidase activity. *Anal Biochem*. 2008;379(1):80-85.

36. Xie H, Zeng F, Wu S. Ratiometric fluorescent biosensor for hyaluronidase with hyaluronan as both nanoparticle scaffold and substrate for enzymatic reaction. *Biomacromolecules*. 2014;15(9):3383-3389.

37. Huang C, Chiang C, Lin Z, Lee K, Chang H. Bioconjugated gold nanodots and nanoparticles for protein assays based on photoluminescence quenching. *Anal Chem*. 2008;80(5):1497-1504.

38. Folmar M, Shtoyko T, Fudala R, et al. Metal enhanced fluorescence of me-ADOTA· cl dye by silver triangular nanoprisms on a gold film. *Chemical Physics Letters*. 2012;531:126-131.

39. Chib R, Raut S, Shah S, et al. Steady state and time resolved fluorescence studies of azadioxatriangulenium (ADOTA) fluorophore in silica and PVA thin films. *Dyes and Pigments*. 2015;117:16-23.

40. Laursen BW, Sørensen TJ. Synthesis of super stable triangulenium dye. *J Org Chem*. 2009;74(8):3183-3185.

41. Maliwal BP, Fudala R, Raut S, et al. Long-lived bright red emitting azaoxa-triangulenium fluorophores. . 2013.

42. Shtoyko T, Raut S, Rich RM, et al. Preparation of plasmonic platforms of silver wires on gold mirrors and their application to surface enhanced fluorescence. *ACS applied materials & interfaces*. 2014;6(21):18780-18787.

43. Sørensen TJ, Laursen BW, Luchowski R, et al. Enhanced fluorescence emission of me-ADOTA by self-assembled silver nanoparticles on a gold film. *Chemical physics letters*. 2009;476(1):46-50.

44. Sørensen TJ, Thyrhaug E, Szabelski M, et al. Azadioxatriangulenium: A long fluorescence lifetime fluorophore for large biomolecule binding assay. *Methods and applications in fluorescence*. 2013;1(2):025001.

45. Raut SL, Rich R, Shtoyko T, et al. Sandwich type plasmonic platform for MEF using silver fractals. *Nanoscale*. 2015;7(42):17729-17734.

46. Bogh SA, Bora I, Rosenberg M, Thyrhaug E, Laursen BW, Sørensen TJ. Azadioxatriangulenium: Exploring the effect of a 20 ns fluorescence lifetime in fluorescence anisotropy measurements. *Methods and Applications in Fluorescence*. 2015;3(4):045001.

47. W Laursen B, C Krebs F. Synthesis, structure, and properties of azatriangulenium salts. *Chemistry-A European Journal*. 2001;7(8):1773-1783.

48. Bora I, Bogh SA, Santella M, Rosenberg M, Sørensen TJ, Laursen BW. Azadioxatriangulenium: Synthesis and photophysical properties of reactive dyes for bioconjugation. *European Journal of Organic Chemistry*. 2015.

49. Deng Y, Feng X, Zhou M, Qian Y, Yu H, Qiu X. Investigation of aggregation and assembly of alkali lignin using iodine as a probe. *Biomacromolecules*. 2011;12(4):1116-1125.

50. Guo Z, Park S, Yoon J, Shin I. Recent progress in the development of near-infrared fluorescent probes for bioimaging applications. *Chem Soc Rev*. 2014;43(1):16-29.

51. Ajayaghosh A, Carol P, Sreejith S. A ratiometric fluorescence probe for selective visual sensing of Zn2. *J Am Chem Soc*. 2005;127(43):14962-14963.

52. Fan J, Hu M, Zhan P, Peng X. Energy transfer cassettes based on organic fluorophores: Construction and applications in ratiometric sensing. *Chem Soc Rev*. 2013;42(1):29-43.

53. Niu L, Guan Y, Chen Y, Wu L, Tung C, Yang Q. BODIPY-based ratiometric fluorescent sensor for highly selective detection of glutathione over cysteine and homocysteine. *J Am Chem Soc*. 2012;134(46):18928-18931.

54. Lokeshwar VB, Lokeshwar BL, Pham HT, Block NL. Association of elevated levels of hyaluronidase, a matrix-degrading enzyme, with prostate cancer progression. *Cancer Res*. 1996;56(3):651-657.

55. Kuppusamy U, Das N. Inhibitory effects of flavonoids on several venom hyaluronidases. *Experientia*. 1991;47(11-12):1196-1200.

56. Tung J, Mark GE, Hollis GF. A microplate assay for hyaluronidase and hyaluronidase inhibitors. *Anal Biochem*. 1994;223(1):149-152.

Chapter 6

Azadioxatriangulenium (ADOTA) fluorophore for imaging of hyaluronidase activity

Abstract

A fluorescence lifetime imaging probe with a long lifetime was used in combination with time-gating for the detection of hyaluronidase using hyaluronic acid as the probe template. This probe was developed by heavily labeling hyaluronic acid with long lifetime azadioxatriangulenium fluorophores (ADOTA). We used this probe to image hyaluronidase produced by DU-145 prostate cancer cell

1. Introduction

Fluorescence microscopy techniques for cellular imaging are essential to explore various physiological and pathological processes occurring inside the cell. Confocal fluorescence imaging is one of the most widely used methods in biomedical research due to its high sensitivity and spatial resolution [1,2]. However, conventional fluorescence intensity based imaging is affected by the laser excitation intensity and fluorophore concentration. As an alternate approach, fluorescence lifetime-based measurements are independent of the excitation intensity and fluorophore concentration [2-4]. Fluorescence lifetime is sensitive to its microenvironment and even slight variations in the microenvironment can trigger easily measured changes in the

fluorescence lifetime of the fluorophore, which are not observable in conventional fluorescence intensity measurements.

Fluorescence lifetime imaging microscopy (FLIM) was first used for live cell imaging in the early 1990s [5]. Imaging of exogenous fluorescent probes that target diseased cells have shown promising results in clinical settings, such as early detection of cancer [6,7]. Developing a fluorescent probe for imaging cancer cells is a challenging approach which requires special fluorescent probes specific to biomarkers produced by the cancer cells. Hence, developing a fluorescent probe, which can easily be recognized by an enzyme overexpressed by cancer cells would be an ideal approach. Hyaluronidase is one such enzyme which is reported to be overexpressed in various cancers like melanoma, prostate, bladder cancer, head and neck carcinoma, *etc* [8-11]. Hyaluronic acid is the substrate for the enzyme hyaluronidase, which is a naturally occurring glycosaminoglycan with a molecular weight ranging from 500-5000 Dalton. It is composed of multiple subunits of glucuronic acid and N-acetyl Glucosamine [12-14]. With rapid growth and development in biomedical nanotechnology, development of novel fluorescent material is gaining increasing attention among the scientific community [15]. For FLIM imaging, it is ideal to use a fluorophore with a long fluorescence lifetime so as to easily distinguish its signal from the autofluorescence. Autofluorescence has a lifetime roughly around 1-7 ns which is comparable to the fluorescence lifetime of commonly available organic fluorophores [16,17]. Even with the long fluorescence lifetime and superior optical properties of quantum dots, they are of limited use due to several disadvantages. Specifically, quantum dots with NIR emission are large in size and can introduce perturbations in the targeted cell. Also, toxicity due to toxic core materials used in synthesis further limits their usage in biomedical research. Lastly, despite their

good photostability, they show photo-blinking which can affects the emission signal during imaging [18-21].

In our previous study, we have developed and characterized a novel probe for the sensing of hyaluronidase activity. This probe was developed by heavy labeling of hyaluronic acid with a triangulenium fluorophore called azadioxatriangulenium (ADOTA) [22]. ADOTA is a triangulenium dye, a group of cationic dyes with excellent photophysical properties. The most important characteristic property of ADOTA dye is the rare combination of relatively low oscillator strength of the emissive transition and high quantum yield, which give rise to a long fluorescence lifetime of ~17 ns with an emission in the orange/red region of the electromagnetic spectrum [23-28].

Hyaluronic acid is the substrate for the enzyme hyaluronidase and heavy labeling of ADOTA results in the aggregation of fluorophore molecules on hyaluronic acid (HA). It is a known phenomenon that aggregation of fluorophore results in a decrease of fluorescence lifetime of the fluorophore. We have previously shown that HA-ADOTA probe can easily be used to detect hyaluronidase activity in spiked PBS solution with 1 U/ml-100 U/ml of hyaluronidase via steady-state and time-resolved fluorescence spectroscopy. We have also shown the application of this probe in detecting hyaluronidase activity in cellular media of DU-145 prostate cancer cell line [22]. However, we wanted to check if the change in the fluorescence lifetime of the HA-ADOTA probe before and after cleavage by hyaluronidase produced by the cancer cells can be used as a contrast mechanism to detect hyaluronidase activity via fluorescence-lifetime imaging. Here in this report, we have used HA-ADOTA probe as a fluorescence lifetime-based sensing agent for the lifetime-based imaging of hyaluronidase in cancer cells. We have used this developed HA-ADOTA probe to detect hyaluronidase activity in DU-145 cells, a prostate cancer

cell line which is reported in the literature to overexpress hyaluronidase enzyme [11,29]. Heavy labeling of HA with ADOTA results in the short lifetime of ADOTA via aggregation. Therefore, it becomes quenched in its native state. However, when the HA-ADOTA probe is cleaved by the enzyme hyaluronidase, and the long chains of the polymer are cleaved into shorter ones, the distance between the fluorophores increases leading to an increase in both fluorescence intensity and fluorescence lifetime. This change in the fluorescence lifetime of the probe is significant enough that it can easily be distinguished by FLIM and works as a contrast agent. To date, various luminescent probes for the detection of hyaluronidase are reported in the literature [30-46]. To the best of our knowledge, this is the first fluorescent probe with long fluorescence lifetime developed for the lifetime-based imaging of hyaluronidase in cancer cells.

As mentioned previously, the presence of autofluorescence is a major problem with cellular imaging. Even with the very sophisticated instruments, it is really difficult to completely eliminate autofluorescence. The popular organic dyes like fluorescein or rhodamine, which are best excited with 470, 488 and 532 nm excitation sources also provide efficient excitation of intrinsic fluorophore like flavoproteins and flavones which contributes to autofluorescence [47,48]. One very successful approach to overcome this problem is to use pulsed excitation and time-resolved detection using a probe with long fluorescence lifetime. By a technique called time-gated detection, the fluorescence signal originating from long lived fluorescent probe can be easily separated from the signal coming from the short lived autofluorescence [49,50]. Due to the long fluorescence lifetime of the probe after digestion compared to the background fluorescence (autofluorescence), we can easily use time-gated detection to completely remove autofluorescence from the image. Also, due to long fluorescence lifetime of this probe after

digestion by hyaluronidase, this probe can be used for the fluorescence lifetime imaging of hyaluronidase.

2. Material and methods

2.1. Materials

Sodium hyaluronate from bacterial fermentation was obtained from Acros Organics (Thermo Fisher Scientific, Fair Lawn, NJ). Dulbecco's phosphate-buffered saline (PBS), Fetal bovine serum (FBS), DMEM media, antibiotic, Insulin transferrin and selenium(ITS) supplement, Slide-A-Lyser dialysis cassettes (10,000 molecular weight cutoff) were purchased from Theromo Fisher Scientific (Waltham, MA). Dimethyl sulfoxide (DMSO), guanidine hydrochloride, acetaldehyde, cyclohexyl isocyanide and centricon filter (30,000 Mol cut off) were obtained from Sigma-Aldrich (Sigma-Aldrich, St. Louis, MO). DU-145 (prostate cancer) and PZ-HPV-7 (Healthy prostate cells) were purchased from ATCC (Manassas, VA). The ADOTA fluorophore (N-(4-Aminophenyl) -azadioxatriangulenium Tetrafluoroborate) was synthesized by a procedure described elsewhere [24]. All compounds, solvents, and materials were used as received; water was used directly from a Millipore (Billerica, MA) purification system.

2.2. Methods

2.2.1. Preparation of HA-ADOTA probe

The starting material for the preparation of the reactive amine of the AzaDiOxaTriaAngulenium (ADOTA-phenyl-NH_2) was prepared according to the method described by Bora et al. [24]. HA was dissolved to 1.25 mg/mL in dH2O and then diluted 1:2 in DMSO. The ADOTA-NH_2 was

dissolved in DMSO and added to the HA solution for a final ADOTA-NH_2 concentration of 25 mg/mL. Acetaldehyde and cyclohexyl isocyanide were added to 0.04 % (v/v) and the reaction was allowed to proceed for 48 hr at 25 °C. Afterwards, the solution was diluted 1:14 in ethanol/guanidine HCl (50 μL of 3 M guanidine HCl per 900 μL of 100 % ethanol) and the HA-ADOTA allowed to precipitate overnight at −20 °C. The precipitate was then dissolved in 1 mL of dH_2O followed by extensive dialysis against dH_2O [51]. The concentration of HA in the probe was measured using ELISA kit for hyaluronidase.

2.2.2. Cellular staining

The DU-145 cell line was grown in 2 mL of DMEM media containing 10% FBS and 1% antibiotic solution in a glass bottom petri dish. After almost 70% confluency, DMEM media with FBS was removed and washed three times with serum free media. Cells were then incubated with serum free media containing ITS supplement. After 72 hours, the prepared petri dishes were used for imaging without any further washing. The PZ-HPV-7 healthy prostate cells were grown in Keratinocyte serum free media. After 70% confluency, the media was replaced, washed three times with fresh media and replaced with fresh 2 mL of Keratinocyte–SFM media. The cells were used for imaging after 72 hours. Apigenin was used as an inhibitor for hyaluronidase in DU-145 cells. A 20 mM stock solution of apigenin was prepared with DMSO for this experimental setup. To the growing DU-145 cells in 2ml of serum free DMEM media, 50 μM of apigenin was added and incubated at 37^{o} C for 30 minutes. After incubation, the cells were used for imaging without any further washing.

2.2.3. Fluorescence lifetime imaging

The HA-ADOTA probe was added to a glass bottom plate (10 μL of HA-ADOTA probe in 2 mL of media) and used for measuring the fluorescence lifetime of HA-ADOTA in the samples of

DU-145 cells and PZ-HPV-7 cells. A confocal microscope equipped with time-correlated single photon counting (TCSPC) detector was used (MicroTime 200, PicoQuant, Germany). A 470 nm laser operating at 5 MHz repetition rate was used. The sample is prepared in a glass bottom petri dish and the laser excitation is used on Olympus 1X71 inverted microscope with a water immersion 60x/1.2 NA objective. The signal from the detector was routed into a PicoHarp 300 (PicoQuant, Germany) time-correlated single counting (TCSPC) module. Fluorescence lifetime measurements were acquired for 15 minutes. All experiments were performed three times and all analyses were performed using SymPho Time, V.5.3.2 software from PicoQuant.

2.2.4. Time-gated intensity imaging

To eliminate the interference from the autofluorescence and scattering light, we have used time-gated detection using the long fluorescence lifetime of cleaved HA-ADOTA probe. In time-gated detection, a time-delay threshold, or gate, is set and only photons collected after the gate are integrated in the total intensity. Since autofluorescence has a decay lifetime of ~ 1-7 ns, depending on the type of tissue or cells, the intensity decay of autofluorescence dies out faster than the fluorescence decay of ADOTA (lifetime ~ 17 ns). Therefore, we may remove the autofluorescence signal by setting the time gate to a few nanoseconds after the excitation pulse. Moreover, since the spectral profile of autofluorescence overlaps with the spectral profiles of commonly available red emitting organic fluorophore, temporal separation of the autofluorescence from the fluorophore of interest is advantageous. However, the commonly used red emitting organic fluorophores have a very short fluorescence lifetime, comparable to that of autofluorescence of tissues and cells. This issue can be resolved by using the ADOTA fluorophore which has a long fluorescence lifetime and can help in time-gated imaging of cells without any background. The fluorescence lifetime of digested HA-ADOTA is much longer than

the autofluorescence lifetime, that is, it continues to fluoresce long after the autofluorescence has decayed completely. In our experiments, we always used a 2 ns gating time to remove scattered excitation light, as all the image are analyzed via tail fitting. After that, 5 ns, 10 ns, 15 ns and 20 ns are used as gating times to completely remove autofluorescence.

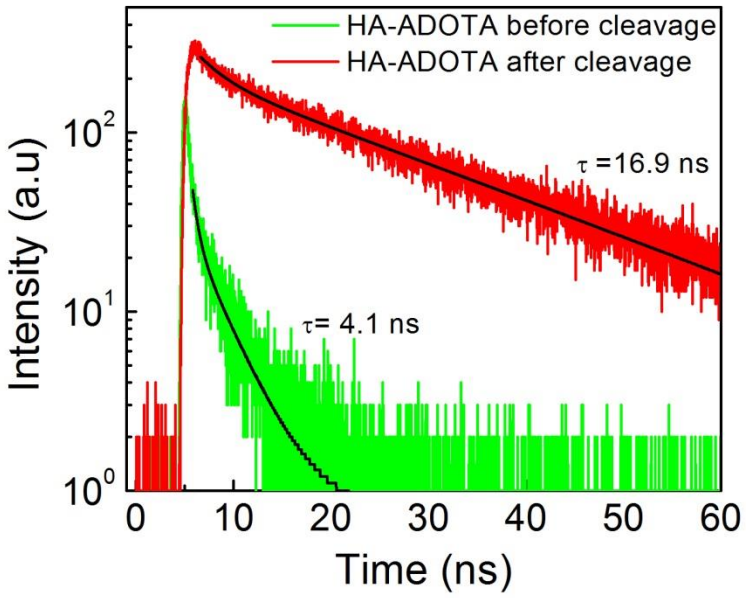

Figure 1: Fluorescence lifetime decay of HA-ADOTA probe in media collected from DU-145 cells after 72 hours. An increase in amplitude weighted fluorescence lifetime was observed after the cleavage of HA-ADOTA by hyaluronidase for 15 minutes produced by the DU-145 cells. The data is the representation of three independent experiments.

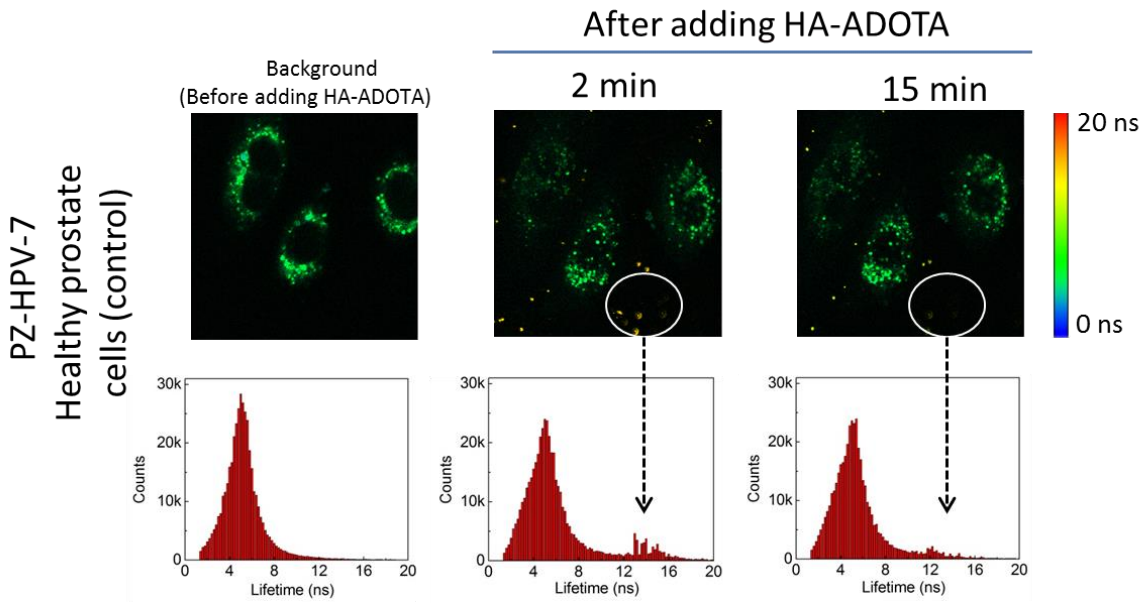
After adding HA-ADOTA
Background
(Before adding HA-ADOTA)
2 min
15 min
20 ns
0 ns
PZ-HPV-7
Healthy prostate
cells (control)
Counts
Lifetime (ns)

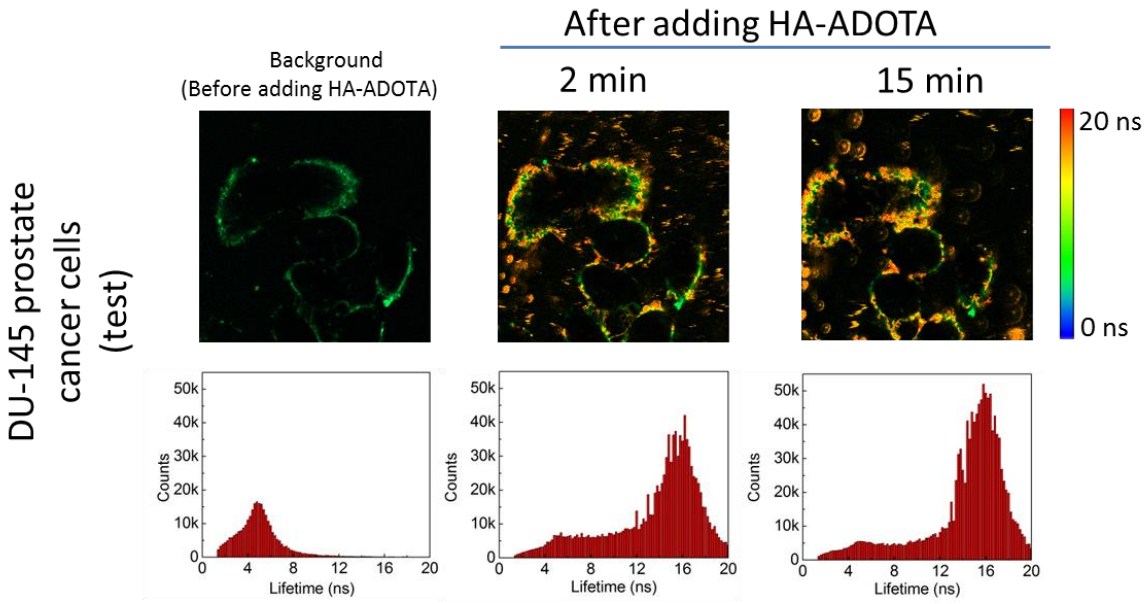
After adding HA-ADOTA
Background
(Before adding HA-ADOTA)
2 min
15 min
20 ns
0 ns
DU-145 prostate
cancer cells
(test)
Counts
Lifetime (ns)

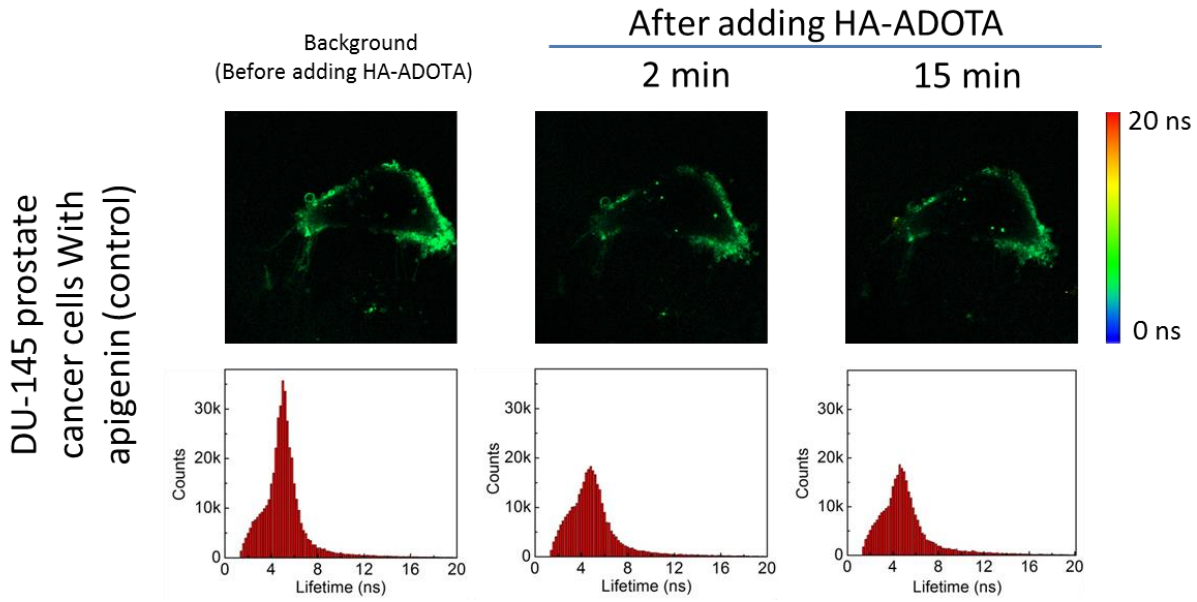

Figure 2: Fluorescence lifetime images of PZ-HPV-7 (Healthy prostate cells) and DU-145 cancer cell lines with and without HA-ADOTA. The long fluorescence lifetime of ~16 ns was observed for digested HA-ADOTA probe by hyaluronidase in DU-145 cells.

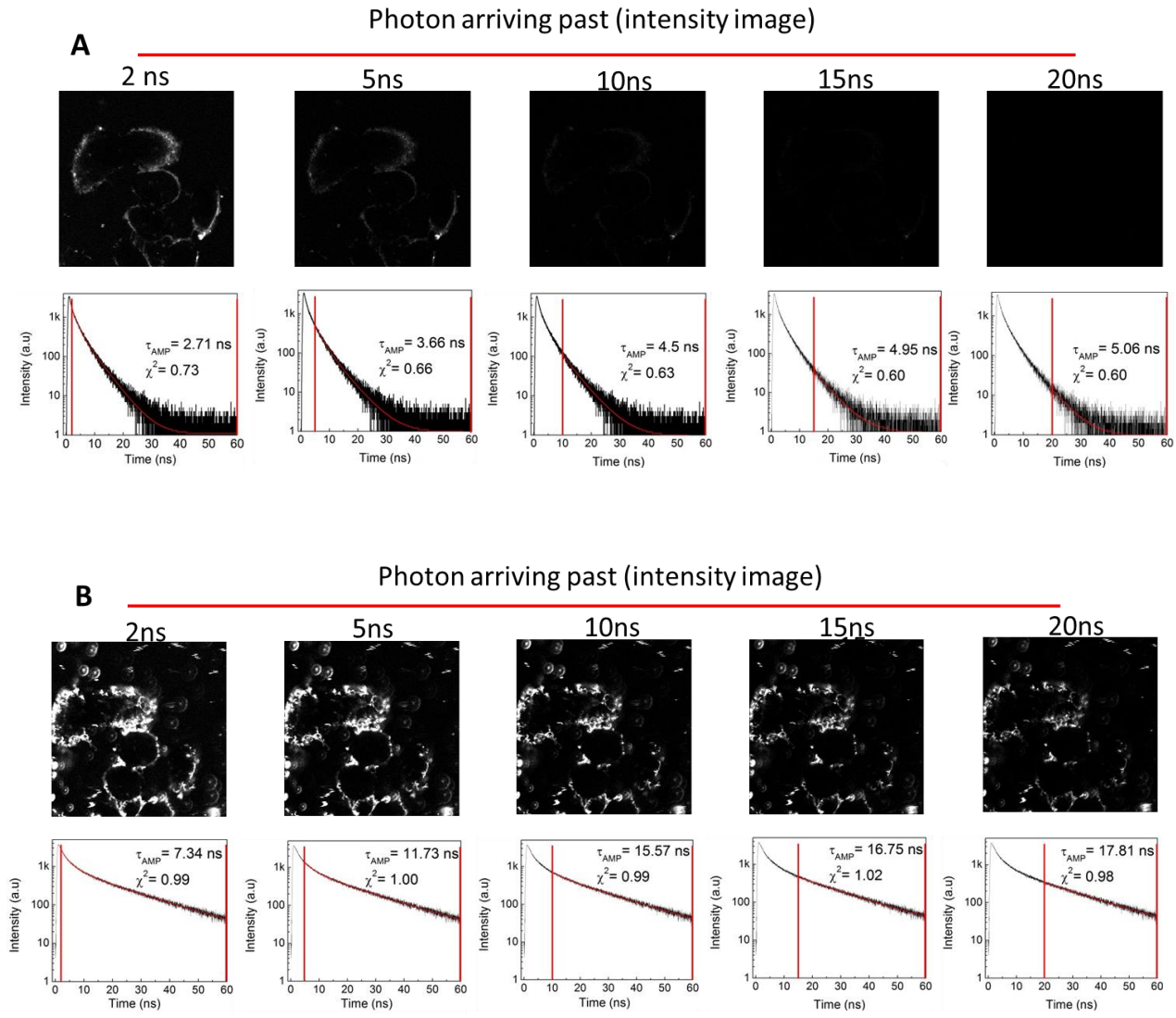

Figure 3: Time gated analysis of background from DU-145 cells (A) and DU-145 cells with HA-ADOTA (B) after 15 minute of incubation with 2ns, 5ns, 10ns, 15ns and 20 ns gating after the excitation pulse. The data is the representation of three independent experiments.

3. Results

In cellular imaging using fluorescence intensity, the contribution from light scattering and sample autofluorescence imparts large background signal to all images. Fluorescence lifetime imaging microscopy (FLIM) offers two big advantages, namely the separation of fluorescence emission not only spectrally by wavelength or emission color but also temporally by fluorescent lifetime. The concentration of HA in the probe was measured using an ELISA kit for hyaluronic acid and was found to be 0.6 mg/mL. The concentration of the ADOTA in the stock HA-ADOTA is 13.96 μM. The concentration of ADOTA used in the final experiment setup is 70 nM. After the addition of HA-ADOTA probe to the media collected from DU-145 cells, a time dependent increase in the fluorescence lifetime was observed when the enzyme starts to cleave the HA-ADOTA probe. The average amplitude weighted fluorescence lifetime of intact HA-ADOTA probe is ~ 4 ns. After cleavage of HA-ADOTA probe by the hyaluronidase present in the media for 15 minutes, a longer fluorescence lifetime of ~ 17 ns was observed (Figure 1). Figure 2 shows the fluorescence lifetime of HA-ADOTA probe in PZ-HPV-7 (Control), DU-145 and DU-145 cells treated with inhibitor (apigenin). All the cells shows a background fluorescence lifetime centred approximately at 4.5 ns which can be observed from the lifetime distribution graph for both PZ-HPV-7 and DU-145 prostate cells. After adding HA-ADOTA probe to all three experimental setup, fluorescence lifetime images were taken and no change in the fluorescence lifetime of HA-ADOTA probe was observed from the PZ-HPV-7 cells (healthy prostate cells). Only a weak signal around 14 ns was observed, which is possibly due to the presence of a very low level of hyaluronidase produced by the healthy prostate cells [29]. This shows that the prepared HA-ADOTA probe is even sensitive to a very small level of hyaluronidase produced by the

healthy prostate cells. However, in case of DU-145 prostate cancer cells, a long fluorescence lifetime was observed just after 2 min, which proves a large concentration of hyaluronidase in the media and the digestion of HA-ADOTA probe immediately after adding HA-ADOTA. It can be observed from Figure 2, in case of DU-145 cell, the counts around 4 ns lifetime are very small compared to the counts around 16 ns lifetime. After 15 min, the signal around 16 ns becomes even higher compared to the signal at 2 min, which proves further cleavage of HA-ADOTA probe by hyaluronidase enzyme produced by the DU-145 cells. It can be observed from the FLIM image of DU-145 cells at 2 and 15 minutes that the main cleavage of HA-ADOTA is occurring around the cell membrane which is represented as orange/red color in the FLIM image. The orange/red color signal representing the long fluorescence lifetime can also be observed from the media of DU-145 cells, which shows the presence of hyaluronidase in the media of DU-145 cells. In case of PZ-HPV-7 cells, no change in fluorescence lifetime was observed. The FLIM data shows that the cleaved HA-ADOTA probe indeed has a longer fluorescence lifetime when digested by hyaluronidase produced by the DU-145 prostate cancer cells. To further confirm that the HA-ADOTA was cleaved by hyaluronidase exclusively produced by DU-145 cells, we used apigenin, which is a known inhibitor for the enzyme hyaluronidase [52-58]. Data from the apigenin experiments shows no change in the fluorescence lifetime of the HA-ADOTA probe (Figure 2). This confirms the cleavage of HA-ADOTA is by the hyaluronidase enzyme. Further time-gating was applied to the images to completely remove autofluorescence. Figure 3A shows the time resolved intensity image of DU-145 cells without HA-ADOTA to represent autofluorescence lifetime. It can be seen from the Figure 3A that autofluorescence completely dies out after 10 ns of gating. If gating is allowed past 10 ns, no significant signal was observed.

Figure 3B, shows the same DU-145 cells treated with HA-ADOTA for 15 min (fluorescence intensity image). It can be seen from the figure that a significant signal was observed even after 15 and 20 ns gating, which is collected from our ADOTA fluorophore, as the autofluorescence completely vanishes at 15 ns. This confirms the collected signal after 15 ns gating is from our fluorophore of interest and guarantees background free cellular imaging.

4. Conclusions

In conclusion, we have demonstrated the use of the FLIM methodology in the detection of hyaluronidase using the long lifetime organic fluorophore ADOTA. The long fluorescence lifetime of cleaved HA-ADOTA facilitates the discrimination between the signal from the probe and the intrinsic fluorescence of the cells and produces a good signal-to-noise ratio. Due to long fluorescence lifetime and efficient time-gated detection, the signal-to-noise ratio was further enhanced showing application of the organic ADOTA fluorophore dye with a long fluorescence lifetime. This fluorescence lifetime-based sensing will be used for the detection of hyaluronidase for any type of cancer which overexpresses hyaluronidase. To the best of our knowledge, this is the first time that FLIM based detection of hyaluronidase has been used in cancer cells. This methodology can be extended to the detection of hyaluronidase in various other cancer cells and exploration of the advantage of a long fluorescence lifetime of the ADOTA fluorophore in the detection of other biomarkers. This method in the future can be used to detect a variety of transient cellular processes or diseases completely free from background fluorescence.

References

1. Amos WB, White J, Fordham M. Use of confocal imaging in the study of biological structures. *Appl Opt*. 1987;26(16):3239-3243.

2. Lakowicz JR, Szmacinski H, Nowaczyk K, Berndt KW, Johnson M. Fluorescence lifetime imaging. *Anal Biochem*. 1992;202(2):316-330.

3. Bastiaens PI, Squire A. Fluorescence lifetime imaging microscopy: Spatial resolution of biochemical processes in the cell. *Trends Cell Biol*. 1999;9(2):48-52.

4. Gadella TW, Jovin TM, Clegg RM. Fluorescence lifetime imaging microscopy (FLIM): Spatial resolution of microstructures on the nanosecond time scale. *Biophys Chem*. 1993;48(2):221-239.

5. Cubeddu R, Taroni P, Valentini G, Canti G. Use of time-gated fluorescence imaging for diagnosis in biomedicine. *Journal of Photochemistry and Photobiology B: Biology*. 1992;12(1):109-113.

6. Savariar EN, Felsen CN, Nashi N, et al. Real-time in vivo molecular detection of primary tumors and metastases with ratiometric activatable cell-penetrating peptides. *Cancer Res*. 2013;73(2):855-864. doi: 10.1158/0008-5472.CAN-12-2969 [doi].

7. Erickson SJ, Martinez SL, DeCerce J, Romero A, Caldera L, Godavarty A. Three-dimensional fluorescence tomography of human breast tissues in vivo using a hand-held optical imager. *Phys Med Biol*. 2013;58(5):1563.

8. Stern R. Hyaluronidases in cancer biology. . 2008;18(4):275-280.

9. Franzmann EJ, Schroeder GL, Goodwin WJ, Weed DT, Fisher P, Lokeshwar VB. Expression of tumor markers hyaluronic acid and hyaluronidase (HYAL1) in head and neck tumors. *International journal of cancer*. 2003;106(3):438-445.

10. Liu D, Pearlman E, Diaconu E, et al. Expression of hyaluronidase by tumor cells induces angiogenesis in vivo. *Proc Natl Acad Sci U S A*. 1996;93(15):7832-7837.

11. Lokeshwar VB, Rubinowicz D, Schroeder GL, et al. Stromal and epithelial expression of tumor markers hyaluronic acid and HYAL1 hyaluronidase in prostate cancer. *J Biol Chem*. 2001;276(15):11922-11932. doi: 10.1074/jbc.M008432200 [doi].

12. Girish K, Kemparaju K. The magic glue hyaluronan and its eraser hyaluronidase: A biological overview. *Life Sci*. 2007;80(21):1921-1943.

13. Stern R. Hyaluronan catabolism: A new metabolic pathway. *Eur J Cell Biol*. 2004;83(7):317-325.

14. Stern R. Hyaluronan metabolism: A major paradox in cancer biology. *Pathologie Biologie*. 2005;53(7):372-382.

15. Chatterjee DK, Gnanasammandhan MK, Zhang Y. Small upconverting fluorescent nanoparticles for biomedical applications. *Small*. 2010;6(24):2781-2795.

16. Berezin MY, Achilefu S. Fluorescence lifetime measurements and biological imaging. *Chem Rev*. 2010;110(5):2641-2684.

17. Sarder P, Maji D, Achilefu S. Molecular probes for fluorescence lifetime imaging. *Bioconjug Chem*. 2015.

18. Derfus AM, Chan WC, Bhatia SN. Probing the cytotoxicity of semiconductor quantum dots. *Nano letters*. 2004;4(1):11-18.

19. Resch-Genger U, Grabolle M, Cavaliere-Jaricot S, Nitschke R, Nann T. Quantum dots versus organic dyes as fluorescent labels. *Nature methods*. 2008;5(9):763-775.

20. Michalet X, Pinaud FF, Bentolila LA, et al. Quantum dots for live cells, in vivo imaging, and diagnostics. *Science*. 2005;307(5709):538-544. doi: 307/5709/538 [pii].

21. Hauck TS, Anderson RE, Fischer HC, Newbigging S, Chan WC. In vivo quantum-dot toxicity assessment. *Small*. 2010;6(1):138-144.

22. Chib R, Mummert M, Bora I, et al. Fluorescent biosensor for the detection of hyaluronidase: Intensity-based ratiometric sensing and fluorescence lifetime-based sensing using a long lifetime azadioxatriangulenium (ADOTA) fluorophore. *Analytical and Bioanalytical Chemistry*. 2016:1-11.

23. Bogh SA, Bora I, Rosenberg M, Thyrhaug E, Laursen BW, Sørensen TJ. Azadioxatriangulenium: Exploring the effect of a 20 ns fluorescence lifetime in fluorescence anisotropy measurements. *Methods and Applications in Fluorescence*. 2015;3(4):045001.

24. Bora I, Bogh SA, Santella M, Rosenberg M, Sørensen TJ, Laursen BW. Azadioxatriangulenium: Synthesis and photophysical properties of reactive dyes for bioconjugation. *European Journal of Organic Chemistry*. 2015;2015(28):6351-6358.

25. Chib R, Raut S, Shah S, et al. Steady state and time resolved fluorescence studies of azadioxatriangulenium (ADOTA) fluorophore in silica and PVA thin films. *Dyes and Pigments*. 2015;117:16-23.

26. Maliwal BP, Fudala R, Raut S, et al. Long-lived bright red emitting azaoxa-triangulenium fluorophores. . 2013.

27. Raut SL, Rich R, Shtoyko T, et al. Sandwich type plasmonic platform for MEF using silver fractals. *Nanoscale*. 2015;7(42):17729-17734.

28. Thyrhaug E, Sørensen TJ, Gryczynski I, Gryczynski Z, Laursen BW. Polarization and symmetry of electronic transitions in long fluorescence lifetime triangulenium dyes. *The Journal of Physical Chemistry A*. 2013;117(10):2160-2168.

29. Lokeshwar VB, Lokeshwar BL, Pham HT, Block NL. Association of elevated levels of hyaluronidase, a matrix-degrading enzyme, with prostate cancer progression. *Cancer Res*. 1996;56(3):651-657.

30. An L, Liu L, Wang S. Cationic conjugated polymers for homogeneous and sensitive fluorescence detection of hyaluronidase. *Science in China Series B: Chemistry*. 2009;52(6):827-832.

31. Huang Y, Song C, Li H, et al. Cationic conjugated polymer/hyaluronan-doxorubicin complex for sensitive fluorescence detection of hyaluronidase and tumor-targeting drug delivery and imaging. *ACS applied materials & interfaces*. 2015;7(38):21529-21537.

32. Liu S, Zhao N, Cheng Z, Liu H. Amino-functionalized green fluorescent carbon dots as surface energy transfer biosensors for hyaluronidase. *Nanoscale*. 2015;7(15):6836-6842.

33. de Belder AN, Wik KO. Preparation and properties of fluorescein-labelled hyaluronate. *Carbohydr Res*. 1975;44(2):251-257.

34. Nagata H, Kojima R, Sakurai K, et al. Molecular-weight-based hyaluronidase assay using fluorescent hyaluronic acid as a substrate. *Anal Biochem*. 2004;330(2):356-358.

35. Zhang L, Mummert ME. Development of a fluorescent substrate to measure hyaluronidase activity. *Anal Biochem*. 2008;379(1):80-85.

36. Murai T, Kawashima H. A simple assay for hyaluronidase activity using fluorescence polarization. *Biochem Biophys Res Commun*. 2008;376(3):620-624.

37. Song Y, Wang Z, Li L, Shi W, Li X, Ma H. Gold nanoparticles functionalized with cresyl violet and porphyrin via hyaluronic acid for targeted cell imaging and phototherapy. *Chemical Communications*. 2014;50(99):15696-15698.

38. Cheng D, Han W, Yang K, Song Y, Jiang M, Song E. One-step facile synthesis of hyaluronic acid functionalized fluorescent gold nanoprobes sensitive to hyaluronidase in urine specimen from bladder cancer patients. *Talanta*. 2014;130:408-414.

39. Wang W, Cameron AG, Ke S. Developing fluorescent hyaluronan analogs for hyaluronan studies. *Molecules*. 2012;17(2):1520-1534.

40. Hu Q, Zeng F, Wu S. A ratiometric fluorescent probe for hyaluronidase detection via hyaluronan-induced formation of red-light emitting excimers. *Biosensors and Bioelectronics*. 2016;79:776-783.

41. Xie H, Zeng F, Wu S. Ratiometric fluorescent biosensor for hyaluronidase with hyaluronan as both nanoparticle scaffold and substrate for enzymatic reaction. *Biomacromolecules*. 2014;15(9):3383-3389.

42. Wang Z, Li X, Song Y, Li L, Shi W, Ma H. An upconversion luminescence nanoprobe for the ultrasensitive detection of hyaluronidase. *Anal Chem*. 2015.

43. Fudala R, Mummert ME, Gryczynski Z, Gryczynski I. Fluorescence detection of hyaluronidase. *Journal of Photochemistry and Photobiology B: Biology*. 2011;104(3):473-477.

44. Chib R, Raut S, Fudala R, et al. FRET based ratio-metric sensing of hyaluronidase in synthetic urine as a biomarker for bladder and prostate cancer. *Curr Pharm Biotechnol*. 2013;14(4):470-474. doi: CPB-EPUB-20130109-1 [pii].

45. Rich RM, Mummert M, Foldes-Papp Z, et al. Detection of hyaluronidase activity using fluorescein labeled hyaluronic acid and fluorescence correlation spectroscopy. *Journal of Photochemistry and Photobiology B: Biology*. 2012;116:7-12.

46. Fudala R, Mummert ME, Gryczynski Z, Rich R, Borejdo J, Gryczynski I. Lifetime-based sensing of the hyaluronidase using fluorescein labeled hyaluronic acid. *Journal of Photochemistry and Photobiology B: Biology*. 2012;106:69-73.

47. Munro AW, Noble MA. Fluorescence analysis of flavoproteins. In: *Flavoprotein protocols*. Springer; 1999:25-48.

48. Visser AJ, Ghisla S, Massey V, Müller F, Veeger C. Fluorescence properties of reduced flavins and flavoproteins. *European Journal of Biochemistry*. 1979;101(1):13-21.

49. Schneckenburger H, Gschwend MH, Sailer R, Mock HP, Strauss WS. Time-gated fluorescence microscopy in cellular and molecular biology. *Cell Mol Biol (Noisy-le-grand)*. 1998;44(5):795-805.

50. Mathejczyk JE, Pauli J, Dullin C, et al. Spectroscopically well-characterized RGD optical probe as a prerequisite for lifetime-gated tumor imaging. *Mol Imaging*. 2011;10:469-480.

51. Rich RM, Mummert M, Gryczynski Z, et al. Elimination of autofluorescence in fluorescence correlation spectroscopy using the AzaDiOxaTriAngulenium (ADOTA) fluorophore in combination with time-correlated single-photon counting (TCSPC). *Analytical and bioanalytical chemistry*. 2013;405(14):4887-4894.

52. Shukla S, Gupta S. Apigenin: A promising molecule for cancer prevention. *Pharm Res*. 2010;27(6):962-978.

53. Podyma KA, Yamagata S, Sakata K, Yamagata T. Difference of hyaluronidase produced by human tumor cell lines with hyaluronidase present in human serum as revealed by zymography. *Biochem Biophys Res Commun*. 1997;241(2):446-452.

54. Kang W, Zhou C, Koga Y, Baba T. Hyaluronan-degrading activity of mouse sperm hyaluronidase is not required for fertilization? *Journal of Reproduction and Development*. 2010;56(1):140-144.

55. Hunnicutt GR, Primakoff P, Myles DG. Sperm surface protein PH-20 is bifunctional: One activity is a hyaluronidase and a second, distinct activity is required in secondary sperm-zona binding. *Biol Reprod*. 1996;55(1):80-86.

56. Caltagirone S, Rossi C, Poggi A, et al. Flavonoids apigenin and quercetin inhibit melanoma growth and metastatic potential. *International Journal of Cancer*. 2000;87(4):595-600.

57. Murai T, Kawashima H. A simple assay for hyaluronidase activity using fluorescence polarization. *Biochem Biophys Res Commun*. 2008;376(3):620-624.

58. Trochon V, Blot E, Cymbalista F, et al. Apigenin inhibits endothelial-cell proliferation in G2/M phase whereas it stimulates smooth-muscle cells by inhibiting P21 and P27 expression. *International journal of cancer*. 2000;85(5):691-696.

Summary

Fluorescence based sensing and imaging has tremendous applications in biomedical sciences. Fluorescent probe specific to a disease biomarker can help in the diagnosis and treatment of various diseases like cancer. Fluorescence emission in the red region of the electromagnetic spectrum provides the best optical window for sensing and imaging, as the contribution of autofluorescence decreases in this region. To distinguish the signal from the fluorophore and autofluorescence, the efforts have been focused on developing red emitting fluorophore preferentially with long fluorescence lifetime (significantly longer than autofluorescence). This improves signal-to-noise ratio and opens the possibility for time-gated detection. However, the commercially available red fluorophores have a very short fluorescence lifetime. The groups of currently developed triangulenium fluorophores like Azadioxatriangulenium (ADOTA), which emits in the orange/red region with long fluorescence lifetime and high quantum yield, present a great opportunity for sensing and imaging.

In this dissertation, novel probes for the sensing and imaging of hyaluronidase have been developed. Both probes are synthesized using hyaluronic acid as a template. One probe has fluorescein and rhodamine as a FRET pair for sensing. Another probe was synthesized by heavy labeling of hyaluronic acid with ADOTA fluorophore.

Our first probe, HA-FRET was labeled with fluorescein and rhodamine, which is a classic FRET pair. The HA-FRET probe was characterized in synthetic urine. Steady-state data showed a time-dependent increase in the fluorescein to rhodamine intensity ratio after cleavage of the HA - FRET probe by hyaluronidase. Our steady-state data is also accompanied by time-resolved data where, an increase in fluorescence lifetime of the donor (fluorescein) was observed after the enzymatic cleavage. Our data confirm that fluorescent probe using hyaluronic acid as a template can be synthesized and used for the detection of hyaluronidase.

To develop another probe using azadioxatriangulenium (ADOTA) fluorophore, we first studied the photophysical properties of ADOTA in PVA film and silica thin films. A 15 nm red shift in the emission spectrum of ADOTA was observed in case of a silica thin film. Also, the fluorescence lifetime of ADOTA in silica thin film was 12 ns compared to 20 ns in PVA film. The lorentzian lifetime distribution showed a broad distribution of emitting species in silica thin film compared to the PVA film. The shorter lifetime and concentration dependent red shift in emission suggest aggregation of dye molecules in the excited state.

Above mentioned studies helped us developing another probe for HA activity. This probe was designed by heavy labeling of hyaluronic acid with ADOTA fluorophore. Heavily labeled probe showed a red shift in the peak emission spectrum. The intact probe has a peak emission spectrum centered at 605 nm, whereas, the cleaved probe moves the emission spectrum of the probe to its original wavelength i.e. 560 nm. The cleavage of the HA - ADOTA probe by hyaluronidase showed an increase in fluorescence intensity and fluorescence lifetime of the probe. The steady-state ratiometric sensing showed a time dependent increase in fluorescence intensity. Time-resolved data showed an increase in fluorescence lifetime of the probe cleaved by hyaluronidase. Intact HA-ADOTA probe has fluorescence lifetime around 4 ns whereas, the cleaved HA-ADOTA probe has lifetime around 18 ns. The HA - ADOTA probe was successfully used to estimate the level of hyaluronidase produced in the media of DU-145 prostate cancer cell line.

Finally, we showed the application of the HA - ADOTA probe in cellular imaging. Significant differences in the fluorescence lifetime of the HA-ADOTA probe before and after enzymatic cleavage, act as a good contrast agent in fluorescence lifetime imaging microscopy (FLIM). It is known from the literature that the DU-145 prostate cancer cells overexpress hyaluronidase activity. We have used the HA-ADOTA to image hyaluronidase activity in DU-145 cells. Our data showed a significant difference in the

fluorescence lifetime of intact and cleaved probe in FLIM images of the DU-145 cells. We also used HA-ADOTA probe with healthy prostate cells, which produces a high levels of hyaluronidase and with an inhibitor of hyaluronidase (apigenin) in DU-145 cells. No change in the fluorescence lifetime was observed, which shows the specificity of the HA - ADOTA probe towards hyaluronidase. We also examined the time-gated intensity imaging capability of this long-lived fluorescent probe to remove autofluorescence. We found that, if the detection is moved 10ns post excitation pulse, we can completely remove autofluorescence background from the DU-145 cells. However, we were still able to get a bright signal from our fluorescent probe even after 15 ns and 20 ns of gating. In summary, a fluorescent probe with long fluorescence lifetime was synthesized and characterized for sensing and imaging applications. This long-lived ADOTA fluorophore has tremendous applications in biomedical sciences for sensing and background-free cellular imaging.

Publications

APPENDIX A – First Author Publications included in this dissertation

- **R. Chib**, M. Mummert, I. Bora, B. W. Laursen, S. Shah, R. Pendry, I. Gryczynski, J. Borejdo, Z. Gryczynski, R. Fudala (2016), Fluorescent biosensor for the detection of hyaluronidase: intensity-based ratiometric sensing and fluorescence lifetime-based sensing using a long lifetime azadioxatriangulenium (ADOTA) fluorophore, Analytical and Bioanalytical Chemistry, 1-11.
- **R. Chib**, S. Raut, S. Shah, B. Grobelna, I. Akopova, R. Rich, T. J. Sørensen, B. W. Laursen, H. Grajek, Z. Gryczynski (2015), Steady state and time resolved fluorescence studies of azadioxatriangulenium (ADOTA) fluorophore in silica and PVA thin films, Dyes and Pigments 117, 16-23.
- **R. Chib**, S. Raut, R. Fudala, A. Chang, M. Mummert, R. Rich, Z. Gryczynski, I. Gryczynski (2013), FRET based ratio-metric sensing of hyaluronidase in synthetic urine as a biomarker for bladder and prostate cancer, Curr. Pharm. Biotechnol. 14(4), 470-474.

APPENDIX B- Other First Author Publications

- **R. Chib**, S. Shah, Z. Gryczynski, R. Fudala, J. Borejdo, B. Zelent, M. G. Corradini, R. D. Ludescher, I. Gryczynski (2015), Standard reference for instrument response function in fluorescence lifetime measurements in visible and near infrared, Measurement Science and Technology 27(2), 027001.
- **R. Chib**, S. Butler, S. Raut, S. Shah, J. Borejdo, Z. Gryczynski, I. Gryczynski (2015), Effect of quencher, denaturants, temperature and pH on the fluorescent properties of BSA protected gold nanoclusters, J Lumin 168, 62-68.
- **R. Chib**, S. Raut, S. Sabnis, P. Singhal, Z. Gryczynski, I. Gryczynski (2014), Associated anisotropy decays of ethidium bromide interacting with DNA, Methods and Applications in Fluorescence 2(1), 015003.

APPENDIX C- Co-author publications

- S. L. Raut, J. D. Kimball, R. Fudala, I. Bora, **R. Chib**, H. Jaafari, M. K. Castillo, N. W. Smith, I. Gryczynski, S. V. Dzyuba (2016), A triazine-based BODIPY trimer as a molecular viscometer, Physical Chemistry Chemical Physics.
- R. A. Kokate, P. Chaudhary, X. Sun, S. I. Thamake, S. Maji, **R. Chib**, J. K. Vishwanatha, H. P. Jones (2016), Rationalizing the use of functionalized poly-lactic-co-glycolic acid nanoparticles for dendritic cell-based targeted anticancer therapy, Nanomedicine(0).
- S. Shah, **R. Chib**, S. Raut, J. Bermudez, N. Sabnis, D. Duggal, J. D. Kimball, A. G. Lacko, Z. Gryczynski, I. Gryczynski (2016), Photophysical characterization of anticancer drug valrubicin in rHDL nanoparticles and its use as an imaging agent, Journal of Photochemistry and Photobiology B: Biology 155, 60-65.
- S. Shah, Z. Gryczynski, **R. Chib**, R. Fudala, A. Baxi, J. Borejdo, A. Synak, I. Gryczynski (2016), Demonstration of FRET in solutions, Methods and Applications in Fluorescence 4(1), 015001.
- Q. Rice, S. Raut, **R. Chib**, A. Hayes, Z. Gryczynski, I. Gryczynski, Y. Kim, B. Tabibi, J. Seo (2016), Defect-mediated spontaneous emission enhancement of plasmon-coupled CuInS 2 and CuInS 2/ZnS, Optical Materials Express 6(2), 566-577.
- S. Raut, **R. Chib**, S. Butler, J. Borejdo, Z. Gryczynski, I. Gryczynski (2014), Evidence of energy transfer from tryptophan to BSA/HSA protected gold nanoclusters, Methods and Applications in Fluorescence 2(3), 035004.
- S. L. Raut, R. Fudala, R. Rich, R. Kokate, **R. Chib**, Z. Gryczynski, I. Gryczynski (2014), Long lived BSA Au clusters as a time gated intensity imaging probe, Nanoscale 6(5), 2594-2597.
- Q. Rice, S. Raut, **R. Chib**, Z. Gryczynski, I. Gryczynski, W. Zhang, X. Zhong, M. Abdel-Fattah, B. Tabibi, J. Seo (2014), Fractional contributions of defect-originated photoluminescence from CuInS 2/ZnS coreshells for hybrid white LEDs, Journal of Nanomaterials 2014, 202.
- S. Raut, R. **Chib, R**. Rich, D. Shumilov, Z. Gryczynski, I. Gryczynski (2013), Polarization properties of fluorescent BSA protected Au 25 nanoclusters, Nanoscale 5(8), 3441-3446.
- S. L. Raut, D. Shumilov, **R. Chib**, R. Rich, Z. Gryczynski, I. Gryczynski (2013), Two photon induced luminescence of BSA protected gold clusters, Chemical Physics Letters 561, 74-76.

Send Orders of Reprints at reprints@benthamscience.net

470 *Current Pharmaceutical Biotechnology,* **2013**, *14*, **470-474**

FRET Based Ratio-Metric Sensing of Hyaluronidase in Synthetic Urine as a Biomarker for Bladder and Prostate Cancer

Rahul Chib[*,1], Sangram Raut[1], Rafal Fudala[1], Aaron Chang[2], Mark Mummert[3], Ryan Rich[1], Zygmunt Gryczynski[1,4] and Ignacy Gryczynski[*,1]

[1]*Department of Molecular Biology and Immunology, Center for Commercialization of Fluorescence Technologies, University of North Texas Health Science Center, Fort Worth, TX 76107, USA;* [2]*Johns Hopkins University, Baltimore, Maryland 410-516 USA;* [3]*Department of Psychiatry and Behavioral Health, University of North Texas Health Science Center, Fort Worth, TX 76107, USA;* [4]*Department of Physics and Astronomy, Texas Christian University, Fort Worth, TX, 76129, USA*

Abstract: Elevated hyaluronidase levels are found in the urine of bladder and prostate cancer patients. Therefore, HA-ase is regarded as an important biomarker for the detection of these cancers. In this report, we use a FRET based ratiometric sensing approach to detect the level of HA-ase in synthetic urine. For this, we have used a HA-FRET probe (hyaluronan) labeled with fluorescein as a donor and rhodamine as an acceptor. We monitor the digestion of our HA-FRET probe with different concentrations of HA-ase in synthetic urine via fluorescence emission. The extent to which FRET is released depends on the concentration of HA-ase. Our fluorescence intensity results are also supported with time resolved fluorescence decay data. This assay can be used to develop a non-invasive technique for the detection of bladder and/or prostate cancer progression.

Keywords: Ratiometric sensing, Hyaluronidase, HA-FRET, Bladder cancer.

1. INTRODUCTION

Bladder and prostate cancer are among the most frequently diagnosed types of cancers worldwide. In the US, a total of 75,510 new cases of bladder cancer and 241,740 new cases of prostate cancer are estimated in 2012 alone [1]. Therefore it is necessary to have simple, ergonomic and non-invasive diagnostic techniques with which the cancer can be detected and monitored at a very early stage, so that proper therapeutic measures can be taken. Increased hyaluronidase (HA-ase) levels in urine has been identified as a promising biomarker of bladder and prostate cancer [2, 3]. Studies by the Lokeshwar group have shown that there is usually a 2.5-6.5 fold increase in hyaluronidase levels in patients with bladder cancer in comparison to healthy individuals [4]. Hyaluronidase level greater than 10mU/mg indicate higher grade of cancer. [4]. Therefore estimating the level of hyaluronidase in urine can help in accurately predicting the progression of bladder and prostate cancer.

Hyaluronidase is an endoglycosidase that catalyzes Hyaluronan (HA) depolymerization via cleavage of the β-N-acetyl-D-glucosaminidic bonds [5] and it belongs to class hydrolase (EC3.2.1.35) [6]. Hyaluronic acid is associated with many biological processes such as cell adhesion, migration and proliferation [7]. HA-ase degrades HA into proangiogenic fragments which help in cancer progression and metastasis. The human genome contains 6 HA-ase like genes. Hyaluronidases (Hyal1, Hyal2, Hyal3) are present on chromosome 3p21.3, and another two genes (Hyal4 and PH-20/SPAM1) and one pseudogene (HyalP1) are present on chromosome 7q31.3 5. Hyal1 is a tumor derived HA-ase [8]. Hyal1 promotes growth, invasion and angiogenesis in prostate cancer [9].

In our previous studies, we have shown that the level of Hyaluronidase can be estimated using HA-FRET probe in PBS (pH 6). We wanted to test if same probe can be used reproducibly for the detection of HA-ase in synthetic urine containing different salts and hydrogen ion concentration (pH) reason being fluorescence is sensitive to the salt concentrations and pH values. In this experiment we have used synthetic urine (pH 7.83) containing different salts of monovalant and divalent ions which mimic the salts present in human urine. Fluorescence emission intensity measurements are based on probe concentration and could lead to experimental variation due to differences in probe preparations. This problem can be resolved using ratio-metric sensing in which spectrum for each sample was recorded and release of FRET was compared in terms of ratio of fluorescein to rhodamine emission intensity. This is more sensitive than measuring only either donor or acceptor emission. Ratiometric sensing reduces undesirable experimental errors [10,11]. Hence in this assay we have used donor to acceptor emission ratio to assay HA-ase in urine samples.

In our experiment we added HA-FRET probe into synthetic urine (pH 7.83) to prepare 2μM solution. Then we added different concentrations of HA-ase to the HA-FRET

*Address correspondence to this author at the Department of Molecular Biology and Immunology, Center for Commercialization of Fluorescence Technologies, University of North Texas Health Science Center, Fort Worth, TX 76107, USA; Tel/Fax: 8177350148;
Emails: rc0307@live.unthsc.edu and ignacy.gryczynski@unthsc.edu

1873-4316/13 $58.00+.00

and synthetic urine mixture at room temperature. The spectrum for each sample was recorded and release of FRET was compared which is used to determine the concentration of hyaluronidase in urine. This technique can be utilized to develop an instrument which can easily estimate the concentration of hyaluronidase in urine and hence the progression of bladder/prostate cancer.

2. MATERIALS AND METHODS

Sodium hyaluronate from bacterial fermentation was obtained from Acros Organics (Thermo Fisher Scientific, NJ, USA). Fluorescein amine, dimethyl sulfoxide (DMSO), guanidine hydrochloride, acetaldehyde, cyclohexyl isocyanide, Sephadex G-75, and bovine testes hyaluronidase (EC 3.2.1.35, type 1-S, 451 U/mg) all were obtained from Sigma–Aldrich). Dulbecco's phosphate-buffered saline (PBS) was purchased from Invitrogen Life Technologies (Invitrogen Corporation, CA, and USA). Synthetic urine (pH 7.83) is obtained from Ricca chemical company (catalog number 8361-1), Slide-A-Lyser dialysis cassettes (10,000 molecular weight cutoff) were purchased from Pierce Chemical (Thermo Fisher Scientific).

2.1. Preparation of HA-FRET

Using the same method as mentioned in our previous paper [11]. HA was covalently conjugated to fluorescein amine and rhodamine B using a condensation reaction. HA was dissolved to 1.25 mg/ml in dH2O. The HA solution was diluted 1:2 in DMSO, and fluorescein amine (predissolved as a DMSO stock solution) was added to a final concentration of 5 mg/ml. Acetaldehyde and cyclohexyl isocyanide were added to 0.04% (v/v), and the reaction was allowed to proceed for 16 hr at 25ºC. Afterward, the solution was diluted 1:14 in ethanol/guanidine HCl (50 µl of 3 M guanidine HCl per 900 µl of 100% ethanol) and HA was allowed to precipitate overnight at -20ºC. The precipitate was then dissolved in 1ml of dH2O, followed by extensive dialysis against dH2O.

2.2. Fluorescence Measurement of Hyaluronan Hydrolysis

The HA–FRET probe was added to synthetic urine to make a solution (2µM) was incubated with different concentrations of hyaluronidase in synthetic urine at room temperature. Fluorescence emission spectra were collected using Cary Eclipse spectrofluorometer (Varian Inc., Australia) every 10 min for 90 minutes. Measurements were performed in 0.4×0.4 cm quartz cell with excitation at 470 nm and emission at 520 nm and 590 nm using 495 nm long pass filter before on emission side.

2.3. Deconvolution of HA-FRET Spectra

The respective emission due to the donor and acceptor was deconvoluted to obtain individual spectrum of donor and acceptor. All spectra were deconvoluted using MATHCAD software. This program is designed to resolve a spectrum consisting of up to three constituent fluorophores which are assumed to combine linearly based on experimental fluorophores reference spectra and the utilization of an algorithm for least squares minimization to produce corresponding unmixed spectra in graph form with error provided in minimal least squares values for flexibility in analysis. This will provide us the corrected intensity of fluorescein and rhodamine in our sample. For this, reference spectra of fluorescein, rhodamine and synthetic urine were collected. The reference spectrum of fluorescein was obtained from hyaluronan labeled with fluorescein only (HA-FL) excited at 470 nm and of rhodamine by exciting our HA-FRET probe at 520 nm. (Fig. **3**) shows the example of how the resolved spectra were obtained.

2.4. Lifetime Measurement of HA-FRET Probe

Fluorescence lifetime measurements were done using FluoTime 200 fluorometer (PicoQuant, GmbH, Berlin, Germany). This time–resolved instrument is equipped with an ultrafast detector, a Hamamatsu R3809U-50 microchannel plate photomultiplier (MCP). For the excitation we used a 470 nm picosecond pulsed laser diode. The detection was through a monochromator supported by 495 nm long wave pass filter in order to eliminate scattered excitation light. The decay data were analyzed with FluoFit, version 5.0 software (PicoQuant, GmbH). Fluorescence intensity decays were analyzed by deconvolution with the instrument response function which is obtained using ludox and analyzed as a sum of experimental terms:

$$I(t)/I_{o=} \sum \alpha_i \exp(-t/\tau_i)$$

where, I(t) is the fluorescence intensity at time t and α_i is a preexponential factor representing the fractional contribution to the time-resolved decay of the component with the lifetime τi ($\sum \alpha_i = 1$). The amplitude average lifetime was calculated as $(\tau) = \sum_i \alpha_i \tau_i$.

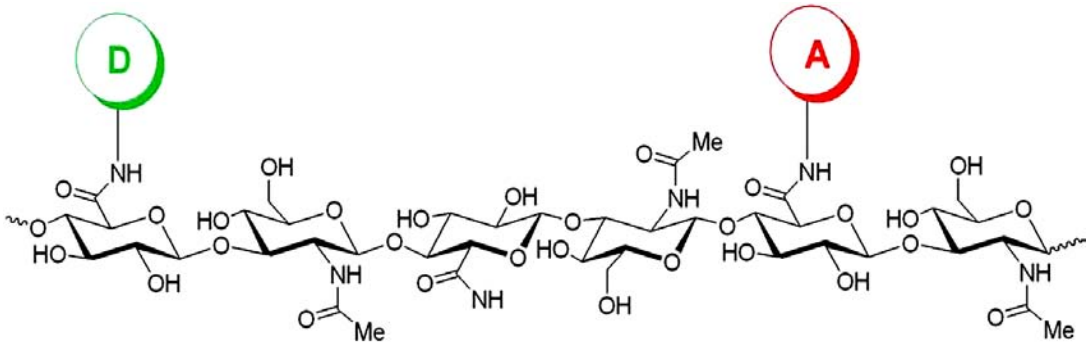

Scheme (1). HA-FRET molecule labeled with fluorescein as donor and rhodamine as acceptor.

3. RESULTS AND DISCUSSION

3.1. Fluorescence Emission

We measured fluorescence spectra of HA-FRET probe in the absence and presence of HA-ase. The sample was incubated in synthetic urine for 90 minutes with different concentrations of enzyme at room temperature (25°C). Without the enzyme, release of FRET was not observed. In the presence of enzyme (Fig. **1**), at 90 minutes, we observed release of FRET and donor emission intensity increases with significant change in the donor to acceptor emission intensity ratio. The increased donor to acceptor ratio is dependent on enzyme concentration. Higher the concentration of HA-ase, greater is release of FRET.

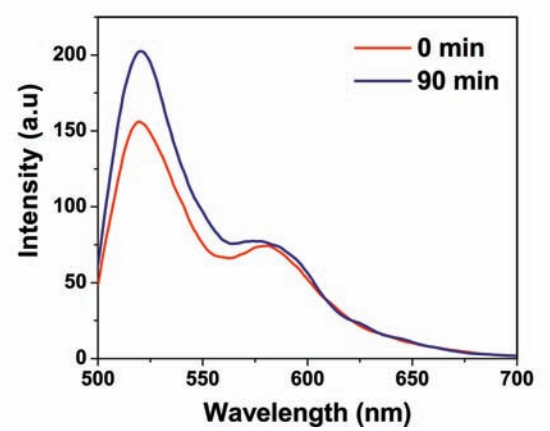

Fig. (1). Difference between emission intensity of HA-FRET when incubated with 35 U/mL HA-ase for 90 min. Excitation used was 470 nm. Experiment was carried out at RT in synthetic urine pH 7.83.

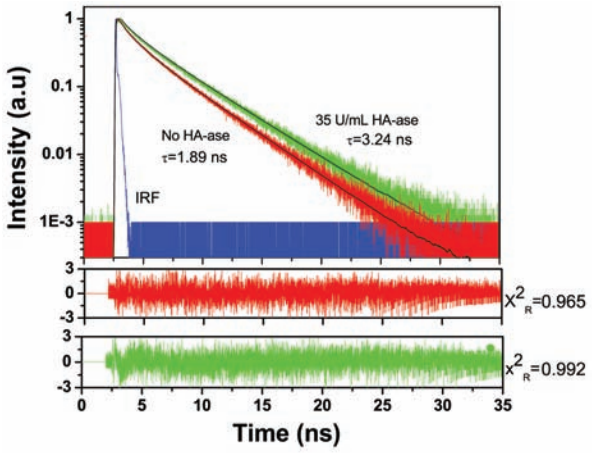

Fig. (2). Fluorescence intensity decays of 2 uM HA-FRET (donor) in synthetic urine when incubated with 35U/mL of HA-ase enzyme for 90 minutes. Excitation used was 470 nm laser. Donor emission was observed at 520 nm using 495 long pass filter before detector. Decays were fitted using multi-exponential function and chi square values were used to access the goodness of fit.

3.2. Fluorescence Lifetime

The fluorescence intensity decay measurement is shown in (Fig. **2**). Each measurement was taken in the presence and absence of HA-ase at 90 minute. The fluorescein is highly quenched in the absence of HA-ase, showing a heterogeneous decay and three components are needed to fit the data with lifetime of 3.65, 1.35 and 0.21 ns and amplitudes: 0.74, 0.22, and 0.35 with amplitude average lifetime of 1.89 ns. With an increase in concentration of HA-ase, amplitude average lifetime increased proportionately (Table **1**). For 10

Table 1. Time Resolved Fluorescence Intensity Decay Parameters for the Donor in HA- FRET with Different Concentration of HA-ase at RT.

	No Enzyme	10 U/ml	35U/ml	100U/ml
τ1 (ns)	3.65	4.04	4.14	4.19
τ2(ns)	1.35	0.79	0.62	0.49
τ3(ns)	0.21	-	-	-
α1	0.74	0.92	0.95	0.96
α2	0.22	0.08	0.05	0.03
α3	0.035	-	-	-
$<\tau>^{i)}$	1.89	3.01	3.24	3.48
$\bar{\tau}^{ii)}$	3.02	3.77	3.97	4.1
X^2_R iii)	0.965	0.966	0.992	0.938

τ 1, τ 2 and τ 3 are different lifetime and α1, α2 and α3 are components of fluorescence lifetime in nanoseconds.

i) $< \tau >= \sum_i \alpha_i \tau_i$

ii) $\bar{\tau} = \sum_i f_i \tau_i$, Where, $f_i = \frac{\alpha_i \tau_i}{\sum_i \alpha_i \tau_i}$

iii) (X^2_R = goodness of fit).

U/ml, 35 U/mL and 100 U/mL of enzyme amplitude average lifetime was 3.01ns, 3.24 ns and 3.48 ns respectively. After addition of HA-ase, components needed to fit the data also decreased from three to two. The time resolved measurements showed increase in donor lifetime with gradual addition of enzyme, strongly indicate release of FRET in the enzyme presence and corroborate our intensity based ratiometric measurements

3.3. Resolution of Spectra

The obtained fluorescence spectrum is a convolution of donor and acceptor emission spectrum therefore doesn't give the exact intensity of donor and acceptor emission. It has been our observation that usually acceptor shows higher emission intensity compared to its corrected emission intensity calculated by resolution of the spectrum. To estimate the corrected emission intensities we deconvoluted each spectrum into its donor and acceptor components. As shown in (Fig. **3**), we used normalized fluorescein and rhodamine spectra as reference spectra for deconvolution. As (Fig. **3**) (B) shows, our synthetic urine had negligible contribution to the observed fluorescence from HA-FRET sample (2uM). (Fig. **3**) (C) shows spectrum to be resolved (black line) and the corrected individual donor (green line) and acceptor (red line) emission spectra after deconvolution of the spectrum to be resolved. As mentioned earlier, we can observe that the corrected intensity of acceptor (rhodamine) is less compared to its observed intensity from the HA-FRET molecule.

3.4. FRET Based Ratio Metric Sensing

We resolved each spectrum as mentioned earlier to calculate intensity ratio every 10 minute for all concentrations of HA-ase. (Fig. **4**) shows donor to acceptor intensity ratio against time for all concentrations (10, 35 and 100 U/mL) of enzyme. HA-FRET solution without enzyme did not show any change in intensity ratio whereas, in the presence of HA-ase release of FRET and increase in intensity ratio was observed. There is an exponential increase in intensity with increase in time. Intensity ratio (green/red emission) of HA-FRET as function of HA-ase concentration at 60 min is shown in (Fig. **5**). After 60 minutes this enzymatic reaction almost reaches a plateau and no significant changes are ob-

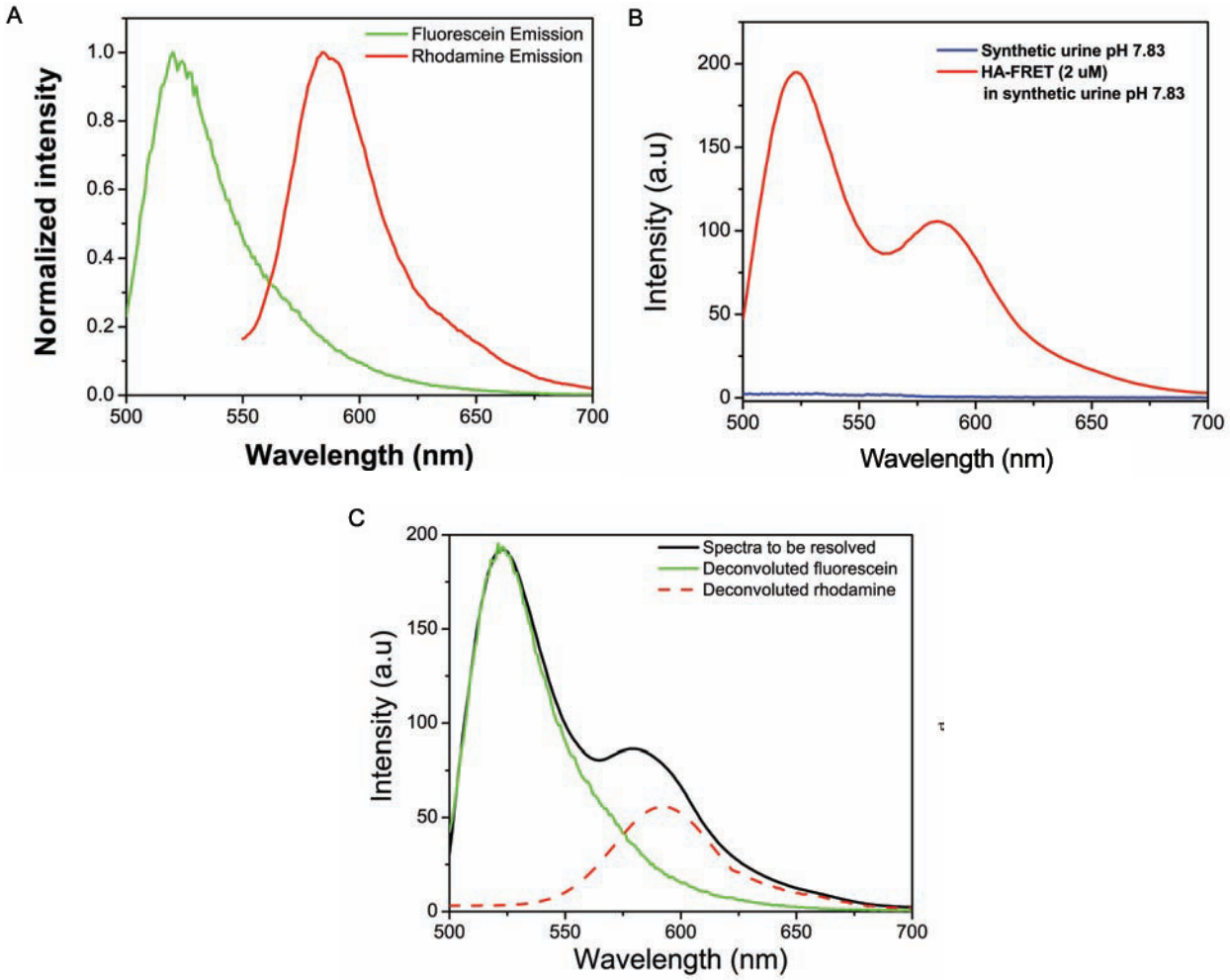

Fig. (3). (**A**) normalized emission spectrum of fluorescein (from HA-FRET labeled with fluorescein only. Exc 470 nm) and rhodamine (from HA-FRET by exciting at longer wavelength. Exc 520 nm) in synthetic urine pH 7.83 at RT (**B**) Emission spectra from 2 μM HA-FRET and background signal from synthetic urine. (**C**) Shows example of how the HA-FRET spectrum was resolved into its components using MATHCAD based program written in our laboratory.

served thereafter. These results indicate a strong dependence of digestion kinetics on the enzyme concentration. (Fig. **5**) shows the standard curve for calculating the unknown concentration of HA-ase. The intensity ratio and concentration of HA-ase shows exponential relationship and can easily be applied to real time urine samples to calculate enzyme concentration in it. Such dependence facilitates the detection of the presence and activity of the HA-ase enzyme

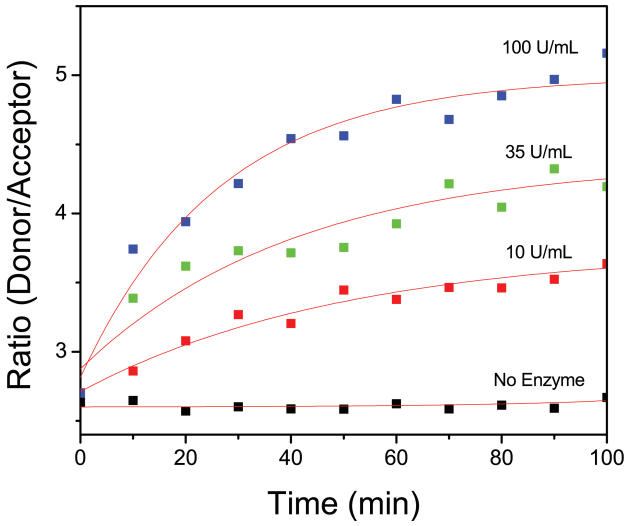

Fig. (4). Time dependant fluorescence intensity ratio (green/red emission) of HA-FRET probe in the presence and absence of HA-ase and exponential fits (red lines) to data. Concentration of HA-FRET sample was 2 uM in each case. The excitation was 470 nm and experiment was done at RT in synthetic urine pH 7.83.

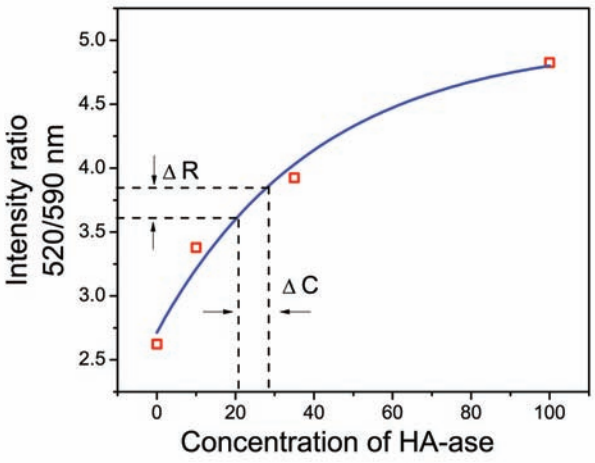

Fig. (5). Intensity ratio (green/red emission) of HA-FRET as function of HA-ase concentration at 60 min and exponential fit (blue line. If ΔR= 3.72 ±0.12 then ΔC= 24.5 ±3.5.

Received: March 11, 2012 **Revised: August 04, 2012** **Accepted: August 08, 2012**

CONCLUSION

With this technique, it is possible to mark the HA-ase activity by fluorescence intensity changes in our HA-FRET probe. Release of FRET is observed with increase in concentration of Hyaluronidase. Lifetime based sensing of HA-ase supports our fluorescence intensity based measurements. Increase in lifetime of donor is noticed in the presence of HA-ase. Release of FRET and hence increase in fluorescein (donor) lifetime was observed. This ratiometric sensing is a very precise method of measuring changes in the fluorescence intensity. As we know, with progressive stage of urinary bladder or prostate cancer, the amount of HA-ase released in urine is increased. With this, we propose that this technique can be potentially used to determine the amount of hyaluronidase in patient's urine and hence the progressive stage of urinary bladder or prostate cancer can be determined.

CONFLICT OF INTEREST

The authors confirm that this article content has no conflicts of interest.

ACKNOWLEDGEMENTS

This work was supported by the NIH GRANT R01EB12003.

REFERENCES

[1] Siege R, Naishadham D, Jemal A. Cancer statistics, 2012. *Can. J. Clinician*, **2012**, *62*, 10.

[2] Lokeshwar VB, Lokeshwar BL, Pham HT, Block NL. Association of elevated levels of hyaluronidase, a matrix-degrading enzyme, with prostate cancer progression. *Cancer Res.*, **1996**, *56*(3), 651-657.

[3] BR, Getzenberg RH. Urine based markers of urological malignancy. *J. Urol.*, **2001**, *165*(2), 600-611.

[4] Lokeshwar VB, Block NL. HA-HAase urine test. A sensitive and specific method for detecting bladder cancer and evaluating its grade. *Urol. Clin. North Am.*, **2000**, *27*(1), 53-61.

[5] Csoka AB, Frost GI, Stern R. The six hyaluronidase-like genes in the human and mouse genomes. *Matrix Biol.*, **2001**, *20*(8), 499-508.

[6] Stern R, Jedrzejas MJ. Hyaluronidases: Their genomics, structures, and mechanisms of action. *Chem. Rev.*, **2006**, *106*(3), 818-839.

[7] Lee JY, Spicer AP. Hyaluronan: A multifunctional, megaDalton, stealth molecule. *Curr. Opin. Cell Biol.*, **2000**, *12*(5), 581-586.

[8] Lin G, Stern R. Plasma hyaluronidase (hyal-1) promotes tumor cell cycling. *Cancer Lett.*, **2001**, *163*(1), 95-101.

[9] Benitez A, Yates TJ, Lopez LE, Cerwinka WH, Bakkar A, Lokeshwar VB. Targeting hyaluronidase for cancer therapy: Antitumor activity of sulfated hyaluronic acid in prostate cancer cells. *Cancer Res.*, **2011**, *71*(12), 4085-4095.

[10] Maa C, Zeng F, Wu G, Wu S. A nanoparticle-supported fluorescence resonance energy transfer system formed via layer-by-layer approach as a ratiometric sensor for mercury ions in water. *Analytica Chimica Acta.*, **2012**, *734*, 69-78.

[11] Fudala R, Mummert ME, Gryczynski Z, Gryczynski I. Fluorescence detection of hyaluronidase. *J. Photochem. Photobiol. B.* **2011**, *104*(3), 473-477.

Dyes and Pigments 117 (2015) 16–23

Contents lists available at ScienceDirect

Dyes and Pigments

journal homepage: www.elsevier.com/locate/dyepig

Steady state and time resolved fluorescence studies of azadioxatriangulenium (ADOTA) fluorophore in silica and PVA thin films

Rahul Chib [a, *], Sangram Raut [a, d], Sunil Shah [a], Beata Grobelna [b], Irina Akopova [a], Ryan Rich [a], Thomas Just Sørensen [c], Bo W. Laursen [c], Hanna Grajek [e], Zygmunt Gryczynski [a, d], Ignacy Gryczynski [a, *]

[a] Department of Cell Biology and Immunology, Center for Fluorescence Technologies and Nanomedicine, University of North Texas Health Science Center, Fort Worth, TX 76107, USA
[b] Faculty of Chemistry, University of Gdańsk, Wita Stwosza 63, 80-952 Gdańsk, Poland
[c] Nano-Science Center and Department of Chemistry University of Copenhagen, Universitetsparken 5, DK2100 København Ø, Denmark
[d] Department of Physics and Astronomy, Texas Christian University, Fort Worth, TX 76129, USA
[e] Department of Physics and Biophysics, University of Warmia and Mazury in Olsztyn, 10-719, Poland

ARTICLE INFO

Article history:
Received 21 November 2014
Received in revised form
27 January 2015
Accepted 29 January 2015
Available online 10 February 2015

Keywords:
Azadioxatriangulenium
Fluorophore
Aggregation
Sol–gel process
Luminescence
Lorentzian lifetime distribution

ABSTRACT

A cationic azadioxatriangulenium dye was entrapped in silica thin films obtained by the sol–gel process and in poly (vinyl) alcohol (PVA) thin films. Azadioxatriangulenium is a red emitting fluorophore with a long fluorescence lifetime of ~20 ns. The fluorescent properties of azadioxatriangulenium in silica thin films and PVA films were studied by means of steady–state and time resolved fluorescence techniques. We have found that the azadioxatriangulenium entrapped in silica thin film has a wider fluorescence lifetime distribution (Lorentzian distribution), lower fluorescence efficiencies, shorter lifetimes compared to Azadioxatriangulenium in a PVA film. The local environment of azadioxatriangulenium molecules in the silica thin film is rich with water and ethanol, which creates the possibility of forming excited state aggregates due to high concentration of dye within a small confined area. In contrast to the PVA matrices, the porous silica films allow restricted rotations of Azadioxatriangulenium molecules, which result in faster and complex fluorescence anisotropy decays suggesting energy migration among dye molecules.

1. Introduction

Over the past decade, the synthesis and characterization of hybrid materials based on silica, in which organic dyes were entrapped has attained considerable attention [1,2]. The use of semiconductor materials for entrapment of the organic fluorophores has been and will remain a very important way to obtain new materials for different applications, including, functional materials in optoelectronic devices, optical sensors [3], optical components like solid state tunable lasers [4] and highly luminescent materials in medicine [5,6].

The initial investigation of entrapping optically active organic molecules with the sol–gel process was performed by Avnir et al. [7] in which they studied the fluorescence properties of rhodamine 6G in different stages of sol–gel development. Since then, various photoactive dyes have been incorporated and studied in the matrices obtained by the sol–gel process [8–10]. Moreover, new hybrid materials provide a great subject of extensive research in materials chemistry [11–13]. To obtain new hybrid materials, an efficient sol–gel process is used which combines the remarkable properties of inorganic and organic materials in a controlled way [14–18]. In particular, because of the good mixing of the starting compounds, it creates the possibility to obtain a homogenous hybrid material at relatively low temperatures [19]. During the sol–gel process, the host molecules are already present in the precursor solution and the conditions of the reactions are mild, therefore the optical properties of the fluorophore remain intact

* Corresponding authors.
E-mail addresses: rc0307@live.unthsc.edu (R. Chib), Ignacy.Gryczynski@unthsc.edu (I. Gryczynski).

http://dx.doi.org/10.1016/j.dyepig.2015.01.027
0143-7208/

[20,21]. Also the entrapment of organic fluorophores in a gel matrix provides better protection of the molecule and higher stability than the free molecules in liquid media [22]. At the same time, silicon dioxide (SiO_2) is well-known as a material with good optical quality, thermal stability, mechanical strength and photochemical stability. Another property of silica, which makes it a good candidate as a host matrix for incorporation of organic fluorophores is the ability to modify the surface by amines, thiols and other coupling agents [23,24]. On the other hand, organic dyes incorporated into silica matrix, sometimes afford more interesting luminescence properties due to strong host–guest interactions. Therefore, preparation of new hybrid materials based on silica in which organic fluorophores are entrapped is suitable for the design of highly luminescent materials.

In the present study, we have introduced an azadioxatriangulenium dye into a silica thin film obtained by the sol–gel process and into a PVA film [25–28]; specifically the acid derivative *N*-(ω-butanoic acid)-azatriangulenium tetrafluoroborate (ADOTA); the molecular structure can be seen in Scheme 1. ADOTA belongs to the class of azaoxa-triangulenium fluorophores which are planar and rigid in structure. Furthermore, ADOTA in water emits in the red region around 560 nm with a fluorescence lifetime of ~20 ns, which makes it the longest orange/red emitting organic fluorophore [29,30].

The spectroscopic properties of the material presented are discussed in this paper. In particular, we compared the absorption, fluorescence emission, steady state anisotropy, time resolved anisotropy and fluorescence lifetime of ADOTA in thin layers of silica and in a PVA film. The use of PVA provides a more rigid environment compared to silica matrix and hence the photophysical properties of the ADOTA can be studied in two different semi-solid matrices. In addition, the photophysical characterization of ADOTA in a heterogeneous environment can be efficiently studied over time by using time resolved fluorescence spectroscopy.

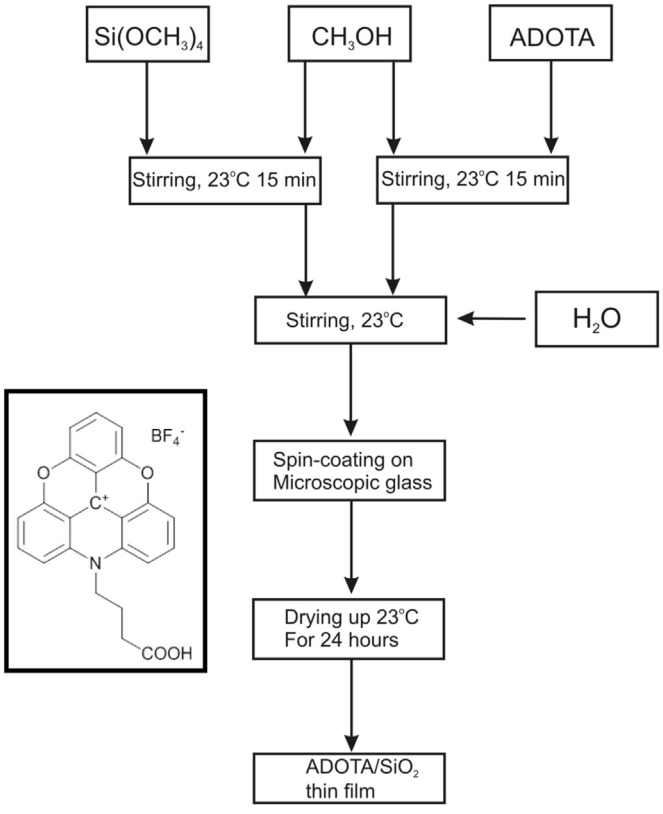

Scheme 1. Flow chart of preparation of ADOTA doped silica thin films. Insert: molecular structure of *N*-(ω-butanoic acid)-azatriangulenium tetrafluoroborate (ADOTA).

2. Materials and methods

All the starting materials for the preparation of silica thin films were of analytical grade. Tetramethoxysilane $Si(OCH_3)_4$ (TMOS) was purchased from Aldrich Co., methanol as a diluent and ammonia were purchased from POCH Company (Poland). Deionized (DI) water was obtained from a Hydrolab system. Polyvinyl alcohol (130, 000 MW) was purchased from Sigma Aldrich (Sigma Aldrich, St Louis, MO USA). *N*-(ω-butanoic acid)-azatriangulenium tetrafluoroborate (ADOTA) was prepared as previously described [27,31].

2.1. Sample preparation and AFM measurements

ADOTA/silica thin films were obtained by the sol–gel spin-coating method, summarized in Scheme 1. Firstly, tetramethoxysilane (TMOS) and methanol were mixed by vigorous stirring for 15 min. After several minutes (which is very important to reach homogeneity of the solution), ADOTA was dissolved in methanol and added to the precursor solution. In order to initiate the sol–gel process, an appropriate volume of water was added. The final molar ratio TMOS/water/methanol was 1:4:12, while the concentration of ADOTA in sol was $2 \cdot 10^{-3}$ M (a low concentration sample with an overall ADOTA concentration of $<10^{-6}$ M was also prepared). The films were distributed over a clean piece of a microscopic slide using the spin-coating technique after 15 min after mixing all of the components. Microscopic glasses were cleaned in a mixture of 33% H_2O_2 and H_2SO_4 in molar ratio 2:1 over 24 h and rinsed with deionized water.

The spin coating was done at 150 rpm for 60 s to disperse the sol. After that, the thin films were allowed to dry in air for 24 h. Moreover, to prepare ADOTA in PVA films, the ADOTA was mixed in PVA solution and spread onto a thin glass slide to evenly coat the slide using spin coating.

Atomic Force Microscopy (AFM) micrographs were produced by using scanning atomic force microscopy on the NTEGRA Prima scanning probe microscope manufactured by NT-MDT (Moscow, Russia). Closed-loop feedback semi-contact mode has been used at rate 0.5 Hz. Scanning was controlled and images were analyzed with NOVA software by NT-MDT instrument manufacturer.

2.2. Absorption measurements

Absorption spectra were measured using a Cary 50 Bio UV–visible spectrophotometer (Varian Inc., Australia). Absorption spectra were scanned from 400 nm to 600 nm using bare glass slide as a baseline. Absorption spectra of silica thin films were corrected for the scattering by subtracting the scattering profile of silica thin films prepared without addition of the dye.

2.3. Steady-state fluorescence measurements

Steady-state fluorescence intensity measurements of all the samples were made using a Carry Eclipse spectrofluorometer (Varian Inc., Australia) by using the front face geometry as shown in Scheme 2. In Scheme 2, S represents the sample used for measurements, M is the mirror, F is a long pass filter before detector and L is the lens. The emission was scanned from 520 nm to 700 nm following a 470 nm excitation and using 495 nm long pass filter on the emission side. Steady-state excitation spectra were measured by observing the emission at 600 nm and excitation was scanned from 400 nm to 560 nm using a 570 nm long pass filter on the

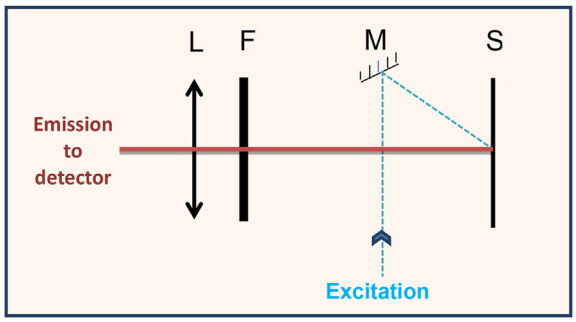

Scheme 2. Schematic of the front face arrangement used for steady state and time resolved fluorescence measurements. In this scheme, S represents the sample used for measurement, M is the mirror, F is long pass filter before detector, L is lens.

emission side. Steady-state fluorescence anisotropy of all the samples were measured using a Carry Eclipse spectrofluorometer (Varian Inc., Australia), with manual polarizers on both the excitation and emission side. Emission anisotropy was measured following 470 nm excitation with a 495 nm long pass filter along the emission side and manually operated parallel and perpendicular polarizers. Anisotropy was calculated using the following formula:

$$r = \frac{I_{VV} - I_{VH}G}{I_{VV} + 2I_{VH}G}$$

where, I_{VV} is the fluorescence intensity measured with the parallel polarizer orientation on the observation path, I_{VH} is the fluorescence intensity at the perpendicular orientation of the polarizer on the emission side and G is the instrumental correction factor calculated by measuring the intensity in HV and HH polarizer orientation.

2.4. Fluorescence intensity decay

Fluorescence lifetimes of all the samples were measured using FluoTime 200 (PicoQuant, GmbH, Berlin, Germany) time resolved spectrofluorometer. This instrument contains a multichannel plate detector (Hamamatsu, Japan) and a 470 nm laser diode was used as the excitation source. The front face geometry as shown in Scheme 2 was used for these measurements as well. The fluorescence intensity decays were measured under magic angle conditions and data was analyzed with FluoFit version 4.5.3 software (PicoQuant GmbH, Berlin, Germany) using both the exponential reconvolution procedure using non-linear regression (multiexponential deconvolution model) and by the lifetime distribution model (Lorentzian model) [32]. In the case of multiexponential analysis, the fluorescence decay was analyzed using:

$$I(t) = \int_{-\infty}^{t} IRF(t') \sum_i \alpha_i e^{\frac{-t-t'}{\tau_i}}$$

where IRF (t′) is the instrument response function at time t′, α is the amplitude of the decay of the ith component at time t and τ_i is the lifetime of the ith component. In case of Lorentzian lifetime distribution, all the data were analyzed using the following equation.

$$I(t) = \int_{-\infty}^{\infty} \rho(\tau) e^{-\frac{t}{\tau}} d_\tau$$

where,

$$\rho(\tau) = \sum_{i=1}^{n} \frac{A_i}{\pi} \frac{\frac{\Delta_{FWHM\ i}}{2}}{(\tau - \tau_i)^2 + (\Delta_{FWHM\ i}/2)^2}$$

where A_i is the amplitude of the ith component, τ_i is the central lifetime value of the ith distribution. The use of the continuous distribution $\rho(\tau)$ minimizes the number of floating parameters in the fitting algorithms.

2.5. Time resolved anisotropy measurements

Excitation used for time resolved anisotropy measurement was 470 nm while emission was observed at 560 nm and 620 nm with vertical and horizontal polarizer position on the emission side using appropriate filters on both excitation and emission side. Anisotropy decays were analyzed with the exponential fitting model in the FluoFit 4.5.3 program from Pico-Quant, Inc. (Germany) using the following equation:

$$r(t) = r_{INF} + \sum_{i=1}^{n} r_i e^{-\frac{t}{\Phi_i}}$$

where, r_i is the anisotropy of the ith component at time t and Φ_i is the rotational correlation time of the ith component. The quality of the fit in lifetime and anisotropy decay analysis was judged by the quality of the residuals and χ^2 square value.

3. Results and discussion

3.1. AFM micrographs of silica thin films

The surface topography of the silica thin film with *N*-(ω-butanoic acid)-azatriangulenium tetrafluoroborate (ADOTA) was studied using the AFM technique as shown in Fig. 1. From this micrograph, we can observe that the surface of the porous silica is rough, with maximum particle size close to 50 nm. The ADOTA-doped PVA films did not show any significant roughness (Supplementary Fig. S1). In order to check how dye is distributed in the prepared silica or PVA layers, confocal fluorescence images were taken and found that ADOTA dye is evenly distributed in all film on the scale of the optical resolution, about 400 nm (see Supplementary information, Fig. S2).

3.2. Absorption spectra

Fig. 2 shows the absorption spectrum of ADOTA in silica thin films and in PVA films dried on a cover-glass. It can be seen from both the figures that the absorption spectra appears somewhat noisy. This is due to the small thickness/path-length (100–150 nm) and small absorptions recovered after correcting for the scattering arising in these samples. The absorption spectrum shape and peak

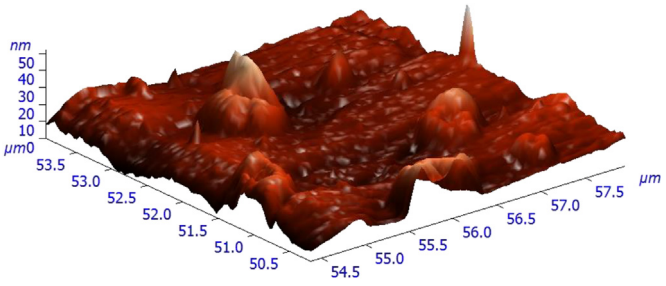

Fig. 1. AFM showing the surface topography of the silica thin layer prepared by the sol gel process.

absorption wavelengths did not change in the silica gel environment compared to the PVA film suggesting no significant perturbation in the immobilized ground state fluorophores population.

3.3. Steady state measurements

Fig. 3 shows the normalized excitation and emission spectra of ADOTA entrapped in a silica thin film (red) and a PVA film (blue). Similar to the absorption data, we did not see any significant change in the excitation spectrum of the dye entrapped within the two different environments. However, a ~15 nm red shift in the emission spectra was observed for the ADOTA in silica thin films.

When we examined the emission spectra of a low concentration ADOTA in the silica layer we found that the emission spectrum was similar to the emission spectrum of ADOTA in PVA film. ADOTA in silica layer shows concentration dependent red shift in emission spectrum. Supplementary information shows all the emission spectra along with measured Full Width Half Maxima (FWHM, Supplementary Fig. S3). For high concentration of the dye in silica layer, the spectrum is red shifted compared to low concentration along with an increase in the FWHM value, suggesting dye aggregation/excimer formation. Although, we have already ruled out the possibility of ground state aggregation since there in no experimental evidence here in this case. However, we cannot rule out the possibility of excimer formation here as the dyes are packed very close to each other and do not require a significant diffusion to form

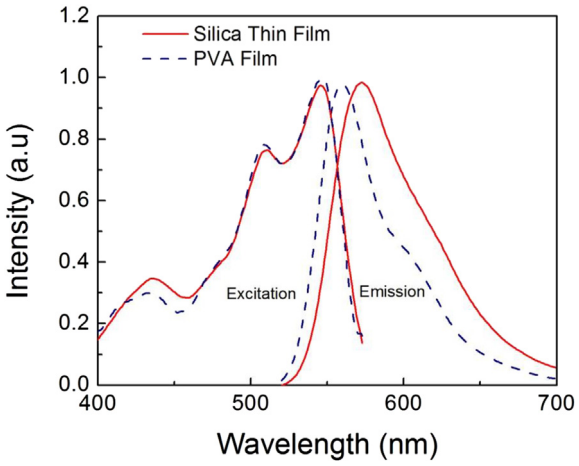

Fig. 3. Normalized excitation and emission spectrum of *N*-(ω-butanoic acid)-azatriangulenium tetrafluoroborate (ADOTA) in silica thin film (red) and in PVA film (blue). (For interpretation of the references to colour in this figure legend, the reader is referred to the web version of this article.)

aggregates in the excited state. The rapid formation of excimers is outside the measurement capabilities of our instrument and hence the rise time (negative exponent) cannot be observed. We ascribe the broadening of the emission spectrum from ADOTA in silica thin films to the heterogeneous environment and aggregation of dye

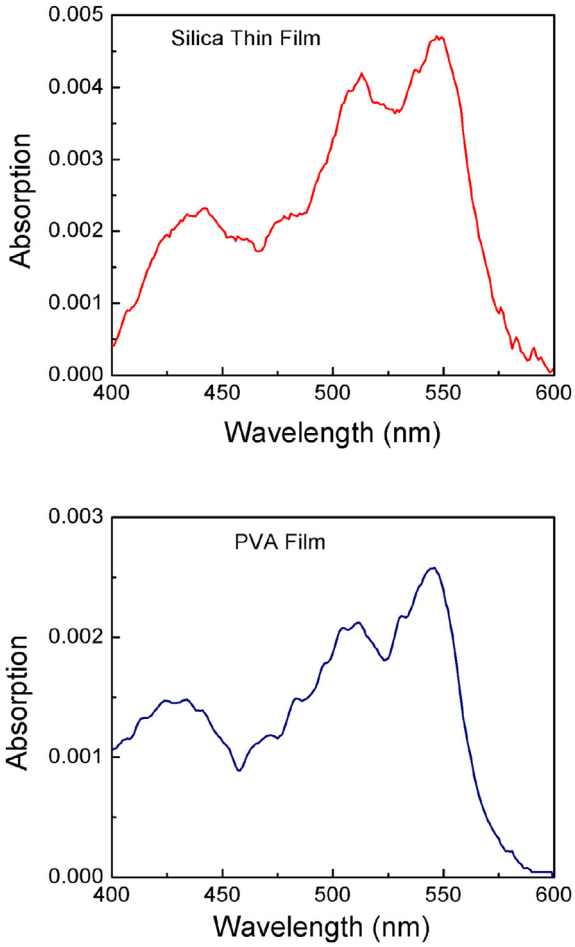

Fig. 2. Top panel: absorption spectrum of *N*-(ω-butanoic acid)-azatriangulenium tetrafluoroborate (ADOTA). in silica thin film. Bottom panel: absorption spectrum of ADOTA in PVA film.

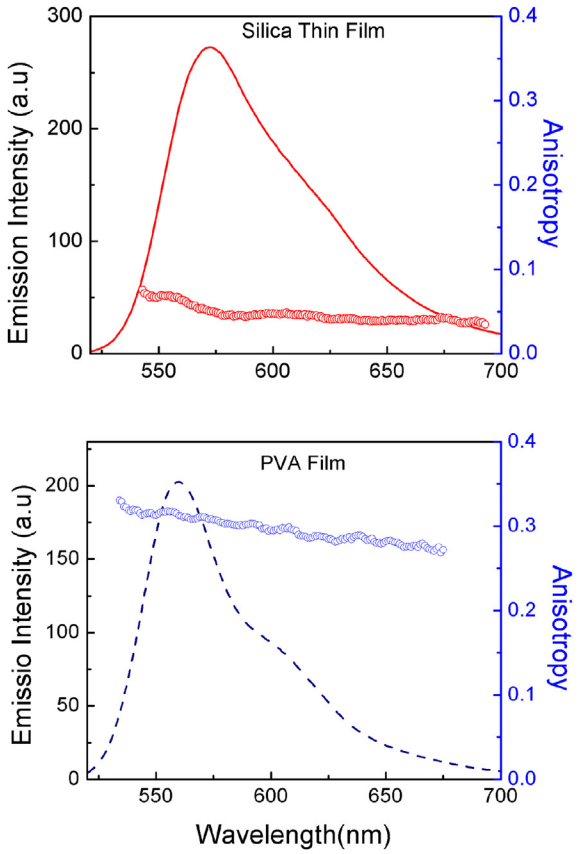

Fig. 4. Top panel: fluorescence emission spectrum (red line) and anisotropy (blue circle) of *N*-(ω-butanoic acid)-azatriangulenium tetrafluoroborate (ADOTA) in silica thin film. Bottom panel: fluorescence emission spectrum (blue line) and anisotropy (blue circle) of ADOTA in PVA film. (For interpretation of the references to colour in this figure legend, the reader is referred to the web version of this article.)

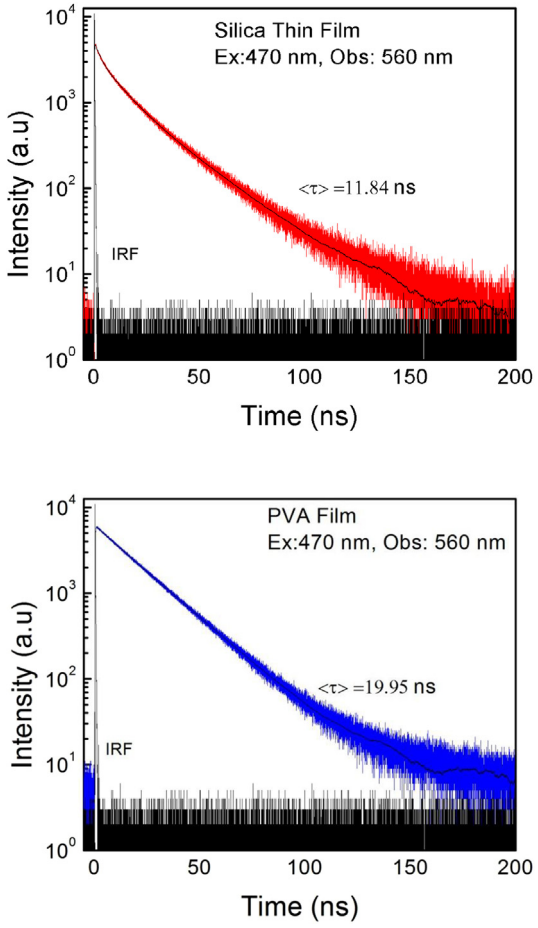

Fig. 5. Top Panel: fluorescence intensity decay of *N*-(ω-butanoic acid)-azatriangulenium tetrafluoroborate (ADOTA) in silica thin film (Ex: 470 nm, Obs: 560 nm). Bottom panel: fluorescence intensity decay of ADOTA in PVA film (Ex: 470 nm, Obs: 560 nm).

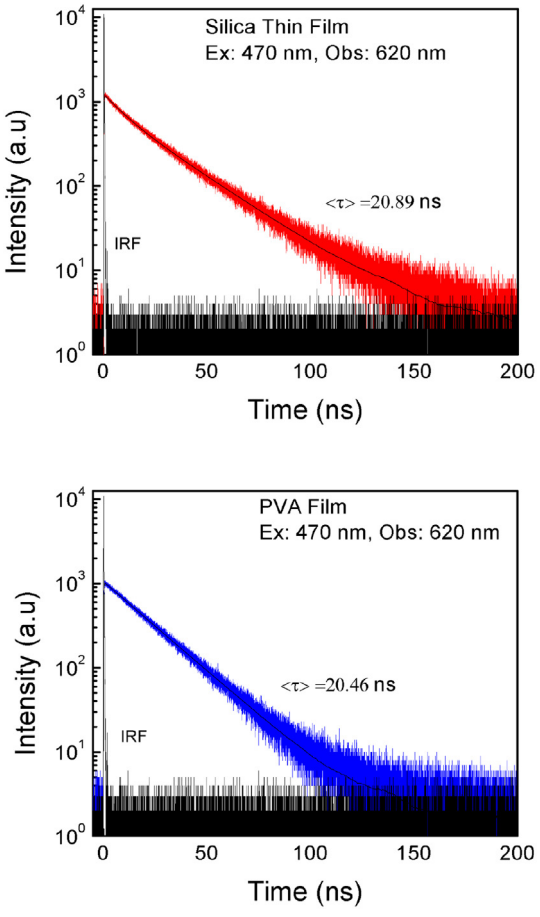

Fig. 6. Top panel: fluorescence intensity decay of *N*-(ω-butanoic acid)-azatriangulenium tetrafluoroborate (ADOTA) in silica thin film (Ex: 470 nm, Obs: 620 nm). Bottom panel: fluorescence intensity decay of ADOTA in PVA film (Ex: 470 nm, Obs: 620 nm).

molecules in the silica matrix. This is a very elaborate problem, because ADOTA entrapped in the pores of the matrix has a possibility to interact not only with itself but also with the surface of three-dimensional network. In the literature this problem is called as the "cage effect" [33]. In the present case, the local environment of the ADOTA molecule is rich with water and methanol. In other words, the cage is filled with solvent and this creates the possibility of forming heterogeneous environment within the confined area.

Steady state anisotropy measurements gave us the overall idea of the mobility of the fluorophore molecules in a silica film and PVA matrix. The steady state anisotropy data are presented in Fig. 4. ADOTA entrapped in a PVA matrix showed high anisotropy reaching a value close to 0.3, thus suggesting a very rigid environment. On the other hand, ADOTA incorporated into silica thin film showed moderate anisotropy of 0.05. This suggests that the dyes are not rigidly linked to the matrix or that the anisotropy is lost due to energy transfer (HOMO- FRET) and that the pores are large on the molecular scale, making the silica matrix less rigid than PVA matrix. These results were confirmed by blowing the argon on to silica film for 1 h and re-measuring the steady state anisotropy to exclude the

Table 1
Analysis of *N*-(ω-butanoic acid)-azatriangulenium tetrafluoroborate (ADOTA) fluorescence intensity decay using multi-exponential model of in Silica thin film and PVA thin film.

Sample	Observation (nm)	Lifetime (ns)			Amplitudes			Average lifetime (ns)		Chi square
		τ_1	τ_2	τ_3	α_1	α_2	α_3	τ_{AMP}	τ_{INT}	χ^2
ADOTA silica thin film	560	25.14	10.10	2.004	0.28	0.41	0.31	11.84	18.60	0.955
	620	26.98	9.33	–	0.65	0.35	–	20.89	20.24	0.892
ADOTA PVA film	560	21.01	13.42	–	0.86	0.14	–	19.95	20.30	0.997
	620	20.46	–	–	1	–	–	20.46	20.46	0.811

Where,

$\tau_{AMP} = \sum_i \alpha_i \tau_i$

$\tau_{INT} = \sum_i f_i \tau_i$

$f_i = \frac{\alpha_i \tau_i}{\sum_i \alpha_i \tau_i}$

possibility of rotational diffusion due to the hygroscopic nature of the silica film. Interestingly, the possibility of ADOTA being covalently linked to the matrices through the acid functional group is not explored and is a topic of further research in this area.

3.4. Time resolved intensity decay/fluorescence lifetime

The fluorescence lifetime of the ADOTA incorporated into a silica thin film was heterogeneous compared to fluorescence lifetime of the ADOTA incorporated into a PVA matrix. The lifetimes measured at 560 nm are shown in Fig. 5. The average lifetime was found to be ~12 ns in the silica matrix and ~20 ns in the PVA matrix. Three components are needed to fit the data at 560 nm for the silica thin film, whereas only two components are needed for the sample in the PVA film (Table 1). The shorter and heterogeneous nature of the decay in silica suggests different environments to which dye molecules are exposed to [28]. Hence, we decided to measure the lifetimes at a longer wavelength (620 nm) which will further allow us to know more about the silica network environment. Fig. 6 shows the lifetime decays at 620 nm wavelength. One can see that the lifetime of ADOTA in the PVA matrix did not change significantly and stayed approximately 20 ns. However, the fluorescence lifetime of ADOTA (at 620 nm) incorporated into the silica matrix is significantly longer than the fluorescence lifetime measured at 560 nm. This could be due to the presence of the dye molecules in the confined space in the silica matrix. Stacking of dyes leads to the restricted motion and less vibrational/torsional losses and hence the longer lifetime at 620 nm observation. Table 1 shows the lifetime values from the data analyzed using multi-exponential reconvolution model.

Table 2
Lorentzian analysis of fluorescence intensity decays of *N*-(ω-butanoic acid)-azatriangulenium tetrafluoroborate (ADOTA).

	Observation (nm)	Lifetime, τ (ns)	FWHM (ns)	Chi square(χ^2)
ADOTA silica thin film	560	13.5	15.1	0.98
	620	21.8	12.7	0.92
ADOTA PVA film	560	20	3.2	0.98
	620	20.4	2.45	0.93

We also analyzed the fluorescence intensity decays using a Lorentzian lifetime distribution model that takes into consideration the average number of emitting species in different environments. The FWHM values of the distribution shows the degree of distribution of the emitting molecules which are much higher in silica thin films than in the PVA films (Fig. 7). The Lorentzian distributions (Table 2) for ADOTA in PVA films are very narrow, about 3 ns at 560 nm observation, and about 2.45 ns at 620 nm observation, which suggests a very uniform environment and lack of interactions between fluorescent molecules. In contrast, the Lorentzian distributions in silica are very wide. In case of ADOTA in

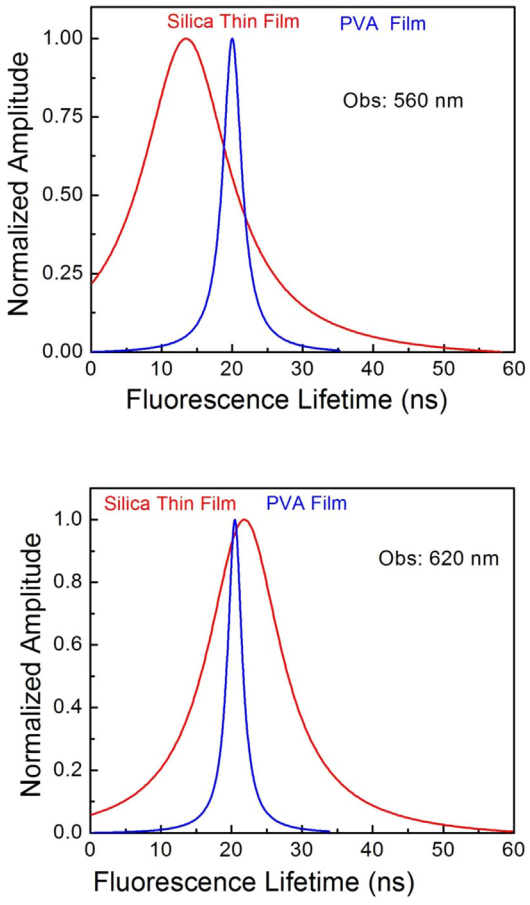

Fig. 7. Lifetime distribution (Lorentzian Model) of *N*-(ω-butanoic acid)-azatriangulenium tetrafluoroborate (ADOTA) in silica thin film and PVA film. (Top Panel) This figure represents the fluorescence lifetime distribution when observed at 560 nm. (Bottom Panel) This figure represents fluorescence lifetime distribution observed at 620 nm. ADOTA is more heterogeneous at 560 nm (Silica Thin $Film_{FWHM}$ = 15.05 ns, PVA $Film_{FWHM=}$3.22 ns) compared to observation at 620 nm (Silica Thin $Film_{FWHM}$ = 12.71 ns, PVA $Film_{FWHM=}$2.45 ns).

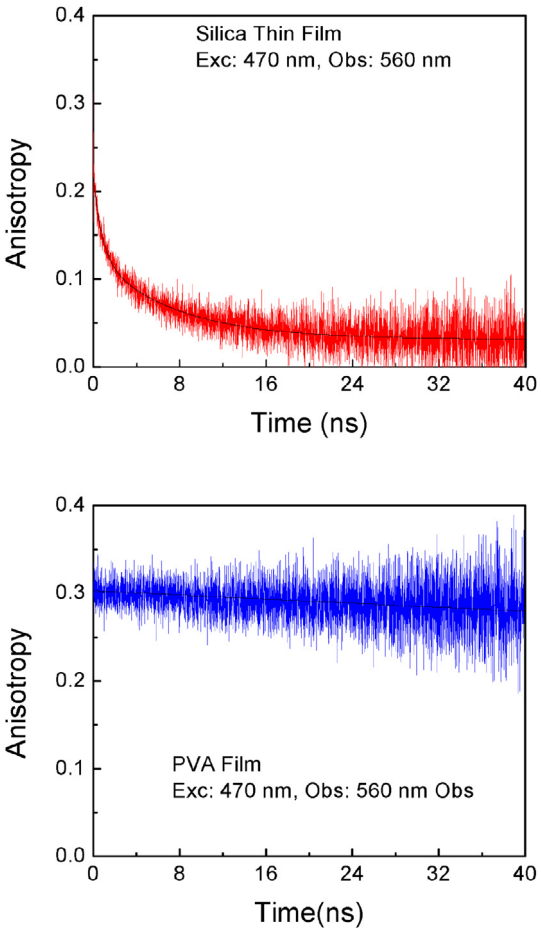

Fig. 8. Top panel: Fluorescence anisotropy decay of *N*-(ω-butanoic acid)-azatriangulenium tetrafluoroborate (ADOTA) in silica thin film (Ex: 470 nm, Obs: 560 nm). Bottom panel: fluorescence anisotropy decay of ADOTA in PVA film (Ex: 470 nm, Obs: 560 nm).

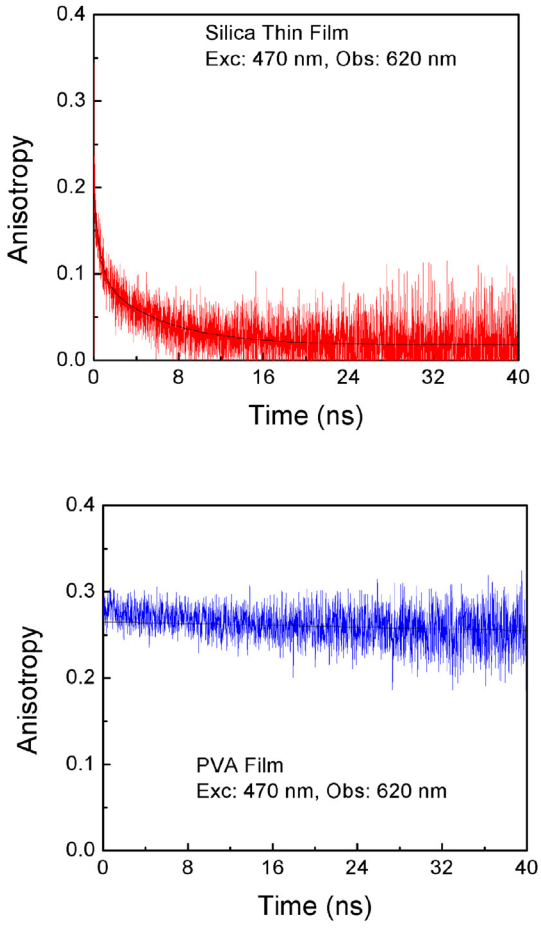

Fig. 9. Top panel: Fluorescence anisotropy decay of *N*-(ω-butanoic acid)-azatriangulenium tetrafluoroborate (ADOTA) in silica thin film (Ex: 470 nm, Obs: 620 nm). Bottom panel: fluorescence anisotropy decay of ADOTA in PVA film (Ex: 470 nm, Obs: 620 nm).

silica thin films, the FWHM value at 560 nm is about 15 ns and at 620 nm about 13 ns. These higher FWHM values show the broader distribution of the emitting molecules in silica thin films.

3.5. Time resolved anisotropy

Time resolved anisotropy measurements presented in Figs. 8 and 9 shows some interesting information. As expected in the case of the PVA matrix, initial anisotropy was high (0.3) with a very long correlation time (>500 ns) (correlation time >> fluorescence lifetime) at both observation wavelengths (560 and 620 nm). However, in case of silica gel matrix the recovered initial anisotropy values are 0.21 and 0.19 for 560 and 620 nm observation and the measured correlation times and r_{INF} values are not significantly different (Table 3). The heterogeneous nature of the correlation times is due to the populations of the dyes in different types of matrix environment. Therefore, it will not be surprising if a part of the dye population is immobilized completely and a part of it has a moderate freedom than the others. It is suggested in the literature that the hydrogen bonding among silica mesh and the dye molecules undergoes reshuffling in excited state and it may give rise to such correlation times [7]. Moreover, the estimated steady state anisotropy values at these wavelengths are 0.069 and 0.042. The drop in the initial recovered anisotropy, in case of anisotropy decay, and steady state anisotropy values suggests energy migration (if the dye molecules are sitting together below 40 A^0 distances which is the approximate Forster distance for such homo-transfer and is a possibility we cannot ignore). Although energy migration is a rapid process which takes place over the lifetime of the fluorophore despite having a relatively long fluorescence lifetime in both matrices.

Table 3
Analysis of *N*-(ω-butanoic acid)-azatriangulenium tetrafluoroborate (ADOTA) anisotropy decay using multiexponential model of on Silica thin film and PVA film.

Sample	Observation (nm)	Anisotropy			Correlation time (ns)	
		r_1	r_2	r_{INF}	Φ_1	Φ_2
ADOTA silica thin film	560	0.088	0.095	0.03	0.81	7.37
	620	0.081	0.093	0.017	6.02	0.58
ADOTA PVA film	560	0.30	–	–	504.4	–
	620	0.26	–	–	1000	–

4. Conclusions

In the present work, the organic fluorophore, *N*-(ω-butanoic acid)-azatriangulenium tetrafluoroborate (ADOTA) was successfully incorporated into silica thin films by the sol–gel process as well as in PVA films. The PVA matrix was chosen to study fluorescence properties of ADOTA in a more rigid environment. Silica matrix provides an unusual environment for the entrapped fluorophores and affects the dye properties in many different ways. A red shift of 15 nm was observed in the emission spectra of ADOTA in silica thin film. In addition, the fluorescence lifetime of ADOTA at 560 nm observation in silica matrix was 12 ns compared to 20 ns in PVA film. However, when the wavelength of observation was placed at 620 nm, the fluorescence lifetimes of ADOTA entrapped in both the matrices are almost similar. The Lorentzian lifetime distribution shows the presence of broad distribution of the emitting species in silica thin layer compared to PVA film. To sum up, considering all the observations such as lower fluorescence efficiencies, shorter lifetimes and concentration dependent red shifted emission suggests aggregation of dye molecules in the excited state. Ultrafast spectroscopy experiments will further support our observations.

Acknowledgments

This work was supported by the NIH grant R01EB12003 (Z.G) and NSF grant CBET-1264608 (I.G), the Carlsberg Foundation (T.J.S), and NCN 2011/03/B/ST5/03094 (B. G).

Appendix A. Supplementary data

Supplementary data related to this article can be found at http://dx.doi.org/10.1016/j.dyepig.2015.01.027.

References

[1] MacCraith BD, McDonagh C. Enhanced fluorescence sensing using sol–gel materials. J Fluoresc 2002;12(3–4):333–42.
[2] Wang X, Wolfbeis OS. Fiber-optic chemical sensors and biosensors (2008–2012). Anal Chem 2012;85(2):487–508.
[3] McDonagh C, Burke CS, MacCraith BD. Optical chemical sensors. Chem Rev 2008;108(2):400–22.
[4] Vannahme C, Leung MC, Richter F, Smith CL, Hermannsson PG, Kristensen A. Nanoimprinted distributed feedback lasers comprising TiO_2 thin films: design guidelines for high performance sensing. Laser & Photonics Rev 2013;7(6):1036–42.
[5] Reisfeld R. Spectroscopy and applications of molecules in glasses. J Non Cryst Solids 1990;121(1):254–66.
[6] Levy D. Sol–gel glasses for optics and electro-optics. J Non Cryst Solids 1992;147:508–17.

[7] Avnir D, Levy D, Reisfeld R. The nature of the silica cage as reflected by spectral changes and enhanced photostability of trapped rhodamine 6G. J Phys Chem 1984;88(24):5956–9.
[8] Lewkowicz A, Bojarski P, Synak A, Grobelna B, Akopova I, Gryczynski I, et al. Concentration-dependent fluorescence properties of rhodamine 6G in titanium dioxide and silicon dioxide nanolayers. J Phys Chem C 2012;116(22):12304–11.
[9] Lewkowicz A, Synak A, Grobelna B, Kułak L, Bojarski P. Spectroscopic properties of rhodamine B entrapped in hybrid porous nanolayers at high dye concentration. Chem Phys 2014.
[10] Synak A, Bojarski P, Grobelna B, Kułak L, Lewkowicz A. Determination of local dye concentration in hybrid porous silica thin films. J Phys Chem C 2013;117(21):11385–92.
[11] Livage J. Sol–gel processes. Curr Opin Solid State Mater Sci 1997;2(2):132–8.
[12] Gomez-Romero P. Hybrid organic ± inorganic materialsÐ in search of synergic activity*. Adv Mater 2001;13(3):5.
[13] Eremenko A, Smirnova N, Rusina O, Linnik O, Eremenko T, Spanhel L, et al. Photophysical properties of organic fluorescent probes on nanosized TiO_2/SiO_2 systems prepared by the sol–gel method. J Mol Struct 2000;553(1):1–7.
[14] Henglein A. Small-particle research: physicochemical properties of extremely small colloidal metal and semiconductor particles. Chem Rev 1989;89(8):1861–73.
[15] Spanhel L, Anderson MA. Synthesis of porous quantum-size cadmium sulfide membranes: photoluminescence phase shift and demodulation measurements. J Am Chem Soc 1990;112(6):2278–84.
[16] Spanhel L, Anderson MA. Semiconductor clusters in the sol–gel process: quantized aggregation, gelation, and crystal growth in concentrated zinc oxide colloids. J Am Chem Soc 1991;113(8):2826–33.
[17] Kamat PV. Photochemistry on nonreactive and reactive (semiconductor) surfaces. Chem Rev 1993;93(1):267–300.
[18] Liu X, Thomas J. Formation and photophysical properties of cadmium sulfide in zeolites with cages and channels. Langmuir 1989;5(1):58–66.
[19] Brinker CJ, Scherer GW. Sol–gel science: the physics and chemistry of sol–gel processing. Gulf Professional Publishing; 1990.
[20] Wohlrab S, Hoppe R, Schulz-Ekloff G, Wöhrle D. Encapsulation of methylene blue into aluminophosphate family molecular sieves. Zeolites 1992;12(7):862–5.
[21] Knobbe ET, Dunn B, Fuqua PD, Nishida F. Laser behavior and photostability characteristics of organic dye doped silicate gel materials. Appl Opt 1990;29(18):2729–33.
[22] Kim M, Seok S, Ahn B, Koo S, Paik S. Encapsulation of water-soluble dye in spherical sol–gel silica matrices. J Sol Gel Sci Technol 2003;27(3):355–61.
[23] Panitz J, Geiger F. Leaching of the anthraquinone dye solvent blue 59 incorporated into organically modified silica xerogels. J Sol Gel Sci Technol 1998;13(1–3):473–7.
[24] Tani T, Namikawa H, Arai K, Makishima A. Photochemical hole burning study of 1,4-dihydroxyanthraquinone doped in amorphous silica prepared by alcoholate method. J Appl Phys 1985;58(9):3559–65.
[25] Laursen BW, Krebs FC. Synthesis of a triazatriangulenium salt. Angew Chem Int Ed 2000;39(19):3432–4.
[26] W Laursen B, C Krebs F. Synthesis, structure, and properties of azatriangulenium salts. Chem A Eur J 2001;7(8):1773–83.
[27] Sørensen TJ, Thyrhaug E, Szabelski M, Luchowski R, Gryczynski I, Gryczynski Z, et al. Azadioxatriangulenium: a long fluorescence lifetime fluorophore for large biomolecule binding assay. Methods Appl Fluoresc 2013;1(2):025001.
[28] Sørensen TJ, Hildebrandt CB, Elm J, Andreasen JW, Madsen AØ, Westerlund F, et al. Large area, soft crystalline thin films of N,N′,N″-trialkyltriazatriangulenium salts with homeotropic alignment of the discotic cores in a lamellar lattice. J Mater Chem 2012;22(11):4797–805.
[29] Thyrhaug E, Sørensen TJ, Gryczynski I, Gryczynski Z, Laursen BW. Polarization and symmetry of electronic transitions in long fluorescence lifetime triangulenium dyes. J Phys Chem A 2013;117(10):2160–8.
[30] Dileesh S, Gopidas K. Photoinduced electron transfer in azatriangulenium salts. J Photochem Photobiol A 2004;162(1):115–20.
[31] Maliwal BP, Fudala R, Raut S, Kokate R, Sørensen TJ, Laursen BW, et al. Long-lived bright red emitting azaoxa-triangulenium fluorophores. PloS One 2013;8(5):e63043.
[32] Bharill S, Sarkar P, Ballin JD, Gryczynski I, Wilson GM, Gryczynski Z. Fluorescence intensity decays of 2-aminopurine solutions: lifetime distribution approach. Anal Biochem 2008;377(2):141–9.
[33] Kaufman VR, Avnir D. Structural changes along the sol–gel–xerogel transition in silica as probed by pyrene excited-state emission. Langmuir 1986;2(6):717–22.

Fluorescent biosensor for the detection of hyaluronidase: intensity-based ratiometric sensing and fluorescence lifetime-based sensing using a long lifetime azadioxatriangulenium (ADOTA) fluorophore

Rahul Chib, Mark Mummert, Ilkay Bora, Bo W. Laursen, Sunil Shah, Robert Pendry, et al.

Analytical and Bioanalytical Chemistry

ISSN 1618-2642

Anal Bioanal Chem
DOI 10.1007/s00216-016-9472-5

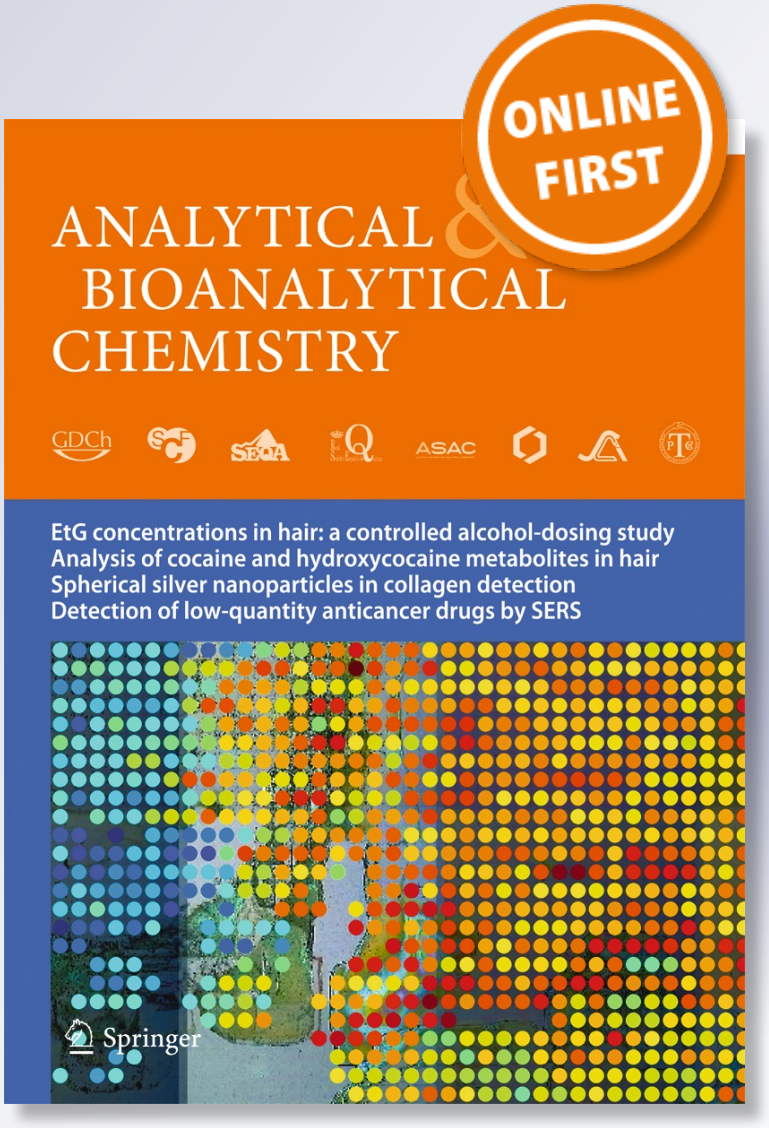

Springer

Anal Bioanal Chem
DOI 10.1007/s00216-016-9472-5

RESEARCH PAPER

Fluorescent biosensor for the detection of hyaluronidase: intensity-based ratiometric sensing and fluorescence lifetime-based sensing using a long lifetime azadioxatriangulenium (ADOTA) fluorophore

Rahul Chib[1] · Mark Mummert[2] · Ilkay Bora[3] · Bo W. Laursen[3] · Sunil Shah[1] · Robert Pendry[4] · Ignacy Gryczynski[1] · Julian Borejdo[1] · Zygmunt Gryczynski[1,4] · Rafal Fudala[1]

Received: 21 December 2015 / Revised: 22 February 2016 / Accepted: 7 March 2016

Abstract In this report, we have designed a rapid and sensitive, intensity-based ratiometric sensing as well as lifetime-based sensing probe for the detection of hyaluronidase activity. Hyaluronidase expression is known to be upregulated in various pathological conditions. We have developed a fluorescent probe by heavy labeling of hyaluronic acid with a new orange/red-emitting organic azadioxatriangulenium (ADOTA) fluorophore, which exhibits a long fluorescence lifetime (~20 ns). The ADOTA fluorophore in water has a peak fluorescence lifetime of ~20 ns and emission spectra centered at 560 nm. The heavily ADOTA-labeled hyaluronic acid (HA-ADOTA) shows a red shift in the peak emission wavelength (605 nm), a weak fluorescence signal, and a shorter fluorescence lifetime (~4 ns) due to efficient self-quenching and formation of aggregates. In the presence of hyaluronidase, the brightness and fluorescence lifetime of the sample increase with a blue shift in the peak emission to its original wavelength at 560 nm. The ratio of the fluorescence intensity of the HA-ADOTA probe at 560 and 605 nm can be used as the sensing method for the detection of hyaluronidase. The cleavage of the hyaluronic acid macromolecule reduces the energy migration between ADOTA molecules, as well as the degree of self-quenching and aggregation. This probe can be efficiently used for both intensity-based ratiometric sensing as well as fluorescence lifetime-based sensing of hyaluronidase. The proposed method makes it a rapid and sensitive assay, useful for analyzing levels of hyaluronidase in relevant clinical samples like urine or plasma.

Keywords Hyaluronidase sensing · Azadioxatriangulenium fluorophore · Ratiometric sensing · Fluorescence lifetime-based sensing · Fluorescence-based assay

Electronic supplementary material The online version of this article (doi:10.1007/s00216-016-9472-5) contains supplementary material, which is available to authorized users.

✉ Rahul Chib
rc0307@live.unthsc.edu

✉ Rafal Fudala
Rafal.Fudala@unthsc.edu

[1] Department of Cell Biology, Immunology and Microbiology, Center for Fluorescence Technologies and Nanomedicine, University of North Texas Health Science Center, Fort Worth, TX 76107, USA

[2] Mental Sciences Institute, University of North Texas Health Science Center, Fort Worth, TX 76107, USA

[3] Nano-Science Center & Department of Chemistry, University of Copenhagen, Universitetsparken 5, 2100 København Ø, Denmark

[4] Department of Physics and Astronomy, Texas Christian University, Fort Worth, TX 76129, USA

Introduction

Hyaluronidase is a family of endoglycosidase that catalyzes the depolymerization of hyaluronic acid (HA) via cleavage of β-*N*-acetyl-D-glucosaminidic bonds [1]. Hyaluronidase is known to be involved in various physiological and pathological conditions like fertilization, embryogenesis, inflammation, tumor growth, and wound healing [2–6]. Initially in the literature, it was described as a "spreading factor" which was found in the testicular extract of animal and humans. It was later characterized as hyaluronic acid-degrading enzyme and called hyaluronidase [5, 7–9]. Recent studies have shown the role of hyaluronic acid and hyaluronidase with the

Published online: 18 March 2016

differentiation, proliferation, migration, and angiogenesis of tumor cells [2, 10, 11]. HA is a linear, non-sulfated glycosaminoglycan composed of multiple subunits of D-glucuronic acid and *N*-acetylglucosamine. In humans, HA is known to maintain various important functions like cartilage integrity, osmotic balance, and homeostasis of water owing to its gel-like properties [12–14]. An overexpression of hyaluronidase is associated in the literature with patients suffering from cancers, such as prostate cancer [15], bladder cancer [6], head and neck carcinoma [4], colon cancer, and malignant melanoma [5]. Therefore, it is of great interest to develop a simple, sensitive, and fast technique with which one can estimate the activity/level of hyaluronidase in biological samples.

Several methods have been reported in the literature for detecting hyaluronidase activity, which mainly depends on the degradation of hyaluronic acid by hyaluronidase. To measure hyaluronidase activity/level, there are several methods reported in the literature which includes turbidimetry [16], viscometry [17], ELISA-like assay [18, 19], colorimetry [20], zymography [21, 22], and fluorescence detection [23–32]. Methods like turbidimetry, colorimetry, and viscometry are not very sensitive and cannot detect the level of hyaluronidase at different time points of an experiment. Zymography is simple yet not very sensitive for quantitative measurements. ELISA-like assays are sensitive and selective but do not allow real-time monitoring of hyaluronidase activity. However, fluorescence-based detection of hyaluronidase is a fast and sensitive method, useful for high-throughput screening, and has a real-time monitoring capability and their usefulness in biological samples makes it an ideal method for hyaluronidase detection.

Various novel fluorescence assays designed to detect hyaluronidase activity have been reported in the literature. These fluorescent probes have been designed for hyaluronidase detection by using hyaluronic acid as a template and labeling it with gold nanoparticles [23, 33], organic fluorescent dyes [34, 35], conjugated small molecules [36], and upconversion luminescence material [29]. Although these fluorescence-based methods have superior properties compared to previous methods in terms of sensitivity, they also have a few drawbacks. For example, gold nanoparticles precipitate in biological high salt environments [26, 37]. Fluorescent probes developed using organic fluorophores are smaller in size compared to probes developed using quantum dots, nanodots, and noble metal nanoparticle as the luminescent material. Some fluorescent probes have a very short fluorescence lifetime and hence cannot be used for lifetime-based sensing or imaging, as the background of the biological sample interferes with the fluorescence signal of the probe and cannot be easily removed as the fluorescence intensity decay of background and probe is almost similar [27, 34].

To make this probe, we heavily labeled hyaluronic acid with an azadioxatriangulenium (ADOTA) fluorophore. ADOTA is an orange/red-emitting organic fluorophore with peak emission centered at 560 nm and a fluorescence lifetime of 20 ns in aqueous solution. Our previous studies have shown that it is the only red-emitting organic fluorophore with a long fluorescence lifetime of 20 ns [38–47]. One major problem encountered using fluorescence detection methods in biological fluids, cells, and tissue is the presence of autofluorescence which reduces the obtainable signal-to-noise ratio. As most biomolecules emit at higher energies, the autofluorescence level decreases towards the red/NIR region of the electromagnetic spectrum. Therefore, using a red-emitting fluorophore can help to overcome this issue.

The goal of this study was to develop a rapid and sensitive ratiometric sensing probe for estimating hyaluronidase activity/level. To achieve this goal, a simple strategy was used where we developed a probe using HA as template and labeled it with an orange/red-emitting organic fluorophore with a long fluorescence lifetime. The design of this probe was created by heavy labeling of HA with an aniline-substituted ADOTA fluorophore (Scheme 1) [48]. When a certain molar ratio of the fluorophore to hyaluronic acid is reached, fluorophores are close enough that dimers or higher order aggregates may form. The aggregated dyes display red-shifted absorption and fluorescence as well as reduced fluorescence lifetime (4 ns). Even a small fraction of aggregates dominates the optical properties due to the close proximity of all dyes bound to HA and the resulting quenching of non-aggregated dyes via energy transfer to the red-shifted aggregates. The fluorescence intensity and fluorescence lifetime of the HA-ADOTA probe are thus significantly reduced compared to the non-aggregated ADOTA dye. The fluorescence signal will recover after the degradation of the probe by hyaluronidase, where the long hyaluronic acid chains of the HA-ADOTA probe are split into shorter fragments and the fluorophore molecules will move apart. It was observed from our previous observations that the aggregation of ADOTA fluorophore causes a red shift in the peak emission wavelength [38]. Similarly, heavy labeling of hyaluronic acid with ADOTA causes a shift in the peak emission wavelength of the probe to 605 nm. Once the hyaluronidase starts degrading this probe, the peak emission wavelength shifts back to its original position at 560 nm. This shift in emission wavelength after degradation of the probe provides a method to develop a ratiometric sensing probe, where the ratio of emission intensity of the digested to undigested probe can be used to calculate hyaluronidase activity/level. Some of the reported methods for the fluorescence detection utilize single fluorescence intensity as the sensing method. Collection of the signal at a fixed wavelength can be tempered due to various reasons like fluctuation in the excitation intensity, emission collection efficiency, change in focal point, etc.[49, 50]. These problems can be overcome by ratiometric collection of signal at two different wavelengths. Ratiometric sensing acts in a self-

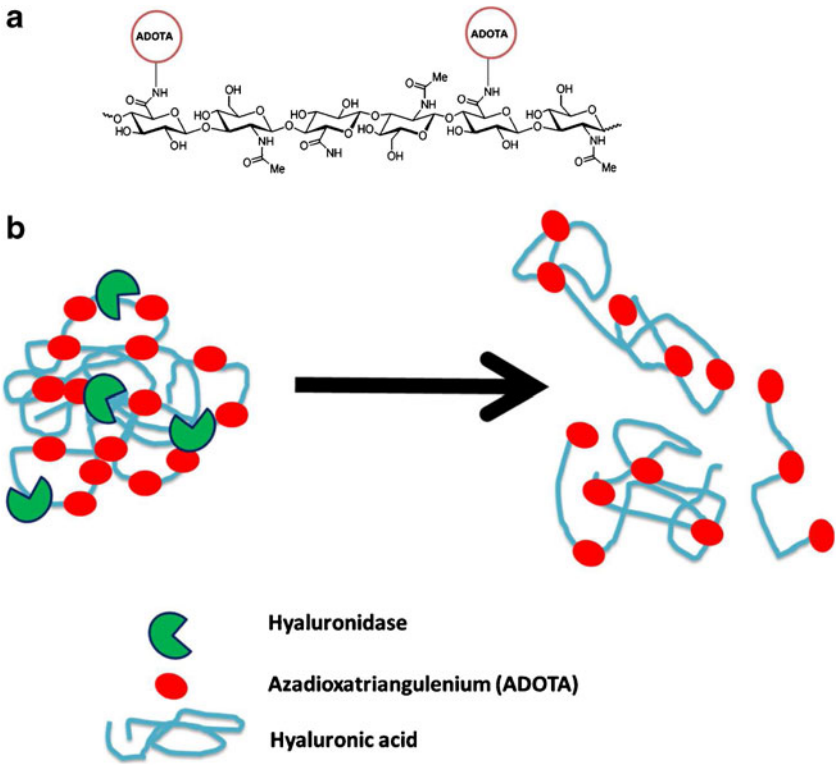

Scheme 1 Schematic representation for the assay system and its response to the enzyme hyaluronidase. (**A**) Covalent binding of ADOTA fluorophore to the COOH group of hyaluronic acid. (**B**) Undigested HA-ADOTA probe and cleaved probe following enzymatic action

calibrating way to minimize interfering factors while allowing for more accurate detection of analyte [51–53].

The activity/level of hyaluronidase can also be estimated using the change in the fluorescence lifetime of the biosensor as the aggregation in the undigested probe leads to a decrease in the fluorescence lifetime (4 ns). After cleavage of the biosensor by hyaluronidase, a recovery in the amplitude-weighted fluorescence lifetime was observed (15 ns). This large difference in the fluorescence lifetime of the probe can be used for the detection of hyaluronidase. Here in this paper, we tested the HA-ADOTA probe in spiked PBS and we also used it to measure hyaluronidase activity/level in cell culture media from a prostate cancer cell line (DU-145) which is known to express higher levels of hyaluronidase [15, 54].

Materials and methods

Sodium hyaluronate from bacterial fermentation was obtained from Acros Organics (Thermo Fisher Scientific, Fair Lawn, NJ). Dimethyl sulfoxide (DMSO), guanidine hydrochloride, acetaldehyde, cyclohexyl isocyanide, centricon filter (30,000 molecular cutoff), and bovine testis hyaluronidase (EC 3.2.1.35, type 1-S, 451 U/mg) were obtained from Sigma-Aldrich (Sigma-Aldrich, St. Louis, MO). Dulbecco's phosphate-buffered saline (PBS), fetal bovine serum (FBS), DMEM media, antibiotic, insulin, transferrin, and selenium (ITS) supplement, and Slide-A-Lyser dialysis cassettes (10, 000 molecular weight cutoff) were purchased from Thermo Fisher Scientific (Waltham, MA). ELISA kit for hyaluronic acid was purchased from R&D Systems (Minneapolis, MN). DU-145 cells were purchased from ATCC (Manassas, VA). The ADOTA fluorophore (*N*-(4-aminophenyl)-azadioxatriangulenium tetrafluoroborate) was synthesized as described elsewhere [48]. All compounds, solvents, and materials were used as received; water was used directly from a Millipore (Billerica, MA) purification system.

Preparation of the active amine form of the azadioxatriangulenium (ADOTA-NH_2) fluorophore

The ADOTA fluorophore with a reactive amine group was prepared according to previously published procedures [48]. Briefly, tris(2,6-dimethoxyphenyl)methylium tetrafluoroborate was reacted with *p*-aminoaniline and 2,6-lutidinein acetonitrile at ambient temperature for 90 min to form the respective acridinium salt. Subsequent twofold ring closure in molten pyridinium hydrochloride at 200 °C in 60 min provided the fluorescent ADOTA. Precipitation as the tetrafluoroborate salt and recrystallization from methanol yield the pure compound in excellent yield as dark crystals (Scheme 2).

Preparation of HA-ADOTA probe

The starting material for the preparation of the reactive amine of the AzaDiOxaTriaAngulenium (ADOTA-phenyl-NH_2)

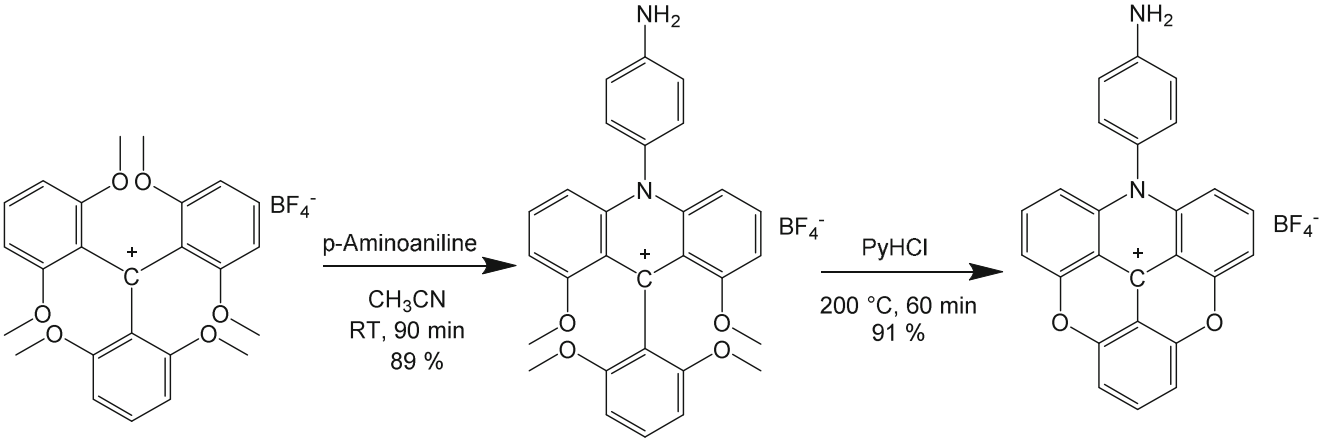

Scheme 2 Synthetic procedure for the preparation of *p*-aminophenyl-ADOTA BF_4

was prepared according to the above-described method (Scheme 2). HA was dissolved to 1.25 mg/mL in dH_2O and then diluted 1:2 in DMSO. The ADOTA-NH_2 was dissolved in DMSO and added to the HA solution for a final ADOTA-NH_2 concentration of 25 mg/mL. Acetaldehyde and cyclohexyl isocyanide were added to 0.04 % (*v*/*v*), and the reaction was allowed to proceed for 48 h at 25 °C. Afterwards, the solution was diluted 1:14 in ethanol/guanidine HCl (50 μL of 3 M guanidine HCl per 900 μL of 100 % ethanol) and the HA-ADOTA allowed to precipitate overnight at −20 °C. The precipitate was then dissolved in 1 mL of dH_2O followed by extensive dialysis against dH_2O. The concentration of HA in the probe was measured using ELISA kit for hyaluronic acid and was found to be 0.6 mg/mL.

Preparation of cell culture media

Concentrated cell culture media were prepared according to the method mentioned by Lokeshwar et al. with slight modifications [54]. DU-145 cells were plated in DMEM media containing 10 % FBS and 1 % antibiotic solution. After 70 % confluency, cells were washed three times with serum-free DMEM media. Cells were then incubated with serum-free DMEM media with ITS supplement. The serum-free media were collected after 72 h and concentrated ten times using 30,000 molecular cutoff centricon filter. Concentrated media from six culture flasks were pooled together and used for analyzing hyaluronidase activity in the media.

Experimental section

Absorption measurements

Absorption spectra were measured using a Cary 50 Bio UV–visible spectrophotometer (Varian Inc., Australia). Absorption spectra were scanned from 350 to 620 nm in PBS at room temperature.

Steady-state fluorescence measurements of hyaluronan hydrolysis

The HA-ADOTA probe was incubated with different amount of hyaluronidase (0–100 U/mL) in PBS, pH 7.4, at room temperature. The fluorescence emission spectra were recorded every 10 min for 150 min for all the concentrations of the enzyme. Steady-state fluorescence intensity measurements of all the samples were made using a Carry Eclipse spectrofluorometer (Varian Inc., Australia) using a 10-mm × 4-mm quartz cuvette. The emission was scanned from 520 to 700 nm following a 470-nm excitation and using a 495-nm-long pass filter on the emission side. Steady-state excitation spectra were measured by observing the emission at 605 nm, and excitation was scanned from 400 to 600 nm using a 590-nm-long pass filter on the emission side.

Fluorescence intensity decay

Same amount of HA-ADOTA probe was added to PBS (pH 7.4) with varying amount of hyaluronidase (0–100 U/mL). The change in fluorescence lifetime was measured for all the concentrations of enzyme every 20 min for 160 min. Fluorescence lifetimes of all the samples were measured using FluoTime 200 (PicoQuant, GmbH, Berlin, Germany) time-resolved spectrofluorometer. This instrument contains a multichannel plate detector (Hamamatsu, Japan), and a 470-nm laser diode was used as the excitation source. The fluorescence intensity decays were measured under magic angle conditions (54.7°), and data was analyzed with FluoFit version 4.5.3 software (PicoQuant GmbH, Berlin, Germany) using the exponential reconvolution procedure using nonlinear

regression (multiexponential deconvolution model). In the case of multiexponential analysis, the fluorescence decay was analyzed using:

$$I(t) = \sum_i \alpha_i \exp(-t/\tau_i)$$

where τ_i are the decay time and α_i are the pre-exponential factors (amplitudes) of the individual components. Amplitude-weighted lifetime is given by:

$$\langle \tau \rangle = \sum_i \alpha_i \tau_i$$

For measuring fluorescence lifetime of HA-ADOTA in solution containing concentrated media from DU-145 cells, a confocal microscope equipped with time-correlated single photon counting (TCSPC) detector was used (MicroTime 200, PicoQuant, Germany). A 470-nm laser operating at 5 MHz repetition rate was used. Sample is prepared in a glass bottom petri dish, and laser excitation is used on Olympus 1X71 inverted microscope. The signal from the detector was routed into a PicoHarp 300 (PicoQuant, Germany) TCSPC module. Fluorescence lifetime was measured every 10 min for 150 min. All analyses were performed using SymPho Time, V.5.3.2 software from PicoQuant.

Results and discussion

Scheme 1 shows the schematic representation of HA-ADOTA probe. The HA-ADOTA probe obtained from heavy labeling of ADOTA fluorophore produces a low fluorescence signal and exhibit a short fluorescence lifetime resulting from aggregation and FRET between ADOTA molecules and aggregates. Nevertheless, the addition of hyaluronidase to the HA-ADOTA biosensor solution causes a strong fluorescence enhancement and an increase in the fluorescence lifetime, which is attributed to the specific cleavage of the hyaluronic acid template by hyaluronidase and the breakup of aggregates and spatial separation of fluorophores.

Figure 1 shows the absorption spectrum of HA-ADOTA probe in PBS solution at room temperature with the maximum absorption peak centered at 540 nm. A second transition is of lower oscillator strength with peak centered at 440 nm. As it can be seen from Fig. 1, even though the main absorption peak is centered at 540 nm, a 470-nm excitation is also enough to excite the probe. Furthermore, a complete emission spectrum can be obtained when the probe is excited using a 470-nm excitation source. The concentration of the ADOTA in the stock HA-ADOTA is 13.96 μM. The probe was diluted 200 times in the assay system (70 nM).

The normalized emission spectra of HA-ADOTA probe and free ADOTA fluorophore in PBS following a 470-nm excitation are shown in Fig. 2A. It can be seen from the graph that the emission spectra of free fluorophore are centered at 560 nm, whereas the peak emission of HA-ADOTA probe is centered at 605 nm. The 45-nm shift in the peak emission wavelength was obtained due to aggregation of the fluorophore molecules. This shift in the peak emission proves the efficient energy transfer between the ADOTA molecules and in fact shows the efficient design of this biosensor.

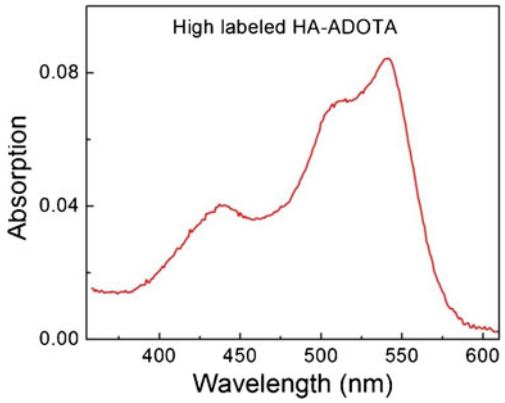

Fig. 1 The absorption spectrum of HA-ADOTA probe in PBS (pH 7.4). The concentration of ADOTA in HA-ADOTA probe is 13.96 μM. HA-ADOTA probe in the assay system is 70 nM

The excitation spectra and emission spectra of HA-ADOTA probe before and after enzymatic cleavage with 100 U/mL of hyaluronidase are shown in Fig. 2B. It can be seen from Fig. 2B that the emission spectrum of the digested probe shifts back to its original peak emission wavelength of 560 nm, whereas the intact probe has a peak emission wavelength centered at 605 nm. This aggregation-induced shift in the emission wavelength allows for an efficient method to ratiometrically detect the enzyme activity by measuring the fluorescence intensity at two wavelengths, i.e. 560 and 605 nm. The ratiometric sensing provides a built-in self-calibration and higher accuracy in terms of quantitative analysis. We also observed a small change in the excitation spectra of HA-ADOTA probe before and after cleavage by hyaluronidase. The shift in the emission wavelength of the HA-ADOTA probe is also visible to the eye. Figure 2C shows the change in the color of the solution containing HA-ADOTA probe before and after enzymatic cleavage, when excited using a handheld blue laser. We also estimated the quantum yield of the ADOTA monomer and aggregates by mimicking the monomer/aggregate system in thin polyvinyl alcohol (PVA) films with low and high concentration of ADOTA. The estimated quantum yield for monomer is 55 %, whereas the quantum yield for aggregate ADOTA system is less than 1 %. The details about quantum yield measurement are given in the Electronic Supplementary Material (ESM, Fig. S1).

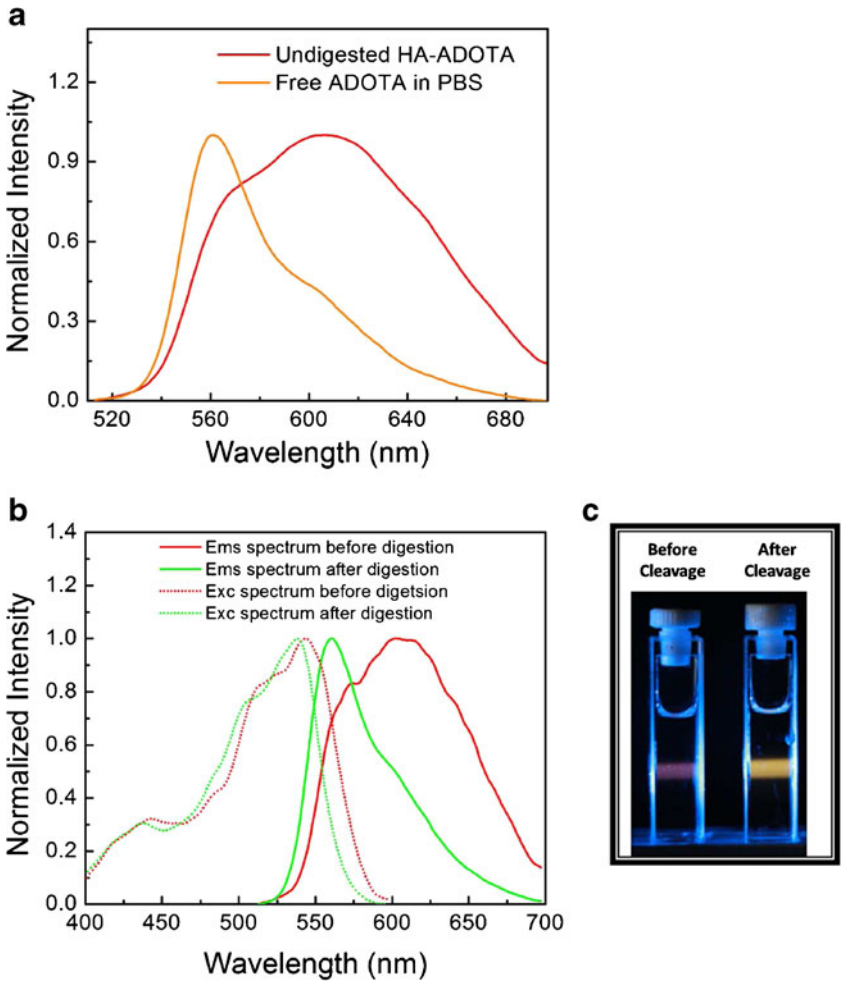

Fig. 2 (**A**) Normalized emission spectra of free ADOTA fluorophore in PBS (pH 7.4) and the emission spectra of HA-ADOTA probe (70 nM ADOTA) in PBS (pH 7.4) when excited using a 470-nm light source. (**B**) The excitation and emission spectra of heavily labeled HA-ADOTA (70 nM ADOTA) probe before and after enzymatic cleavage. The large spectral overlap between excitation and emission spectra is responsible for an efficient excitation energy migration (HOMO-FRET) between ADOTA molecules. The energy migration between ADOTA molecules is responsible for the self-quenching process. (**C**) Pictorial representation of the change in the color of HA-ADOTA solution before and after hyaluronidase cleavage

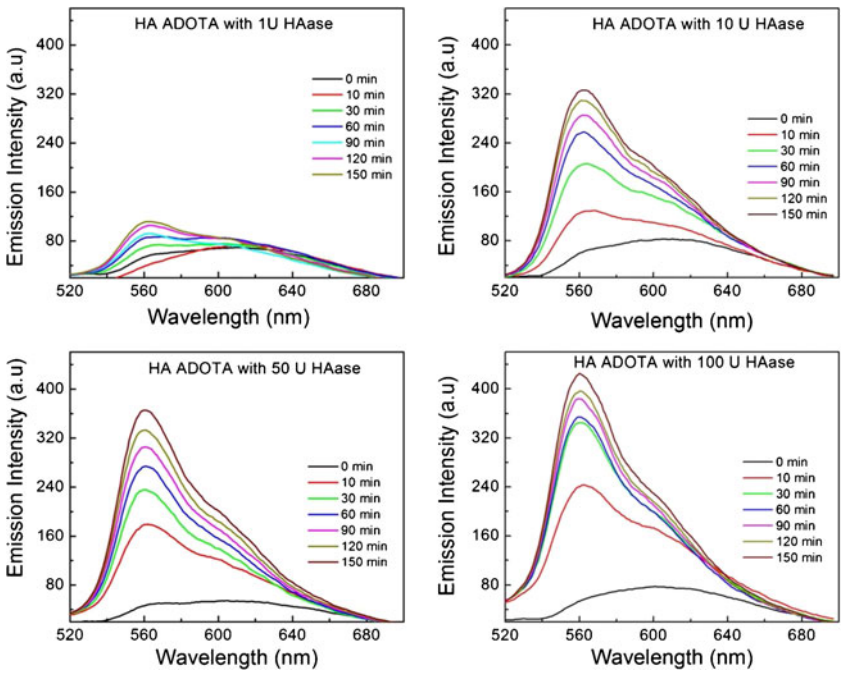

Fig. 3 The change is fluorescence emission of HA-ADOTA probe (70 nM ADOTA, PBS pH 7.4) after incubation with different amount of hyaluronidase enzyme. The fluorescence emission spectra were collected for 150 min. A 470-nm laser was used for the excitation, and the experiments were performed in triplicate and a similar increase in fluorescence intensity was observed

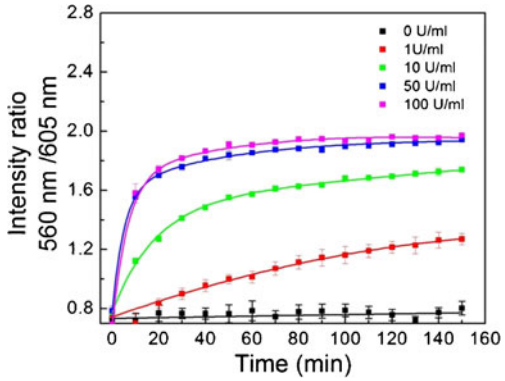

Fig. 4 Change is the ratio of emission intensity (560 nm/605 nm) of the assay system (70 nm ADOTA) in PBS buffer (PBS 7.4) at room temperature vs reaction time in the presence of different amount of hyaluronidase. A 470-nm laser was used for excitation, and all the experiments were performed in triplicate

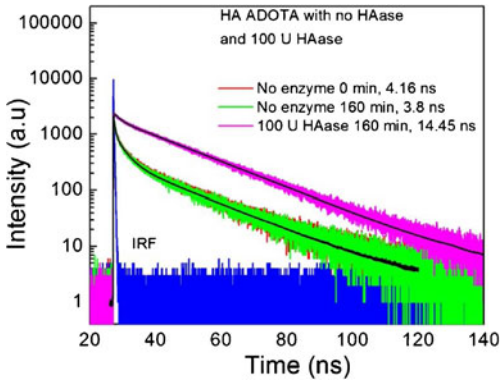

Fig. 6 The fluorescence intensity decay of HA-ADOTA probe (70 nm ADOTA, 0.6 mg/mL HA) in PBS (pH 7.4) in the absence and presence of hyaluronidase. In the presence of enzyme, an increase in the fluorescence lifetime was observed. Without the enzyme at 0 min, three components are needed to fit the data with amplitudes of 0.16, 0.53, and 0.31 with the lifetime of 18, 0.41, and 3.23 ns. With 100 U/mL of hyaluronidase at 160 min, the decay was fitted using two components with amplitudes of 0.74 and 0.26 and with lifetime of 18.85 and 1.83 ns. All fluorescence lifetime measurements were performed in triplicate

Response of HA-ADOTA probe with hyaluronidase

As mentioned, the HA-ADOTA probe was synthesized by heavy labeling of hyaluronic acid with ADOTA fluorophore through covalent bond formation. To investigate the response of the biosensor towards hyaluronidase, the fluorescence response of HA-ADOTA probe to hyaluronidase at varying concentration was investigated by adding hyaluronidase to HA-ADOTA probe (70 nM ADOTA) in PBS (pH 7.4) at room temperature. Figure 3 shows the hyaluronidase concentration-dependent change in the fluorescence intensity of the HA-ADOTA probe. The fluorescence intensity of the reaction system increases with increasing concentration of hyaluronidase from 0 to 100 U/mL of hyaluronidase. Even 1 U/mL of hyaluronidase was enough to increase the fluorescence intensity and causes the shift in the peak emission of the HA-ADOTA probe. In the case of 1 U/mL of hyaluronidase, the fluorescence intensity shows 1.7 times enhancement in the fluorescence signal, whereas, in the case of 100 U/mL of enzyme, 5.6 times enhancement in the fluorescence signal was observed. The emission intensity for different amount of hyaluronidase are drawn to the same scale so as to easily distinguish the change in the fluorescence enhancement with different amount of enzyme.

The kinetic assay of the enzymatic reaction was determined by measuring the time-dependent change in the fluorescence intensity of the HA-ADOTA probe in the absence and presence of hyaluronidase. We assessed the change in fluorescence intensity for all concentrations of enzyme every 10 min for 150 min and calculated the change in the intensity ratio using the fluorescence intensity at 560 and 605 nm as the observation points. From Fig. 4, it can be seen that in the absence of hyaluronidase, we did not notice any change in the ratio of fluorescence intensity, which proves the stability of HA-ADOTA probe. The time-dependent fluorescence intensity measurement shows that the emission intensity ratio at 560 and 605 nm gradually increases with increasing amount of enzyme and time. It was also observed from Fig. 4 that the emission intensity ratio almost reaches a plateau after 80 min of reaction when the enzyme concentration was 50 U/mL or higher. To ensure the reaction was complete, we took 100 min

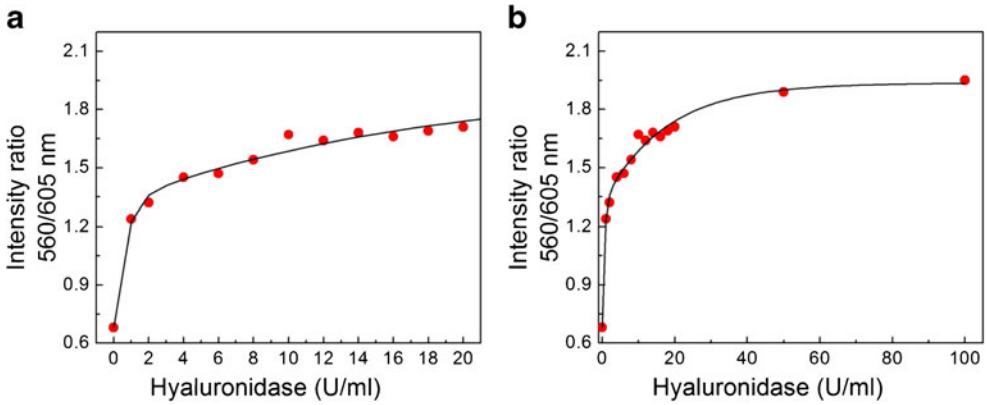

Fig. 5 The calibration curve for the intensity ratio of HA-ADOTA (70 nM ADOTA) probe in PBS (pH 7.4) at 100 min as a function of hyaluronidase levels (**A**) 0–20 U/mL and (**B**) 0–100 U/mL

as the end point in our experiment. Figure 5A represents the calibration curve obtained by measuring the change in the fluorescence intensity after 100 min as a function of hyaluronidase activity for enzyme within 0–20 U/mL, whereas Fig. 5B represents the entire region with 0–100 U/mL. Both the curves were fitted using exponential model ($Y = A_1 \times e^{(-X/t1)} + A_2 \times e^{(-X/t2)} + Y_o$, $R^2 = 0.98$). Details about the fitting method are given in the ESM. Using this standard curve, the level of hyaluronidase from an unknown sample can be easily determined.

Fluorescence lifetime-based sensing of hyaluronidase

We also desired to determine if the observed spectral changes are as well accompanied by the change in the fluorescence lifetime of the HA-ADOTA probe. The fluorescence intensity decay measurements are presented in Fig. 6 for HA-ADOTA probe in PBS at room temperature. The emission of the HA-ADOTA probe is highly quenched in the absence of hyaluronidase and shows a heterogenous decay. Three exponentials are needed to fit the data, and an amplitude-weighted lifetime of 4 ns is determined as compared to 20 ns lifetime for free fluorophore in PBS. In the presence of hyaluronidase, the amplitude-weighted lifetime increases with the increasing amount of enzyme. Table 1 shows the detailed analysis of the intensity decay of HA-ADOTA probe with different concentrations of hyaluronidase (0, 1, 10, 50, and 100 U/mL). The recovered average amplitude-weighted lifetime of HA-ADOTA probe with 100 U/mL of hyaluronidase was 15 ns, and two components were needed to fit the decay with amplitudes of 0.74 and 0.26 and lifetime of 18.85 and 1.83 ns. Figure 7 shows the change in the amplitude-weighted fluorescence lifetime of HA-ADOTA probe with different amounts of enzyme. It can be observed from the graph that with an increasing concentration of hyaluronidase and increasing time, an increase in the fluorescence lifetime is also observed. The time-resolved measurements demonstrate the generation of free unquenched ADOTA dyes ($\tau \sim 19$ ns) in the presence of hyaluronidase.

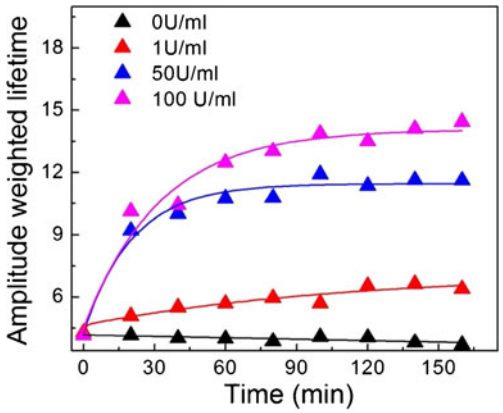

Fig. 7 The time-dependent change in the fluorescence lifetime of HA-ADOTA probe (70 nM ADOTA) in PBS (pH 7.4) in the absence and presence of hyaluronidase

Estimating hyaluronidase activity in cell culture media

It has been previously reported that several prostate cancer cell lines overexpress hyaluronidase activity. DU-145 is one such cell line which is reported to have overexpression of hyaluronidase. To investigate the activity of hyaluronidase produced by DU-145 prostate cancer cell line, we measured enzyme activity in concentrated serum-free culture media using an HA-ADOTA probe. In a solution of 100 μL of concentrated media and PBS (pH 7.4), HA-ADOTA probe (70 nM ADOTA in assay system) was added (total volume 1000 μL). The change in fluorescence intensity ratio was calculated every 10 min for 150 min (Fig. 8). The intensity ratio at 100 min was used to estimate hyaluronidase level using the standard curve obtained from spiked PBS buffer solution (Fig. 5). The calculated hyaluronidase level was 5 U/mL. To confirm if the fluorescence enhancement was caused by hyaluronidase, the effect of apigenin (inhibitor of hyaluronidase) was also examined on the activity of hyaluronidase [5, 55, 56]. Stock solution (20 mM) of apigenin was prepared in DMSO. The final concentration of apigenin in experimental solution was 50 μM. It was observed that the apigenin inhibited the fluorescence enhancement of HA-ADOTA probe. To confirm our steady-state fluorescence intensity data, we also measured the change in

Table 1 Amplitude-weighted lifetime of HA-ADOTA with different amount of hyaluronidase

Hyaluronidase concentration (U)	Time (min)								
	0	20	40	60	80	100	120	140	160
0	4.16 ns	4.16 ns	4.02 ns	4 ns	3.86 ns	4.08 ns	4.05 ns	3.8 ns	3.8 ns
1	4.3 ns	5.09 ns	5.51 ns	5.69 ns	6.07 ns	8.35 ns	8.63 ns	8.77 ns	8.89 ns
50	4.16 ns	9.22 ns	10.03 ns	10.75 ns	10.78 ns	11.91 ns	11.36 ns	11.64 ns	11.62 ns
100	4.16 ns	10.13 ns	10.44 ns	12.47 ns	13.03 ns	13.88 ns	13.5 ns	14.11 ns	14.45 ns

Averaged amplitude-weighted lifetime of HA-ADOTA probe was estimated every 20 min of the enzymatic reaction

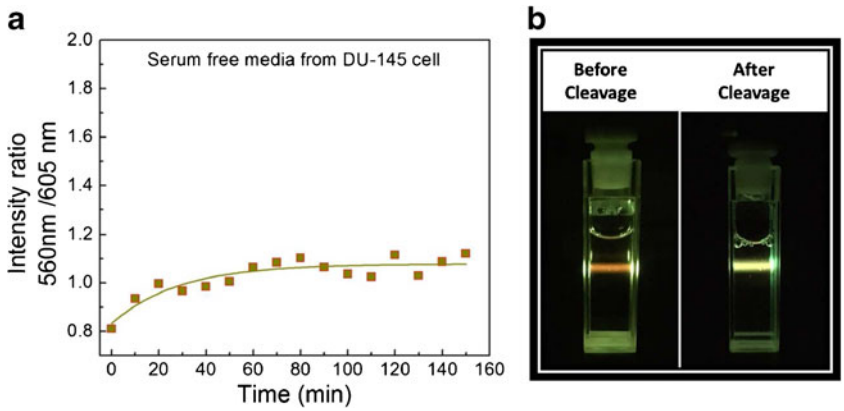

Fig. 8 (**A**) Change is the ratio of emission intensity (560 nm/605 nm) from cell culture media as a function of change in time. A 470-nm excitation was used and the reaction was continued for 150 min at room temperature. All the experiments were performed in triplicate. (**B**) Change in the color of fluorescence emission of HA-ADOTA probe in culture media before and after enzymatic cleavage

the fluorescence lifetime of HA-ADOTA probe in the concentrated serum-free media. Of concentrated media with PBS and HA-ADOTA probe (100 μL total volume), 10 μL was added to a glass bottom petri dish. Fluorescence lifetime was measured using a time-resolved microscope (MicroTime 200, PicoQuant, Germany). The main advantage of using confocal microscope with TCSPC abilities can help us to focus exactly at the center of the media while simultaneously only needing a small volume of the biological sample. The measured amplitude-weighted fluorescence lifetime of the undigested probe was around 4.5 ns. However, after 150 min of enzymatic reaction in the concentrated culture media, a fluorescence lifetime of 18 ns was measured. We also measured the effect of apigenin (hyaluronidase inhibitor) on the fluorescence lifetime of HA-ADOTA probe. Apigenin solution (50 μM) was prepared with 10 μL concentrated media and PBS (total volume = 100 μL). We found that the apigenin inhibited the activity of hyaluronidase and fluorescence lifetime of HA-ADOTA probe stayed constant (4.5 ns). These data suggest that the increase in fluorescence intensity and fluorescence lifetime indeed arises from the hyaluronidase activity. The amplitude-weighted fluorescence lifetime of HA-ADOTA probe in concentrated media with and without apigenin is given in Table 2.

Table 2 Amplitude-weighted fluorescence lifetime of HA-ADOTA probe media collected from DU-145 cell line

Time (min) apigenin	DU-145 media	DU-145 media with apigenin
Background	2.56 ns	2.07 ns
10	4.81 ns	2.8 ns
20	11.09 ns	4.3 ns
30	13.97 ns	5.1 ns
40	14.93 ns	4.14 ns
50	15.25 ns	5.28 ns
60	16.35 ns	3.48 ns
70	18.13 ns	4.56 ns
80	17.74 ns	5.24 ns
90	18.21 ns	4.03 ns
100	17.74 ns	3.85 ns
110	18 ns	4.28 ns
120	17.72 ns	4.3 ns
130	18.37 ns	4.12 ns
140	17.94 ns	4.78 ns
150	17.9 ns	4.87 ns

Data also shows the effect of apigenin on the inhibition of hyaluronidase activity from culture media

Conclusions

In summary, we have successfully developed a biosensor for hyaluronidase using an orange/red-emitting organic ADOTA fluorophore with a long fluorescence lifetime. This probe serves as an intensity-based ratiometric sensor and fluorescence lifetime-based sensor of hyaluronidase. Moreover, due to ratiometric sensing ability, a higher sensitivity can be achieved. The change in color of the fluorescence emission of undigested (red) and digested (yellow) HA-ADOTA probe can also be observed by the naked eyes using an appropriate excitation. Compared to other biosensors developed over nanoparticles, the biosensor developed using organic fluorophore is much smaller in size. The large difference between the fluorescence lifetime of undigested and digested probe helps to easily quantify hyaluronidase level using fluorescence lifetime as detection parameter. Emission in the orange/red region where there is a long fluorescence lifetime makes this probe highly useful for biological samples which possess a large amount of autofluorescence. It is a widely understood phenomenon that the contribution of autofluorescence decreases in the orange/red region of the electromagnetic spectrum. We successfully estimated the level of hyaluronidase in serum-free culture media of DU-145 prostate cancer cells. In conclusion, this HA-ADOTA biosensor can be easily used to measure hyaluronidase activity/level in complex pathological samples where the enzyme hyaluronidase is overexpressed.

Acknowledgments This work was supported by UNTHSC intramural grant RI6120 (R.F.), Sigma Xi grants in aid of research G20141015656984 (R.C.), UNTHSC pre-doctoral bridge grant RI6171 (R.C.), NIH grant R01EB12003 (Z.G.), and NSF grant CBET-1264608 (I.G.). We would like to thank Dr. Andras Lacko and Dr. Nirupama Sabnis for providing us the DU-145 cell line.

Compliance with ethical standards

Conflict of interest The authors declare that they have no competing interests.

References

1. Stern R. Hyaluronidases in cancer biology. Semin Cancer Biol. 2008;18(4):275–80.
2. Chao KL, Muthukumar L, Herzberg O. Structure of human hyaluronidase-1, a hyaluronan hydrolyzing enzyme involved in tumor growth and angiogenesis. Biochemistry (N Y). 2007;46(23):6911–20.
3. Bollet AJ, Bonner WM, Nance JL. The presence of hyaluronidase in various mammalian tissues. J Biol Chem. 1963;238:3522–7.
4. Franzmann EJ, Schroeder GL, Goodwin WJ, Weed DT, Fisher P, Lokeshwar VB. Expression of tumor markers hyaluronic acid and hyaluronidase (HYAL1) in head and neck tumors. Int J Cancer. 2003;106(3):438–45.
5. Liu D, Pearlman E, Diaconu E, Guo K, Mori H, Haqqi T, et al. Expression of hyaluronidase by tumor cells induces angiogenesis in vivo. Proc Natl Acad Sci U S A. 1996;93(15):7832–7.
6. Lokeshwar VB, Estrella V, Lopez L, Kramer M, Gomez P, Soloway MS, et al. HYAL1-v1, an alternatively spliced variant of HYAL1 hyaluronidase: a negative regulator of bladder cancer. Cancer Res. 2006;66(23):11219–27.
7. Chain E, Duthie E. Identity of hyaluronidase and spreading factor. Br J Exp Pathol. 1940;21(6):324.
8. Hobby GL, Dawson MH, Meyer K, Chaffee E. The relationship between spreading factor and hyaluronidase. J Exp Med. 1941;73(1):109–23.
9. McCUTCHEON M, COMAN DR. Spreading factor in human carcinomas. Cancer Res. 1947;7(6):379–82.
10. Turley EA, Noble PW, Bourguignon LY. Signaling properties of hyaluronan receptors. J Biol Chem. 2002;277(7):4589–92.
11. Girish K, Kemparaju K. The magic glue hyaluronan and its eraser hyaluronidase: a biological overview. Life Sci. 2007;80(21):1921–43.
12. Stern R. Hyaluronan catabolism: a new metabolic pathway. Eur J Cell Biol. 2004;83(7):317–25.
13. Stern R. Hyaluronan metabolism: a major paradox in cancer biology. Pathol Biol. 2005;53(7):372–82.
14. Stern R, Asari AA, Sugahara KN. Hyaluronan fragments: an information-rich system. Eur J Cell Biol. 2006;85(8):699–715.
15. Lokeshwar VB, Rubinowicz D, Schroeder GL, Forgacs E, Minna JD, Block NL, et al. Stromal and epithelial expression of tumor markers hyaluronic acid and HYAL1 hyaluronidase in prostate cancer. J Biol Chem. 2001;276(15):11922–32.
16. DORFMAN A, OTT ML. A turbidimetric method for the assay of hyaluronidase. J Biol Chem. 1948;172(2):367–75.
17. Knudsen P, Koefoed J. Viscometric determination of hyaluronidase activity in biological fluids. Scand J Clin Lab Invest. 1961;13(4):673–82.
18. Stern M, Stern R. An ELISA-like assay for hyaluronidase and hyaluronidase inhibitors. Matrix. 1992;12(5):397–403.
19. Pham HT, Block NL, Lokeshwar VB. Tumor-derived hyaluronidase: a diagnostic urine marker for high-grade bladder cancer. Cancer Res. 1997;57(4):778–83.
20. Bonner W, Cantey EY. Colorimetric method for determination of serum hyaluronidase activity. Clin Chim Acta. 1966;13(6):746–52.
21. Steiner B, Cruce D. A zymographic assay for detection of hyaluronidase activity on polyacrylamide gels and its application to enzymatic activity found in bacteria. Anal Biochem. 1992;200(2):405–10.
22. Podyma KA, Yamagata S, Sakata K, Yamagata T. Difference of hyaluronidase produced by human tumor cell lines with hyaluronidase present in human serum as revealed by zymography. Biochem Biophys Res Commun. 1997;241(2):446–52.
23. Cheng D, Han W, Yang K, Song Y, Jiang M, Song E. One-step facile synthesis of hyaluronic acid functionalized fluorescent gold nanoprobes sensitive to hyaluronidase in urine specimen from bladder cancer patients. Talanta. 2014;130:408–14.
24. Chib R, Raut S, Fudala R, Chang A, Mummert M, Rich R, et al. FRET based ratio-metric sensing of hyaluronidase in synthetic urine as a biomarker for bladder and prostate cancer. Curr Pharm Biotechnol. 2013;14(4):470–4.
25. Fudala R, Mummert ME, Gryczynski Z, Rich R, Borejdo J, Gryczynski I. Lifetime-based sensing of the hyaluronidase using fluorescein labeled hyaluronic acid. J Photochem Photobiol B Biol. 2012;106:69–73.
26. Huang Y, Song C, Li H, Zhang R, Jiang R, Liu X, et al. Cationic conjugated polymer/hyaluronan-doxorubicin complex for sensitive fluorescence detection of hyaluronidase and tumor-targeting drug delivery and imaging. ACS Appl Mater Interfaces. 2015;7(38):21529–37.
27. Liu S, Zhao N, Cheng Z, Liu H. Amino-functionalized green fluorescent carbon dots as surface energy transfer biosensors for hyaluronidase. Nanoscale. 2015;7(15):6836–42.
28. Murai T, Kawashima H. A simple assay for hyaluronidase activity using fluorescence polarization. Biochem Biophys Res Commun. 2008;376(3):620–4.
29. Wang Z, Li X, Song Y, Li L, Shi W, Ma H. An upconversion luminescence nanoprobe for the ultrasensitive detection of hyaluronidase. Anal Chem. 2015;87(11):5816–23.
30. Rich RM, Mummert M, Foldes-Papp Z, Gryczynski Z, Borejdo J, Gryczynski I, et al. Detection of hyaluronidase activity using fluorescein labeled hyaluronic acid and fluorescence correlation spectroscopy. J Photochem Photobiol B Biol. 2012;116:7–12.
31. Fudala R, Mummert ME, Gryczynski Z, Gryczynski I. Fluorescence detection of hyaluronidase. J Photochem Photobiol B Biol. 2011;104(3):473–7.
32. Hu Q, Zeng F, Wu S. A ratiometric fluorescent probe for hyaluronidase detection via hyaluronan-induced formation of red-light emitting excimers. Biosens Bioelectron. 2016;79:776–83.
33. Song Y, Wang Z, Li L, Shi W, Li X, Ma H. Gold nanoparticles functionalized with cresyl violet and porphyrin via hyaluronic acid for targeted cell imaging and phototherapy. Chem Commun. 2014;50(99):15696–8.
34. Wang W, Cameron AG, Ke S. Developing fluorescent hyaluronan analogs for hyaluronan studies. Molecules. 2012;17(2):1520–34.
35. Zhang L, Mummert ME. Development of a fluorescent substrate to measure hyaluronidase activity. Anal Biochem. 2008;379(1):80–5.
36. Xie H, Zeng F, Wu S. Ratiometric fluorescent biosensor for hyaluronidase with hyaluronan as both nanoparticle scaffold and substrate for enzymatic reaction. Biomacromolecules. 2014;15(9):3383–9.
37. Huang C, Chiang C, Lin Z, Lee K, Chang H. Bioconjugated gold nanodots and nanoparticles for protein assays based on photoluminescence quenching. Anal Chem. 2008;80(5):1497–504.

38. Chib R, Raut S, Shah S, Grobelna B, Akopova I, Rich R, et al. Steady state and time resolved fluorescence studies of azadioxatriangulenium (ADOTA) fluorophore in silica and PVA thin films. Dyes Pigments. 2015;117:16–23.
39. Folmar M, Shtoyko T, Fudala R, Akopova I, Gryczynski Z, Raut S, et al. Metal enhanced fluorescence of Me-ADOTA Cl dye by silver triangular nanoprisms on a gold film. Chem Phys Lett. 2012;531: 126–31.
40. Laursen BW, Sørensen TJ. Synthesis of super stable triangulenium dye. J Org Chem. 2009;74(8):3183–5.
41. Maliwal BP, Fudala R, Raut S, Kokate R, Sørensen TJ, Laursen BW, et al. Long-lived bright red emitting azaoxa-triangulenium fluorophores. Plos one. 2013;8(5):0063043.
42. Shtoyko T, Raut S, Rich RM, Sronce RJ, Fudala R, Mason RN, et al. Preparation of plasmonic platforms of silver wires on gold mirrors and their application to surface enhanced fluorescence. ACS Appl Mater Interfaces. 2014;6(21):18780–7.
43. Sørensen TJ, Laursen BW, Luchowski R, Shtoyko T, Akopova I, Gryczynski Z, et al. Enhanced fluorescence emission of Me-ADOTA by self-assembled silver nanoparticles on a gold film. Chem Phys Lett. 2009;476(1):46–50.
44. Sørensen TJ, Thyrhaug E, Szabelski M, Luchowski R, Gryczynski I, Gryczynski Z, et al. Azadioxatriangulenium: a long fluorescence lifetime fluorophore for large biomolecule binding assay. Methods Appl Fluoresc. 2013;1(2):025001.
45. Raut SL, Rich R, Shtoyko T, Bora I, Laursen BW, Sørensen TJ, et al. Sandwich type plasmonic platform for MEF using silver fractals. Nanoscale. 2015;7(42):17729–34.
46. Bogh SA, Bora I, Rosenberg M, Thyrhaug E, Laursen BW, Sørensen TJ. Azadioxatriangulenium: exploring the effect of a 20 ns fluorescence lifetime in fluorescence anisotropy measurements. Methods Appl Fluoresc. 2015;3(4):045001.
47. Laursen BW, Krebs FC. Synthesis, structure, and properties of azatriangulenium salts. Chem-A Eur J. 2001;7(8):1773–83.
48. Bora I, Bogh SA, Santella M, Rosenberg M, Sørensen TJ, Laursen BW. Azadioxatriangulenium: synthesis and photophysical properties of reactive dyes for bioconjugation. Eur J Organ Chem. 2015: 6351–6358.
49. Deng Y, Feng X, Zhou M, Qian Y, Yu H, Qiu X. Investigation of aggregation and assembly of alkali lignin using iodine as a probe. Biomacromolecules. 2011;12(4):1116–25.
50. Guo Z, Park S, Yoon J, Shin I. Recent progress in the development of near-infrared fluorescent probes for bioimaging applications. Chem Soc Rev. 2014;43(1):16–29.
51. Ajayaghosh A, Carol P, Sreejith S. A ratiometric fluorescence probe for selective visual sensing of Zn2. J Am Chem Soc. 2005;127(43): 14962–3.
52. Fan J, Hu M, Zhan P, Peng X. Energy transfer cassettes based on organic fluorophores: construction and applications in ratiometric sensing. Chem Soc Rev. 2013;42(1):29–43.
53. Niu L, Guan Y, Chen Y, Wu L, Tung C, Yang Q. BODIPY-based ratiometric fluorescent sensor for highly selective detection of glutathione over cysteine and homocysteine. J Am Chem Soc. 2012;134(46):18928–31.
54. Lokeshwar VB, Lokeshwar BL, Pham HT, Block NL. Association of elevated levels of hyaluronidase, a matrix-degrading enzyme, with prostate cancer progression. Cancer Res. 1996;56(3):651–7.
55. Kuppusamy U, Das N. Inhibitory effects of flavonoids on several venom hyaluronidases. Experientia. 1991;47(11–12):1196–200.
56. Tung J, Mark GE, Hollis GF. A microplate assay for hyaluronidase and hyaluronidase inhibitors. Anal Biochem. 1994;223(1):149–52.